DEPARTAMENTO DE ASTROFISICA

Universidad de La Laguna

QUASAR VARIABILITY: AN ASTROSTATISTICAL CHALLENGE

Thesis submitted by

Dña. Jana Poledniková

as a requirement for the degree of

Doctor of Physical Science

INSTITUTO Đ ASTROFISICA Đ CANARIAS

La Laguna, Septiembre de 2016

Examination date: ?????
Thesis supervisor: Jordi Cepa Nogué, Alessandro Ederoclite

ISBN: xx-xxx-xxxx-x
Depósito legal: xx-xxxx/xxxx

Results from 'San Pedro Mártir observations of microvariability in obscured quasars' was published in *Astronomy & Astrophysics*: Polednikova et al. (2015) and from 'Detecting microvariability in type 2 quasars with the enhanced F-test' in *Monthly notices of Royal Astronomical Society*: Polednikova et al. (2016).

Acknowledgements

This work would have been impossible without support of my great supervisors Jordi Cepa and Alessandro Ederoclite, who had great patience with me, as well as my amazing collaborator José Antonio de Diego, with whom I spent long hours discussing statistics and clever ways to use it to asses out challenges. On top of that I would like two people who made my life on Tenerife even more amazing. First of all, Agnieszka Ryś, my first flatmate ant the person without whom I would have had no idea that I can do a graduate school on a subtropical island. Without her personal involvement, I would have hardly goten here, as she helped with all the paperwork. Thank you Aga for all the evenings re-watching Friends! Second, my other amazing flatmate Klaus Rübke Zuñiga, who was there to help me out with all the phone calls I couldn't make at the beginning due to my inability to speak Spanish. He was possibly the best flatmate in the Universe, with Mojito ready for every occasion.Thank you Klaus for making my life much more fun! Last but not least I wish to thank my family who always supported me in my decisions, even if the decision meant seeing me only handful of times during the year.

On the more official note, I would like to acknowledge support by the Spanish Ministerio de Economía y Competitividad (MINECO) under the grant AYA2014-58861-C3-1, as well as the observatories which were essential in obtaining the data for this work: Nordic Optical Telescope operated on the island of La Palma by the Nordic Optical Telescope Scientific Association in the Spanish Observatorio del Roque de Los Muchachos of the Instituto de Astrofísica de Canarias and 1.5 meter telescope at San Pedro Mártir Observatory in México as well as the RATIR team.

Summary/Abstract

Variable behavior on all time scales seems to be ubiquitous phenomenon in almost all classes of active galactic nuclei. This work deals with two topics. One being detection of microvariability (intra-night variability) in the sources which are obscured and were believed to be non variable - type 2 quasars. The detection of a variable behavior in obscured sources is challenging as the detection is hampered by the low contrast between the presumably variable nucleus and the host galaxy. The second part deals with comparing of the variable behavior with larger amplitudes amongst two types of unobscured quasars: core dominated radio loud quasars (CRLQ) and radio quiet quasars (RQQ).

Microvariability studies of obscured quasars are the focus of chapters 2 and 3. We have explored the possibility to search for short, small amplitude variations, with statistical tests, namely the F-test and one-way analysis of variance, ANOVA. The data for our sample were obtained during two observing runs, one using the 1.5 m telescope at San Pedro Mártir observatory in Mexico and another one with Nordic Optical Telescope (NOT) at Observatorio Roque de los Muchachos, La Palma. Both samples were observed in optical wavelengths.

The fourth chapter is dedicated to a study independent on the previous two chapters, which studies data set obtained during a year long campaign carried out at San Pedro Mártir observatory. The data set contains observations of a paired set of unobscured CRLQ and RQQ. The observations were obtained in a weekly cadence, in optical wavelengths, thus focusing on a low frequency observations. We used Bartels test to search for variability in this case.

As a result, we report detection of microvariability phenomenon in a subset of targets observed during the microvariability campaigns described in chapters 2 and 3. It is a result previously unaccounted for in obscured type 2 quasars. We explore possible explanations such as structure in the obscuring medium. In the second part of the thesis, we focused no comparing whether it is more likely that CRLQ are variable than RQQ. We have conducted this study on a set of targets which was studied previously. The previous study focused on a similar comparison on high frequencies. We have confirmed the results of the previous study using low frequency observations and report no statistically significant difference between RQQ and CRLQ. We have demonstrated feasibility of different statistical tests in variability studies.

Resumen

Casi todos los núcleos galácticos activos muestran variabilidad en todas las escalas temporales. En el presente trabajo se abordan dos aspectos: la detección de microvariabilidad (intranoche) en cuásares de tipo 2, oscurecidos, que por tanto se cre e que no pued en ser variables, y la comparació n del comportamiento variable, de mayor amplitud, entre cuásares emisores radiocompactos (CRLQ) y cuá sares no emisores en radio (RQQ), en ambos casos no oscurecidos.

La detección de microvariabilidad en cuásares oscurecidos es un reto, debido a la dificultad que representa el bajo contraste entre el núcleo presumiblemente variable y la galaxia huésped. En los capítulos 2 y 3, se explora la posibilidad de detectar variaciones de pequeña amplitud y corta escala temporal, mediante pruebas estadísticas. Estas pruebas son la prueba F y el análisis unidireccional de varianza ANOVA. La muestra a estudiar se observó a longitudes de onda ópticas durante dos periodos, uno de ellos mediante el telescopio de 1.5m del Observatorio de San Pedro Mártir (BC, México) y otro mediante el telescopio NOT del Observatorio del Roque de Los Muchachos en la Isla de La Palma.

El capítulo cuarto se dedica a un estudio, independiente de los anteriores, de la diferencia entre CRLQ y RQQ. Para ello se ha observado, con una cadencia semanal durante un periodo de tiempo de un año, una muestra de pares de ambas clases de cuásares, a longitudes de onda ópticas, en el Observatorio de San Pedro Mártir. Se ha aplicado la prueba de Bartels, en busca de variabilidad de baja frecuencia temporal.

Entre los resultados obtenidos en la primera parte de la tesis, cabe destacar que se ha detectado microvariabilidad en un subconjunto de cuásares oscurecidos de tipo 2, para los que no se habí a detectado este fenómeno con anterioridad. Se han explorado posibles explicaciones tales como la presencia de estructura en el medio que los oscurece. En cuanto a los resultados obtenidos en la segunda parte, se confirma que no existe una diferencia significativa entre RQQ y CRLQ ni a altas frecuencias temporales, como ya se habí a demostrado en estudios anteriores, ni a bajas frecuencias temporales, como muestra el estudio actual. Finalmente, como resultado global de la tesis, se ha demostrado la viabilidad de diferentes pruebas estadí sticas aplicadas a los estudios de variabilidad.

Index

Chapter 1

Introduction

Changes in the sky have been in the focus of astronomical studies since the mankind started paying attention to the sky, dating back to second millennium BC. One of the first notions of the changes in the sky comes from observing wandering stars - planétai, or in modern words, planets. The observed changes had to be severe to be noticed. After nearly four millennia of astronomical exploration, we have come to an consensus that nearly all the objects in the universe are variable on different time scales and modern statistical methods allow us to detect variations otherwise not noticeable by eye. This work focuses on detecting variability in active galactic nuclei (AGN hereafter), using statistical methods. The following chapter provides an overview of the topics which need to be brought together the current work, which are unified model of the active galactic nuclei, variability of active galactic nuclei and brief overview of the statistical methods we used to study the variable phenomenon in AGN.

1.1 Objectives

Detection of variability in type II quasars is elusive due to the nature of the source. The natural assumption is that due to the presence of the obscuring torus, blocking our view, the variability is not detectable, as seen further in Figure 1.8. This thesis is centered on three sets of photometric observations obtained with different telescopes, where two sets are focused on type II quasars. The first search for microvariability in type II quasar is conducted using the SITe4 detector on the Harold J. Johnson 1.5 meters telescope situated at the Observatorio Astronómico Nacional at San Pedro Mártir, Baja California. The sample includes three sources. This effort was further broadened by observing four more targets with ALFOSC on the Nordic Optical Telescope (NOT). Previous attempts aimed at detection on large time scales, while the focus of our pilot sample was on short term variations with small amplitudes. With the third dataset, we have shifted our focus to the observations of variability with a larger amplitude and longer time scale. The third set of the data consists of weekly observations of core dominated radio loud and radio quiet quasars, observed using the RATIR instrument, nowadays mounted on the Harold J. Johnson 1.5 meters telescope at San Pedro Mártir observatory. The RATIR instrument permits simultaneous observations in different filters resulting in a multi-color campaign.

The objectives of this thesis can be summarized as follows:

- Investigation of variability of type 2 quasars.
- Search of possible explanations of microvariable behavior.
- Obtain precise photometry of all sources.

- Identify the appropriate astrostatistical method to search for photometric variations in every data set.
- Apply the chosen technique to search for variability. See if the chosen technique is feasible.
- Compare with the results on microvariability in the literature, searching for a possible physical explanation of the phenomenon.

1.2 Active galactic nuclei

The basic definition of the Active Galactic Nuclei (AGNs hereafter) states that AGNs are an energetic phenomena in the nucleus of galaxies, which cannot be attributed directly to the stars. More rigorously, an AGN is a compact region at the center of a galaxy, which contains a massive accreting black hole, with Eddington ratio (the accretion rate in units of the maximum possible accretion rate) exceeding the limit of $L_{AGN}/L_{Edd} = 10^{-5}$, where L_{AGN} is the bolometric luminosity of the AGN and $L_{Edd} = 1.5 \times 10^{38} M_{BH}/M_{\odot}$ erg s^{-1} is the Eddington luminosity for a solar composition gas.

1.2.1 Discovery of AGNs

The first observations of an AGN date back to 1909 when Edward A. Fath observed emission lines in the bright galaxy NGC 1068, which made it stand out between the quiescent galaxies with only absorption lines (Fath 1909). This discovery was followed by observations by Slipher (1917) who noted similarities between the emission lines in NGC 1068 and the planetary nebulae. Slipher (1917) was also the first one to notice that the emission lines are resolved and have widths of hundreds of kilometers per second. Seyfert (1943) reported that a fraction of galaxies with bright, stellar-like nuclei, produce broad emission lines. His work was centered on a group of galaxies (NGC 1068, NGC 1275, NGC 4051, NGC 4151 and NGC 7469). The major conclusions of Seyfert's work were:

1. The lines are broad (up to 8500 km s^{-1}, full width at zero intensity).
2. The hydrogen lines sometimes are broader than the other lines.

There was not much attention paid to the galaxies Syfert studied, up till 1950s, when some of them (NGC 1068 and NGC 1275) were observed to be radio sources.

Radio astronomy was essential for the AGNs. By 1950s, radio telescopes were able to identify the strongest radio sources in the sky. Most of the sources emitting at radio wavelengths at the high galactic latitudes were identified with resolved galaxies, however some of them vere coinciding with sources with stellar appearance. One of the first examples of such was 3C 48, reported by Matthews & Sandage (1963), whose position coincided with a 16 mag star. Another example of similar nature is 3C 273, reported in the work of Hazard et al. (1963).

The major breakthrough came with the work of Schmidt (1963) who realized that the broadened lines are corresponding to Balmer-series emission lines, forbiden line [O III] (λ5007) and Mg II (λ2798) line redshifted at $z = 0.158$. This redshift meant discovery of the furthermost object till date. Even most shocking was the bolometric brightness of the source. Given the Hubble law and the computed redshift

$$m - M = 5 \log(cz/H_0) + 25, \tag{1.1}$$

where cz/H_0 is measured in Mpc, the absolute magnitude of 3C 273 is $M_B = -25.3 + 5 \log H_0$, which is almost 100 times more bright than for example M31. We assume $H_0 = 75$ km s^{-1} Mpc^{-1}.

As the nature of the sources was not fully understood at the given time, the objects were referred to as 'quasi - stellar radio sources'. From this came the shortened term 'quasar'.

The description of quasar objects by the end of 1960s went as (Schmidt 1969):

1. Star-like objects identified with radio sources.
2. Time-variable continuum flux.
3. Large UV flux.
4. Broad emission lines.
5. Large redshifts.

These characteristics served as a prime for initial identifications and discoveries of quasars, as well as for the first attempts to understand the underlying physics. Over the course of the upcoming years, it was shown that there are different kinds of objects falling into the quasar class, which resulted in a classification based on almost purely phenomenological approach.

1.2.2 Classification of AGNs

The AGNs can be divided into several classes and subclasses according to the appearance of their spectra as can be seen in Figures 1.1 – 1.3. In the course of almost 50 years, when there was no clear connection between the different classes of the AGNs, the taxonomy rose to a significant number of classes of objects. Nevertheless as the detailed classification is not the crucial point of this work, only the most basic and important classes of AGNs are discussed below.

Type I AGNs: sources which have broad (1000 - 20,000 km s^{-1}) permitted emission lines, H_α, H_β, C IV λ1549, Mg II λ 2798 etc. The broad emission lines are easier to detect in bright sources. Type I AGNs can be further divided into Seyfert 1 galaxies (Sy 1) and type I quasars. The distinction between them can be established based on the bolometric luminosity. AGNs with bolometric luminosity $M_B > -21.5 + 5 \log h_0$ are considered to be Seyfert galaxies. In the cases of low to medium luminosities, the high ionization narrow emission lines, both permitted and forbidden, are also present. These lines are missing in many of the high-luminosity type I AGNs.

Type II AGNs: objects with spectra similar to type I AGN but without the broad line component. The only lines present are narrow (300 - 1000 km s^{-1}). As well as type I AGNs, type IIs can be divided into two groups, Seyfert 2 (Sy2) galaxies and type II quasars. However the distinction between these two classes is not as clear as in the case of type I AGNs, as type II AGNs are dust obscured and therefore in order to obtain their bolometric luminosity one needs to find a probe of the accretion rate. The proxy to measure bolometric luminosities is the measurement of [OIII] luminosity, which is easily accessible. AGNs with $L_{[OIII]} \geq 10^{8.3} L_\odot$ are considered a high luminosity counterparts, named type II quasars. Some of the type II AGNs display broad line component when observed in the polarized light. The phenomenon was first observed in NGC1068 (Antonucci & Miller 1985). It prompted a further division of the type II AGNs into the "real" ones and the ones with hidden broad line region. The real type II AGNs lack any broad line. Moran et al. (2000) reports that at least 35% of the nearby classical Sy2 galaxies show polarized broad emission lines. Nevertheless detection of the hidden broad line region is typically time consuming as the results can be obtained only by deep spectropolarimetry or by mid-infrared spectroscopic observations. There are undergoing efforts to determine whether such division can be made based on simpler observations (e.g. Tommasin et al. 2010). All in all, type II AGNs are notoriously hard to classify as often there are no hard X-ray data which would help with the classification. On top of that, objects like HII galaxies show the same strong emission lines as type II AGNs. Therefore we

rely on the classification based on the ratios of the intensities of the emission lines, as proposed by Baldwin et al. (1981). Most notable ratios used in the literature are [O III]λ5007/Hβ, [N II]λ/Hα and [O I]λ6300/Hα. Type II AGNs have the ratios higher than other sources (see Figure 1.4).

Intermediate AGNs: Osterbrock & Koski (1976) discovered Seyfert galaxies of an 'intermediate' properties. In broader sense, the intermediate AGN is an AGN which has weak broadened lines in comparison with the narrow ones. The notation goes as Seyferts 1.2, 1.5, 1.8 and 1.9. The appendage of a given galaxy to a subgroup is based on the characteristics of the hydrogen Balmer lines. A Sy 1.2 galaxy resembles Sy1, but Hβ line is not as broad as in regular Sy 1. Sy 1.5 has Hβ line as strong as the narrow component. Sy 1.8 and 1.9 show only some broad line components, for example Sy 1.9 shows broadening only in Hα. The refinement in the classification is a consequence of a higher spectroscopic resolution available. In the past, there were only low resolution spectra, which allowed only the basic distinctions between the types I and II.

Blazars: most notably variable sources, which also show a high degree of polarization (30-40% linear polarization). The luminosity of a blazar can change by 30% within 24 hours. Blazars include the subclasses of BL Lac[1] objects, named after the prototype BL Lac, which are devoid of emission lines and show strong radio emission, and that of flat spectrum radio quasars (FSRQs; historically also known as optically violently variable quasars). The major difference between the two groups is the presence of emission lines in the spectrum. While the BL Lac type of sources is line deficient, FSRQs have some noticeable lines. The general lack of emission lines provides a challenge for determining the redshift of blazars. Nevertheless based on few lines (mostly in FSRQs) observed, several blazar redshifts were obtained.

Low ionization narrow emission line regions (LINERs): usually synonymous with the low-luminosity AGNs (LLAGN). Those targets are relatively common in the local universe. Their spectrum has strong optical emission lines of [O III], [O II], [O I], [N II] and Balmer series. All of the mentioned lines are also present in the 'normal' highly ionized AGNs. The intensity of the lines in LINERs points to a lower ionization state. One of the convenient ways to distinguish between the LLAGNs and ionized AGNs is the ratio of [O III]/Hβ. The ratio is significantly smaller in LINERs than in AGNs.

LINERs can be divided in two groups, based on the appearance of the broad line region in the spectra. The broad lines are almost exclusively Hα lines as the wings of the profile of the other Balmer lines is likely to be lost in the strong stellar continuum. Therefore correct distinguishing between the two classes of LINERs is often ambiguous.

In the most known LINERs , photoionization by a nuclear radiation source seems to be the main source of ionization and excitation of the gas. However photoionization by evolved stellar populations like post-AGB stars also results in LINER-looking emission-line ratios. The usual way of distinguishing between truly LINERs and AGB stars the ratio of emission lines intensity to continuum, which is significantly higher in LINERs than in post AGB stars.

Broad absorption line AGNs (BAL AGNs): are type I AGNs with the rest wavelength UV spectrum showing deep, blue-shifted absorption features, or troughs, associated with most cases with strong resonance lines of C IV, Si IV, N V, O VI and Lyα (for the highly ionized sources) or Mg II and Fe II (lower ionization sources). The feature was first observed by Lynds (1967). The widths of the absorption troughs are typically 10 000 km s^{-1}. The usual explanation lies in the assumption that all high luminosity AGNs contain high-outflow-velocity systems (e.g. Turnshek et al. 1988; Chartas et al. 2002).

[1]The name follows the notation for variable stars. This is due to the fact that the source was originally considered a variable star.

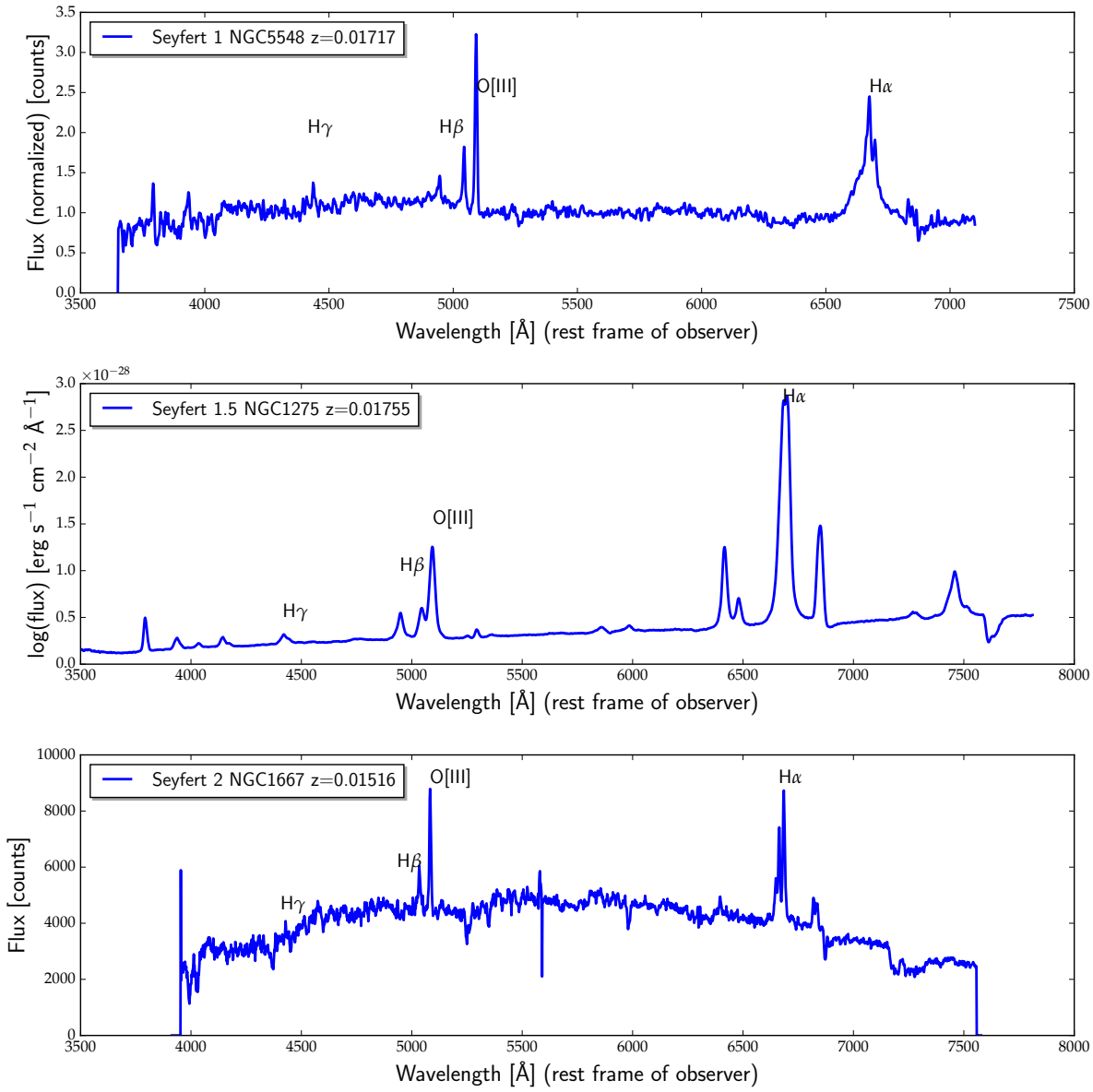

Figure 1.1: Optical spectra for the representatives of the various classes of Syfert galaxies. The most prominent Balmer lines are marked along with the O[III] line, whose prominence makes it a strong feature in most of the AGNs. Top panel: Seyfert 1 galaxy with a noticeable broad line component in Hα. Adopted from Kennicutt (1992), observed with 2.3 telescope at the Steward observatory. Middle panel: optical spectrum of Seyfert 1.5 galaxy. In Seyfert 1.5 galaxy, the strength of the broad and narrow lines are comparable. Adapted from Buttiglione et al. (2009), observed with the TNG telescope on Roque de los Muchachos. Bottom panel: Seyfert 2 galaxy, missing the broad line component. Adopted from Jones et al. (2009), observed by the Anglo-Australian telescope as a part of 6dF survey (Jones et al. 2004).

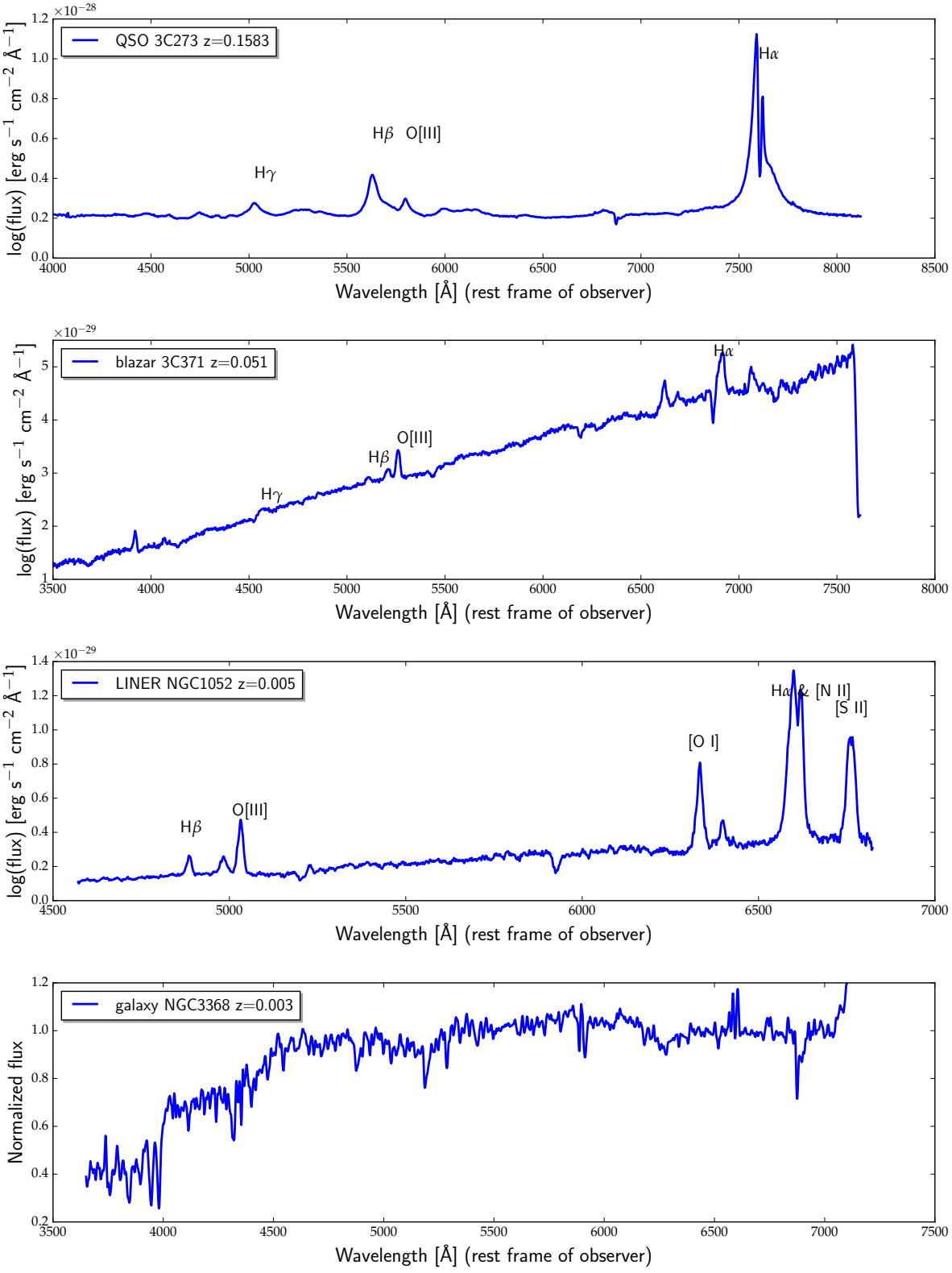

Figure 1.2: Spectral based classification of the AGNs with a comparison to the quiescent galaxy. Top panel: Spectrum of quasar 3C 273, the brightest known quasar and also the flagship of quasar discovery with prominent Balmer lines. Adopted from Torrealba et al. (2012), observed with the 2.1 meter telescope at OAN San Pedro Martír. Second top panel: spectrum of blazar (Bl Lac type object), mostly lacking strong features, in comparison with the other AGN classes. Adopted from Buttiglione et al. (2009), observed with the TNG telescope on Roque de los Muchachos observatory. Third from the top: spectrum of a LINER. Spectrum resembles a regular Seyfert 2 galaxy, except for strong low-ionization lines like [O I] or [N II]. Adopted form Torrealba et al. (2012), observed with the 2.1 meter telescope at OAN San Pedro Martír. Bottom: A sample spectrum of a regular galaxy, deprived of Balmer lines, adopted from Kennicutt (1992), observed with the 2.3 meter telescope at Steward observatory. .

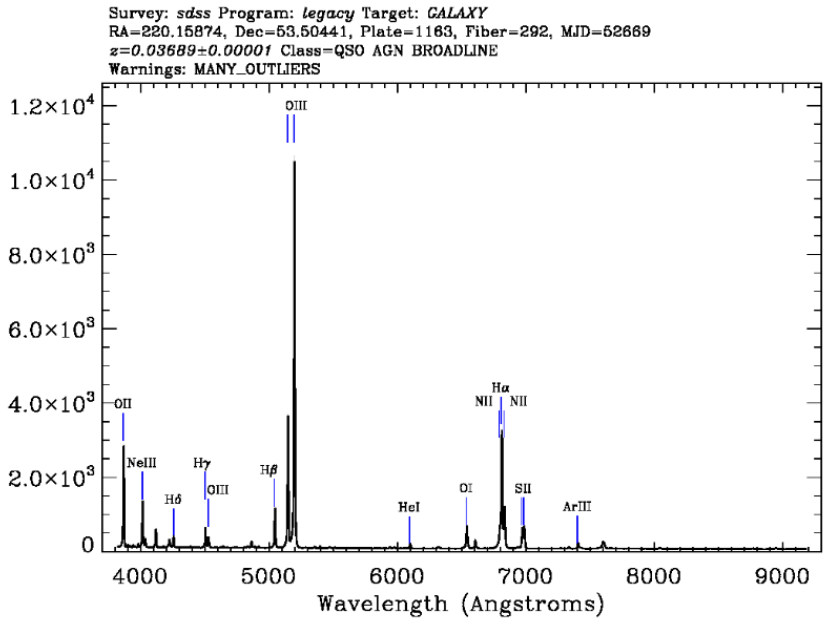

Figure 1.3: SDSS spectra of Markarian 477, the brightest type II quasar. The y-axis is flux 10^{-17}[erg^{-1} cm^{-2} Å^{-1}]. .

A typical BAL AGN has weaker X-ray luminosity relative to the optical luminosity, than an ordinary AGN. Few BALs were detected in radio wavelengths. BAL AGNs tend to be more polarized in both, continuum and the absorption troughs. The sources with Mg II absorption line tend to have redder continuum.

Ultra-luminous Infrared Galaxies (ULIRGs): and their more luminous counterparts hyperluminous infrared galaxies (HLIRGs) and extremely-luminous infrared galaxies (ELIRGs) are, as the name points out, extremely luminous in the red part of the spectrum, quantitatively at $\lambda > 10\mu$m (Soifer et al. 1987). The luminosities $L(8-1000\mu\text{m}) \gtrsim 10^{12}\text{L}_\odot$ exceed the optical luminosities typically by a factor of 10. Many of the galaxies were associated with starburst galaxies, nevertheless some of them proved to host an AGN. The excess in the infrared emission is attributed to the thermal radiation from dust (at $T \approx 100K$ or less) which is either heated by the massive star formation or by a hidden AGNs. ULIRGs make outstanding candidates for discovering new AGNs.

Radio loud and radio quiet AGNs: most of the AGNs show some radio emission. The customary way of describing the strength of the emission is defining the radio-loudness parameter R, which separated the so-called radio-loud from the so-called radio-quiet AGNs. R is computed as the ratio of radio emission to optical monochromatic luminosity:

$$R = \frac{L_\nu(5\text{GHz})}{L_\nu(4400\text{Å})} = 1.36 \times 10^5 \frac{L(5\text{GHz})}{L(4400\text{Å})}, \tag{1.2}$$

where $L(5\text{GHz})$ and $L(4400\text{Å})$ represents the value of monochromatic luminosity at those energies. The division is set at $R = 10$. Approximately 10% of the observed AGNs are radio loud. The spectrum is represented by a single power-law $F_\nu \propto \nu^{\alpha_R}$. Sources with $\alpha_R < 0.5$ are reffered to as flat-spectrum radio sources, while the $\alpha_R > 0.5$ are steep-spectrum radio sources.

1.2.3 Unified Model of Active Galactic Nuclei

As the studies of various classes of the AGNs progressed, it became apparent that there are several components that make up an AGN. A basic overview of the components is provided below.

A central engine and the accretion disc: AGN activity is thought to be powered by accretion of gas onto a supermassive black hole (SMBH hereafter). The masses of the central SMBH are estimated to be the order of $10^8 M_\odot$. Most of the radiation is believed to be emitted by the central areas and due to accretion flow onto the central SMBH. The accretion disc is believed to be optically thick. For a disc surrounding a $10^8 M_\odot$ black hole accreting at the Eddington rate, the emission from the inner part of the disc maximizes at a wavelength around 100 Å which corresponds to the extreme UV or soft X-ray region of the spectrum. The structure will have a dimension $\sim 1000 r_g$, where r_g is a gravitational radius. AGNs have angular momentum, which permits only certain geometries: optically thick, geometrically thick disc; optically thick, geometrically thin disc or a combination of both.

Broad line region: is found relatively close to the central part of the AGN. In concordance with the taxonomy above, it is directly observed in the type I sources. It is a major feature in the spectra of the AGN, often used to distinguish AGNs from different sources. The proximity of the broad line region (BLR hereafter) to the central SMBH makes it an ideal probe to the physics of the innermost parts of the AGNs. The bulk motions in the BLR are most certainly directly affected by the changes in the central engine. The width of the lines ranges from $\delta v_{FWHM} \approx 500$ km s^{-1} to extremes such as $\delta v_{FWHM} \approx 30000$ km s^{-1}, with typical values around $\delta v_{FWHM} \approx 5000$ km s^{-1}. The line profiles do not have to follow the same structure in all the AGNs.

Narrow line region (NLR): is of crucial importance to AGN studies as it is the largest spatial scale where the ionizing radiation from the central source dominates over other sources. It is the only region we can resolve spatially with optical observations and the dynamics are possibly linked to processes in the innermost, spatially unresolved parts of the AGN. This is probably the best studied part of the AGN. There are more than 100 spectral lines recognized for the nearby AGNs, with the most prominent ones summarized in table 1.1.

The NLR has smaller column density (compared to BLR; $\sim 10^{20-21}$cm^{-2}) and low density ($10^3 - 10^6$cm^{-2}). The typical velocities observed in the narrow line region fall within the interval of of 300 – 1000 km s^{-1}. One of the typical Sy2 galaxies, NGC 1068 stands out as extreme with full-width half maximum (FWHM) of the [O III] line 1140 km s^{-1} (Meyer et al. 2004). The level of ionization of the NLR is comparable with that of BLR, albeit the physical conditions are diverse than in BLR. The gas is optically thin and as the density is low, transitions in such environment are not collisional and therefore measuring the spectral lines intensity ratios allows us to measure the electron densities and temperatures. The size of the NLR, in other words, the region where the spectrum is of the typical AGN-ionized gas, can be extended up to 20kpc. Such regions are called extended narrow lines region (ENLRs). Defining the border, where the NLR ends is very challenging, given the fact that we can see the ENLR under different inclination angles. The vast expansion of the NLR and the assumption of the geometry based on the unified scheme, makes the strong lines in the NLR an ideal tool to determine additional parameters. For the cases of the nearby AGNs, the NLR is resolvable in the sky and therefore can be used directly to estimate the distribution of the gas and the kinematics (e.g. Walker 1968). Using emission lines ratios, one can produce maps, which can be used as spatially resolved diagnostics of density, temperature, ionization and excitation.

Together with the BLR, the NLR can be used in diagnostic diagrams to distinguish between the emission line galaxies. The usual ratios used are: [O III] λ5007 / Hβ, [N II] λ6583 / Hα, and [S II] λ6716, 6731 / Hα flux ratios. The diagnostics diagrams are named BPT diagrams (Baldwin, Phillips, Terlevich) introduced by Baldwin et al. (1981), see Figure 1.4.

Table 1.1: Strong narrow emission lines in AGNs. Adopted from Ferland & Osterbrock (1986). For the case of the ionized lines, the ionization potential is the one needed to achieve the observed ionization state.

Line	Relative flux	Ionization potential (eV)	Critical density $n_{crit}[\mathrm{cm}^{-3}]$
Lyα (1216Å)	55	13.6	...
C IV (1549 Å)	12	47.9	...
[C III] (1909 Å)	5.5	24.4	3.0×10^{10}
Mg II (2798 Å)	1.8	7.6	...
[Ne V] (3426 Å)	1.2	97.1	1.6×10^{7}
[O II] (3727 Å)	3.2	13.6	4.5×10^{3}
[Ne III] (3869 Å)	1.4	40.0	9.7×10^{6}
[O III] (4363 Å)	0.21	35.1	3.3×10^{7}
He II (4684 Å)	0.29	54.4	...
Hβ (4861 Å)	1.0	13.6	...
[O III] (4959 Å)	3.6	35.1	7.0×10^{5}
[O III] (5007 Å)	11	35.1	7.0×10^{5}
[N I] (5199 Å)	0.15	0.0	2.0×10^{3}
He I (5876 Å)	0.13	24.6	...
[Fe VII] (6087 Å)	0.10	100	3.6×10^{7}
[O I] (6300 Å)	0.57	0.0	1.8×10^{6}
[Fe X] (5375 Å)	0.04	235	4.8×10^{9}
[N II] (6548 Å)	0.9	14.5	8.7×10^{4}
Hα (6563 Å)	3.1	13.6	...
[N II] (6583 Å)	2.9	14.5	8.7×10^{4}
[S II] (6716 Å)	1.5	10.4	1.5×10^{3}
[S II] (6731 Å)	...	10.4	3.9×10^{3}
[Ar III] (7136 Å)	0.24	27.6	4.8×10^{6}

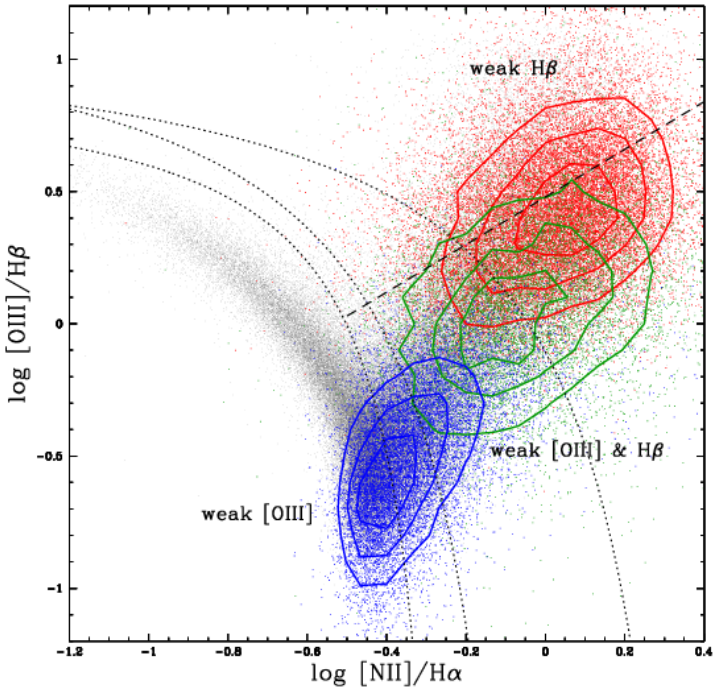

Figure 1.4: BPT diagram as presented in the work of Cid Fernandes et al. (2009) and references therein. Grey dots correspond to objects with signal to noise ratio > 3 in all BPT lines. Dotted curves correspond to the division between AGN and starburst galaxies, according to different works. The diagonal dashed line represents the division between Seyfert galaxies and LINERs. Contours mark different types of weak lines.

The highly ionized gas (HIG region): highly ionized gas region is found between the NLR and the BLR. In terms of distance, we can assume 0.1–10 pc from the central engine. The ionization is up to 100× larger than in the BLR. This part of the AGN is dominantly detected in the X-ray and is referred to as a 'warm absorber'. The HIG is transparent to the UV and the soft X-ray radiation and thus is subjected to strong radiation pressure force (in comparison with the opaque BLR). Such physical conditions result in mass outflows from the AGN. The mass outflow estimation was further explored in local AGNs by Crenshaw & Kraemer (2012) who estimated mass loses of order of $\sim 0.1 M_{\odot}\mathrm{yr}^{-1}$ with an exception of NGC 3783, where the outflow ranges between $5.2 - -30 M_{\odot}\mathrm{yr}^{-1}$.

Broad and narrow absorption line region: broad line, blue-shifted, regions are detected in 10 - 20% of the high luminosity type I AGNs. The sources with such feature usually have significantly reddened continuum, are highly polarized and have weak X-ray and radio emission. Even in the case of the nearest AGNs, the absorption line regions are spatially unresolved.

Torus: one of the most discussed parts of the AGNs is the dusty torus. The phenomenological models (ad hoc models) are in general three: continuous gas distribution models (e.g. Pier & Krolik 1992; Fritz et al. 2006), clumpy torus models (e.g. Nenkova et al. 2008; Hönig et al. 2010) and composite of both (Stalevski et al. 2012). The common property of all phenomenological models is the axial symmetry. It is assumed that the torus inner walls are at the dust sublimation radius. Nevertheless such radius' definition varies between the models as the assumed properties of the dust differ between the models as well as the way of determining the bolometric luminosity of the central

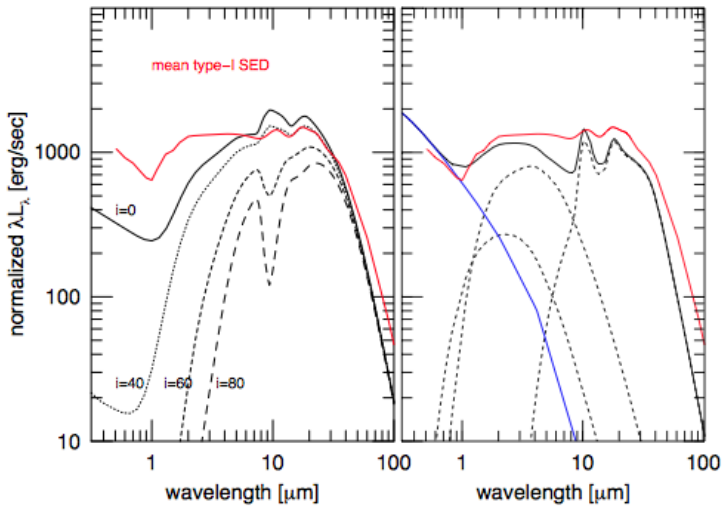

Figure 1.5: Left: Comparison of the composite model SED (Stalevski et al. 2012) (black line) and the observed data (Mor & Netzer 2012) (red line) that contains dust emission from the narrow line region. Right: SED of a three cloud obscurer. Two clouds contain graphite grains and one contains ISM type of dust and is located approximately 100 times further than the first cloud. The covering factors are 0.1, 0.3 and 0.3 respectively. The solid line is combination of the three dashed lines. The blue line is the SED of the central disc. Adapted from Netzer (2015).

source.

The crucial parameter for the phenomenological models are the inner and outer radii of the torus, the density profile and the opening angle. In the case of clumpy torus, additional parameters are the column density of the individual clumps and their radial distribution (in opposition to the gas density in the smooth model), the filling factor and the density distribution of the clumps. Naturally the clumps pose a challenge for e.g. radiative transfer.

The main difference between the clumpy and the smooth model is in the appearance of the spectral energy distribution. The SED expected from the clumpy model exhibits broader range of temperatures as the illuminated and back sides of individual clumps have a broader range of temperatures, unlike the smooth torus. The smooth torus also cannot explain the silicate absorption at 9.7 μm (Nenkova et al. 2008). More importantly, the gaps between the clumps potentially allow unobscured view onto the central parts of the AGN.

The general consensus seems to agree that most realistic model is the composite model which involves combination of the smooth torus and the clumps (see Figure 1.5). In this scenario, the gaps between the clumps are filled with diluted dusty gas which absorbs part of the incident optical / UV radiation and part of the locally emitted NIR and MIR radiation. Therefore the specific features of the clumpy scheme with an additional dust attenuation due to the smooth torus component are maintained.

The jet: almost all powerful radio-loud AGNs show central radio core or radio jet. The point which seems to be the origin of the jet is coinciding with the location of the UV / optical and X-ray continuum source. The emission from the jet is dominated by the synchrotron processes. There is a classification scheme for blazar jets, so called Fanaroff and Ripley types - FR I and FR II. FR II have higher radio luminosity and the jets are highly collimated. The typical FR II jet shows strong linear polarization, perpendicular to the jet direction. The lobes are common in this class of sources. The lobes are not beamed and they act like an extended contours around the central point source. FR I sources tend to be less luminous and usually contain two antiparallel jets. It

seems that the distinction between the flat and steep spectrum radio sources is directly related to the viewing angle and reflects the beaming of the radiation along the axis of the central jet direction. The creation of the jet itself is an important question. One of the most viable explanation lies in the Blandford-Znajek process (Blandford & Znajek 1977). The mechanism describes an extraction of energy from the rotating (Kerr) black hole surrounded by the accretion disc. The extracted power is proportional to $B^2 M_{BH}^2$. As an example, for a black hole $10_{\odot}^8$ with a magnetic field of 10^4 gauss, the maximum extracted energy is 10^{44}ergs^{-1}. Along with the radio detected jets, blazars have γ-ray jets. A γ-ray jet is described in two major models, leptonic or hadronic and possible combination of the two. The leptonic model considers electrons and positrons as relativistically emitted particles, while the hadronic model includes mostly protons and electrons. However the pure leptonic model seems to fall short of the energy necessary to power the jet. The hadronic model on the other hand poses a question of the origin of the hadrons. The signature of the jet is detectable also at other wavelengths. The X-ray observations, for example, show a formation of the structure along the jet.

Assembling the whole image together, we can relate the different parts of the image to the different classes of AGNs observed. Blazars are the sources, where the angle to the line of sight is close to 0°. Therefore the observer is looking almost straight into the jet and the spectrum is dominated by the synchrotron radiation, which provides an explanation of the line deficiency in the spectra of blazars. When the line of sight angle grows, we observe type I AGNs, where the observer maintains a direct view onto the innermost parts of the AGN. When the line of the sight viewing angle reaches $\sim 90°$, the view of the central engine is blocked by the dusty torus and we are observing type II AGN. The basic idea is depicted in Figure 1.6.

The imprints of the different parts of the AGNs can be traced in the spectral energy distribution (SED) of the AGN. SED contains some of the characteristic AGN signatures and therefore helps to distinguish AGN from other classes of sources. SED of AGN is often described, over a limited energy range as

$$L_{\mu} \approx \mu^{-\alpha}, \tag{1.3}$$

where α is the frequency spectral index. In general, there are many underlying features which are overlooked by the simple power-law model, which distinguish between AGN as a synchrotron source and AGN as a multi-component continuum source. The existence of those features points towards different underlying physical processes. Some of the most prominent features being:

- **'Big blue bump'** is a strong broad feature which dominates the spectrum betwen ~ 4000 Å and ~ 1000 Å. The short end being inaccessible by ground based observations and is often called 'soft X-ray excess'.
- **'Local minimum'** around $1\mu m$, attributed to the minimum between the hot thermal spectrum (big blue bump) and a cool termal spectrum caused by the emission by warm (≤ 2000 K) dust. The smooth bump following in the wavelengths longward of the minimum is often called 'IR bump'.
- **'Submillimeter break'** is present in the radio-quiet sources, where there is a rapid decrease in the SED.

Some of the features are marked in the sample SED of two sources, radio loud (4C 34.47) and radio quiet (Mrk 586) in Figure 1.7.

Despite the differences among the various classes of objects, all AGNs show Eddington ratio (L_{AGN}/L_{Edd}, where $L_{Edd} = 1.5 \times 10^{38} M_{BH}/M_{\odot}\text{ergs}^{-1}$) exceeding 10^{-5}. The value is somewhat arbitrary, nevertheless it serves as a good proxy to demonstrate the overall brightness of all AGN classes. Antonucci (1993) proposed a unifying scheme which is nowadays commonly known as

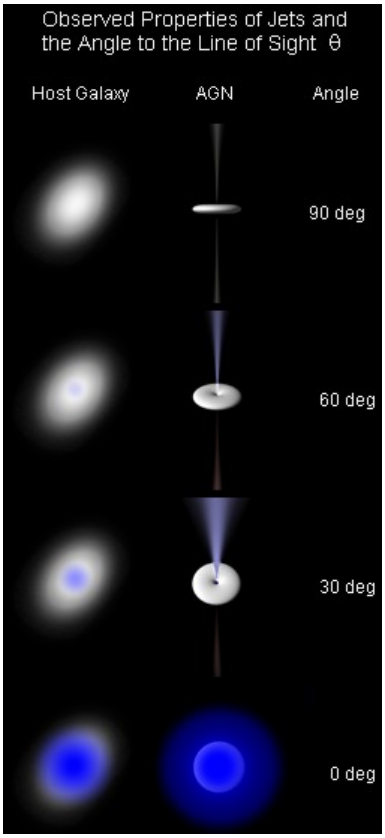

Figure 1.6: Demonstration of the jet contribution to the observed spectra based on the line of sight angle of the AGNs. Credited under Wikimedia commons, author: Ron Kollgaard.

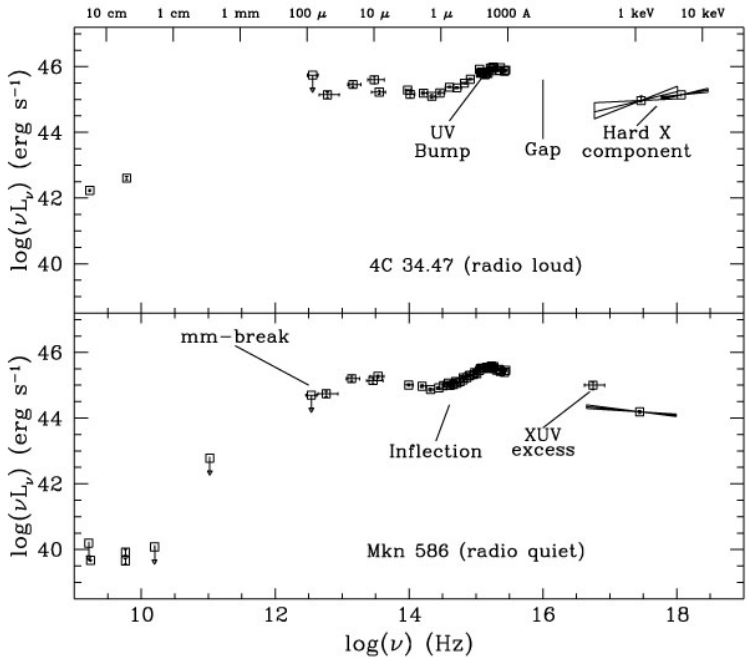

Figure 1.7: Rest frame radio to X-ray spectral energy distribution for a low-redshift radio-loud (upper panel) and radio-quiet (lower panel) quasars. Adapted from Elvis et al. (1994).

the 'Unified model of Active Galactic Nuclei'. The whole image was further accompanied by unified model for radio-loud AGNs presented by Urry & Padovani (1995).

The Unified model was prompted by the seminal work of Antonucci & Miller (1985) who observed Sy1 type spectra in the polarized light of the Sy2 object NGC 1068. Such observation was a strong hint that the objects might be of a similar nature. It was supported by the observations in the infrared and X-ray regimes. In the case of the infrared observations, as the wavelength lengthens, the optical depth decreases and therefore provides a better probe into the structure of the AGN. Compact bright sources and/or independent linear polarization have been found in several sources (i.e. Fabbiano et al. 1986; Djorgovski et al. 1991). X-ray observations further supported the idea that type II sources show weak X-ray continuum in comparison with type I objects. Mulchaey et al. (1992) showed similar high column densities from X-ray measurements, consistent with the central source of type IIs obscured from the direct view.

Antonucci (1993) later showed that all the classes of AGNs can be explained by one model, which can be dissected into several components where the differences in the observed spectrum are result of the geometrical orientation towards the line of the sight of the observer. The result is depicted in Figure 1.8. In following paragraphs, we will describe the features of the unified model.

1.3 Variability

Transient phenomena on the sky can be ascribed to a variety of physical mechanisms and are found in many (if not all) astrophysical sources. It is out of the scope of this work to describe the whole motivation behind the studies of variations of different objects, therefore the focus is kept on AGNs. This section consists of a brief discussion of the types of variability detected in the AGNs, variability detection in different wavelengths and overview of some techniques used to extract information from

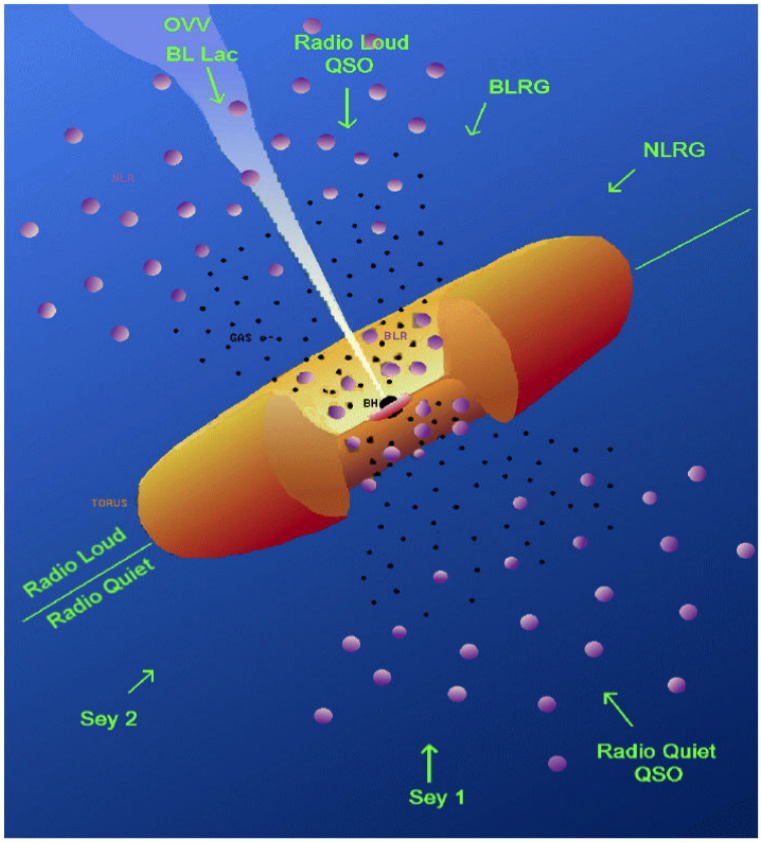

Figure 1.8: Scheme of the unified model of Active Galactic Nucleus (Urry & Padovani 1995).

the variability studies.

1.3.1 Variability of AGNs at different wavelengths

AGNs exhibit variations over the whole electromagnetic spectrum, from radio to gamma rays. The variations are believed to be aperiodic and of variable amplitudes, although some reports of quasi-periodic behavior exists, e.g. in source PG 1553+113 (e.g. Ackermann et al. 2015). The discovery of the variable behavior of AGNs followed closely after their discovery. The first observations of variability were reported in the work by Matthews & Sandage (1963) in quasars. The variability of the lower luminosity counterparts of quasars, Seyfert 1 galaxies was reported later, in the work by Fitch et al. (1967). The detected variations in the optical regime were of $\gtrsim 0.1$ mag and occurred on scales as short as days (in the cases of quasars).

Optical and UV variability of AGNs: since the discovery of the variable behavior of AGNs, most studies in the optical regime have been focused on the study of blazars, which exhibit biggest amplitudes of the changes. *BlLac*, the prototype blazar's apparent magnitude ranges between $mag_{\rm v} \approx 14 - 17$. The variability in the case of the blazar comes most likely from the non-thermal component as this one dominates the spectrum of such objects. Variability of other AGN classes is not so prominent, yet holds important implications. Especially in the case of radio-quiet AGNs, the changes are most likely attributable to the accretion disc. By probing the variations of the accretion flow, a set of significant constraints can be placed on fundamental properties of AGN. One of the examples is the viscosity parameter (Starling et al. 2004) and correlation of parameters such as black hole mass and accretion rate with disc variability properties.

Historically, the vast majority of variability campaigns observed with a low cadence , e. g. Palomar-Green quasars observed for seven years with the Wise observatory (Giveon et al. 1999) or SDSS Stripe 82 (Sesar et al. 2007).

The aim of the optical studies was mostly finding correlations between the variability and various physical parameters of the AGNs. For example, the timescale of the variability gives us an idea about the rate at which the region varies and it gives us an upper limit to the ratio of the size of the region to velocity at which changes propagate and hence giving us an idea about the approximate size of the region, while the amplitude of the variation hints the relative importance of the variability. The correlations between the AGN properties and properties of the light curve are important because they are a consequence of the activity condition and the evolutive history of the nuclei. It was discovered that variability amplitude was found to correlate with redshift (Cristiani et al. 1990; Hook et al. 1994; Trevese et al. 1994; Vanden Berk et al. 2004) and with black hole mass on time scales > 100 days (Wold et al. 2007; Bauer et al. 2009). It was also found to be anticorrelated with luminosity (Cristiani et al. 1997; Giveon et al. 1999; Vanden Berk et al. 2004; Bauer et al. 2009), Eddington ratio (Wilhite et al. 2008; Bauer et al. 2009) and with the rest frame wavelength (Cutri et al. 1985; di Clemente et al. 1996; Giveon et al. 1999; Vanden Berk et al. 2004).

Based on these studies, some constraints were placed on the models of AGNs as to explain the variable phenomenon which seems to be ubiquitous. The proposed phenomena which should be related to variations were multiple supernovae and starburst activity in the vicinity of the nucleus (Terlevich et al. 1992; Aretxaga & Terlevich 1994), stellar collisions (Torricelli-Ciamponi et al. 2000) or gravitational microlensing by small compact objects passing along the line of sight (Hawkins 1993). Several studies also found that on the long time scales (> 100 days), the variations are likely to be the result of changes in the accretion rate (Wold et al. 2007; Li & Cao 2008; Arévalo et al. 2008; Wilhite et al. 2008). However the changes in accretion rate fail to explain shorter time scales variability. X-ray observations of the AGNs seem to be essential for explanation of the short time scale variability.

X-ray variability: X-ray emission is a common property of AGNs and much of the observed luminosity is in fact radiated in the X-ray domain (Elvis et al. 1978). X-ray flux shows some of the most rapid variations of the AGNs, which points out to the origin in a small region close to the central black hole. The variations in X-ray are rather large. Terrell (1986) reported X-ray variations of Cen A, which showed X-ray outbursts during a period of 10 days, where the changes of the intensity were of factor 2 or 3. Some of the most striking examples of large amplitude variability is found amongst Sy1 galaxies. For example source IRAS 13224-3809 exhibited five significant flares in a 30 day observing campaign (Boller et al. 1997). It was also noted that X-ray variability is more prominent in the soft X-rays (below 5 keV) than in hard X-rays (Nandra et al. 1997; Turner et al. 1999; Markowitz & Edelson 2001). The variations in X-ray are connected with the fundamental energy mechanism.

In comparison with time scales of the UV/optical observations, variations in X-rays are more rapid. The mentioned source IRAS 13224-3809 (Boller et al. 1997) shows a factor 2 variations in 20 minutes. In order to interpret these rapid changes in the work frame of AGN, we have to assume that the central black hole is rotating. Following this assumption, the emission has to be relativistically boosted (Boller & Brandt 1999).

As well as in optical / UV wavelengths, there is an effort to link the variability to the measured properties of the AGNs. Uttley & McHardy (2001) discovered the linear relation between the X-ray variability and the flux level of the stellar black hole Cyg X-1 and the accreting millisecond pulsar SAX J1808.4-3658. In the study, the authors suggested similar relation for AGNs. Gaskell (2004) showed that the linear relation between X-ray flux and X-ray variability indeed holds even for AGNs.

Gamma rays variability: the extragalactic sky in gamma rays is dominated by AGNs. The dominating targets are blazars and optically violently variable objects. It was reported by Thompson et al. (1995) that blazars emit enormous amounts of energy and are highly variable in GeV gamma rays. The vast majority of blazars are strongly variable in time scales of months (Hartman et al. 1996). There are cases when rapid variations are reported (3C 279 Kniffen et al. 1993). One of the most prominent variations occurred in PKS 1622-297 (Mattox et al. 1995; Mattox & Wagner 1996) which brightened by a factor of 10 in two days. Another extreme case is Mrk 421, which emits even in TeV energies and changes by a factor of 10 within one day (Kerrick et al. 1995) and by a factor 5 on a time scale of 30 minutes (Gaidos et al. 1996).

The gamma ray emission is of non-thermal nature, implying that the origin of the emission lies most likely in the jets, which in the case of blazars, are pointed roughly towards the observer (Urry & Padovani 1995). The emission is Doppler boosted in intensity as well as in frequency, overpowering any other emission source in these wavelengths. The variations / flaring observed in the AGNs in gamma ray domain therefore most likely originates in the jet. As well as in the case of X-ray observations, the spectrum flattens during the brightening periods of the source (Xue et al. 2006; Krennrich et al. 2002). Nevertheless the mechanism behind the flaring is not known. The theories include internal shock in the jets (Rees 1978; Spada et al. 2001), major ejection of new components of relativistic plasma into the jet (Boettcher & Schlickeiser 1997; Mastichiadis & Kirk 1997) or to magnetic reconnection events (Lyutikov 2003).

Radio variability: in radio wavelengths, AGNs are divided in radio loud and radio quiet sources. The major difference between the two groups is an open question. Ulrich et al. (1997) suggest that the major difference lies in jet collimation. The radio loud sources' jets are collimated while the well collimated jets are missing in radio quiet sources. Another explanation lies in differences in spin of the black hole (Sikora et al. 2007) or differences in the viewing angle (Kellermann et al. 1989). Radio wavelengths variability range from long time scales (years, Hovatta et al. 2007) to short variations within tens of minutes in blazars (Schödel et al. 2007; Kim & Trippe 2013).

There is a connection between the variations in gamma ray and in radio domain (Valtaoja & Terasranta 1995; Kovalev et al. 2009). The temporal association between the gamma rays and radio

pointed out to the conclusion that the shocks in the jet, observed in radio, are also responsible for the gamma ray emission (Valtaoja & Teraesranta 1996).

1.3.2 Emission line variability

AGNs are variable not only in continuum, but also in the emission lines. The first observation of emission line variations were reported by Andrillat & Souffrin (1968) in the Seyfert 1 galaxy NGC 3516. The spectral variationsappear in both, narrow and, more prominently, broad lines. The broad lines are variable, not only in terms of intensity, but also in the profile. The profile variations led to the assumption that there has to be a connection between the variations and inhomogeneities propagating through the BLR. Therefore by characterizing the emission line response to the continuum variations must provide constraints on the kinematics and geometry of the BLR (Bahcall et al. 1972; Blandford & McKee 1982; Antokhin & Bochkarev 1983; Capriotti et al. 1982; Fabrika 1980).

Some of the most important results from the studies of variations of emission lines include the stratification of the medium; amongst the highly ionized lines, the higher ionization there is, the shorter delays and larger amplitudes (e.g. Krolik et al. 1991; Dietrich et al. 1993; Wamsteker et al. 1990). The general picture is that of a stratified highly ionized BLR with the most highly ionized and fastest moving gas closest to the center and the degree of ionization and velocity of the gas decreasing outwards.

The stratification is also detectable in the Balmer line emission region. The line wings vary faster than the core and the higher Balmer lines vary with larger amplitudes and shorter time delays than the lower ones (Kollatschny & Dietrich 1996; Shapovalova et al. 2004; Dietrich et al. 2012).

Some large variations of the Balmer decrement are associated with variations of the spectral shape of the optical continuum on the long time scale (5 – 10 years) and are consistent with transient, strong and variable dust extinction, possibly caused by clouds (Villar-Martin 1996) located in the narrow line region.

1.3.3 Microvariability

The discovery of rapid variations lead to important constraints regarding the anatomy of the AGN. Short time scales imply that the source of the varying emission must be of order of light days, in order to preserve causality arguments. Microvariability helps to constrain the size of the variable region and thus the power engine. If the region is as small as a few light-hours across, it cannot be powered by anything else but a black hole.

Microvariability in radio wavelengths: there are reports of intra day variability (microvariability) in radio wavelengths. Lovelace & Backer (1972) suggested to look for interstellar scintillation in 12 flat-spectrum radio sources (Condon & Backer 1975). The first hints of short term variability came from observations at 3.3 GHz with the 300 ft radio telescope (Heeschen 1982, 1984). The reported time scales were as short as 2 days due to technical constraints of the telescope. The work was followed up by Witzel et al. (1986), who reported observation of the flickering phenomenon (on an intra day basis) observed by 100 meter Effelsberg telescope. Quirrenbach et al. (1992) concluded that the flickering phenomenon is present in $\sim 20\%$ of flat-spectrum sources.

The origin of the intra-day variability in radio sources proved to be interstellar scintillation. As reported by Jauncey et al. (2003), the understanding of the intra-day variability is based on observations of three rapidly variable sources, PKS 0405-385 (Kedziora-Chudczer et al. 1997), PKS 1257-326 (Bignall et al. 2003) and J1819+3845 (Dennett-Thorpe & de Bruyn 2000). The interstellar scintillation is supported by detection of patterns in time delays. Moreover the variability characteristics repeat in an annual cycle. As an example, Kedziora-Chudczer et al. (1997) reports

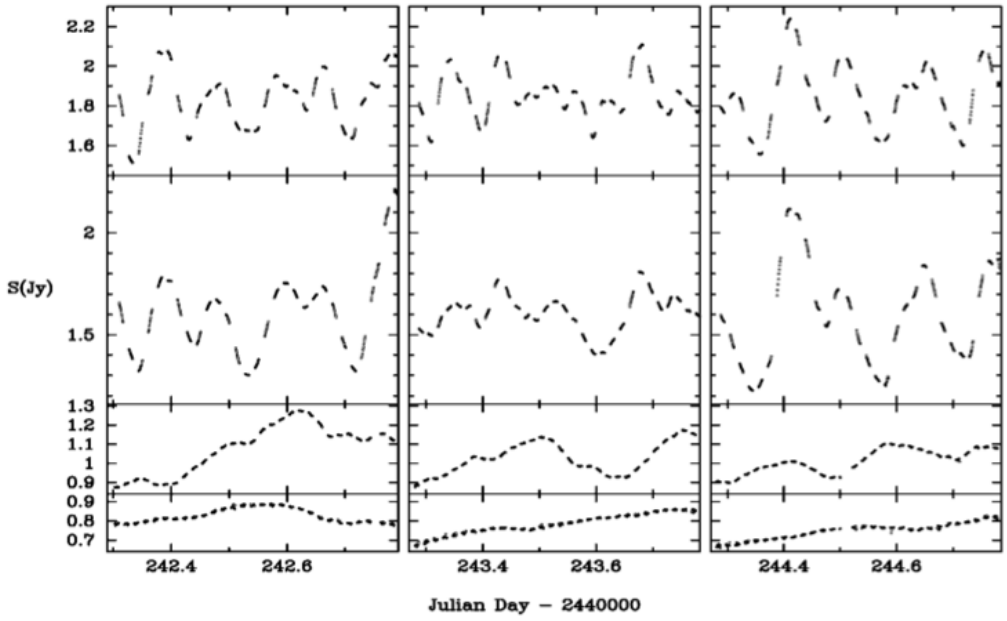

Figure 1.9: The 12 hours long observing cycle of PKS 0405-385 between June 8 - 10, 1996 at four frequencies: 8.6 GHz, 4.8 GHz, 2.4 GHz and 1.4 GHz from top to bottom, respectively. Adapted from Kedziora-Chudczer et al. (1997).

observations of quasi periodic observations and correlations between the variations at 4.8 and 8.6 GHz, which breaks down at 2.4 and 1.4 GHz in PKS 0405-385 as can be seen in Figure 1.9.

The annual cycle provided to be a confirmation that the microvariations in radio wavelengths comes from the movement of the Earth in the interstellar medium. During part of the year, Earth moves with the interstellar medium irregularities and the scintillation pattern changes only very slowly, while when the Earth moves in the opposite direction, the relative speed rises and the scintillation pattern changes more rapidly. Jauncey et al. (2003) reports year long monitoring program with the ACTA on 8.6 GHz and 4.8 GHz which directly showed the change in the annual cycle as can be seen in Figure 1.10.

Optical microvariability: the first reports of short time variations of small amplitudes (microvariability) in the AGNs can be found in Matthews & Sandage (1963) who observed 0.04 mag change in the quasar 3C 48 in 15 minutes. However the detection of such small variations was hard to believe at the time as the amplitude of the variation was at the detection border and could have been mistaken for an error of the observation. The crucial development came with the introduction of the CCD cameras, which showed that microvariability is a phenomenon common in blazars (Kinman 1975). The discovery prompted studies which furthermore established microvariability as a common phenomenon in the infrared wavelengths (Lorenzetti et al. 1990; Takalo et al. 1992; Kidger et al. 1992, 1994; de Diego et al. 1997).

Microvariability was detected not only in blazars, but soon after also in many radio loud AGNs (Wagner & Witzel 1995). On the other hand, detection of the same phenomenon in the radio quiet sources was initially elusive. Some of the first detections of microvariability in radio quiet sources were reported by Jang & Miller (1997). It was later showed by de Diego et al. (1998); Ramírez et al. (2009) that there is no difference in frequency of detection of microvariations in radio

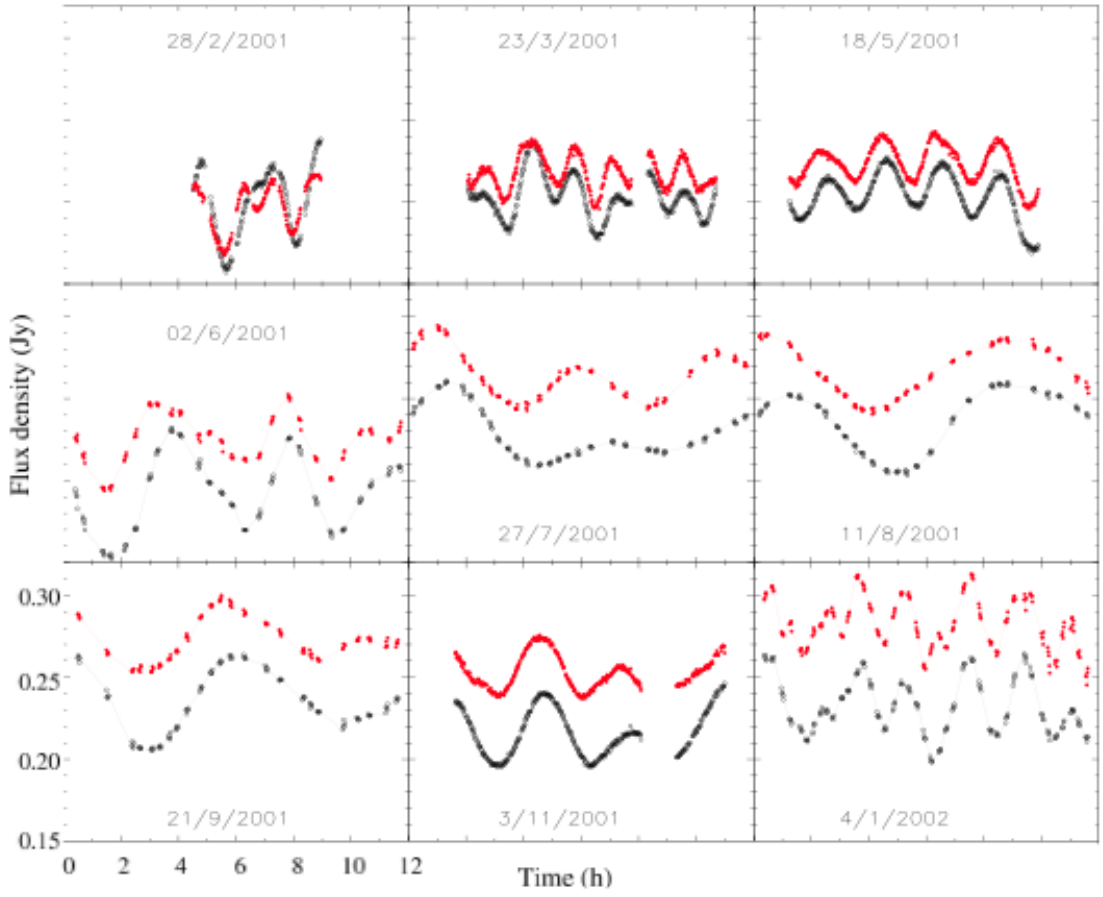

Figure 1.10: The year cycle of PKS 1257-326. The plots have the same scale, 4.8 GHz data are plotted in black, while the 8.6 GHz data are in red. Adapted from Bignall et al. (2003).

quiet quasars and core-dominated radio loud quasars at the experiment resolution level. The result was unexpected as another class of radio loud sources, blazars, is known to be very variable. It was therefore believed that the variability originates in the jet. However for non-blazar radio loud sources, the microvariations are similar to radio quiet objects. Ramírez et al. (2010) argues that the microvariations can be attributed to the disk and the optical jet in both cases.

The origin of the optical microvariability is a matter of dispute. The possibility of the extrinsic microvariability origin was explored in the terms of an intervening galaxy or in the host galaxy, causing a transient microlensing effect (Chang & Refsdal 1979; Jaunsen et al. 1995), enhancing the quasar brightness. In the case of intrinsic origin, there are several competing suggestions of origin. Miller & Wiita (1992) has suggested that the major part of the emission in radio loud AGNs originates in the relativistic jet. Of the proposed models for the microvariability origin, as an example, Blandford & Königl (1979); Marscher (1992) suggested shocks propagating through the jet, Marscher et al. (1992) proposed jet turbulences, Qian et al. (1991) attributed microvariability to light-echo effects and Gopal-Krishna & Wiita (1992) proposed changes in the direction of the jet. All of the mechanisms mentioned can be enhanced by relativistic effects. On the other hand, radio quiet sources are believed to not have a strong relativistic jet (Antonucci et al. 1990; Miller et al. 1993; Kellermann et al. 1994). Nevertheless detection of microvariability in radio quiet AGNs suggests that different mechanisms might be responsible. The majority of works have concentrated on different kinds of instabilities in the innermost part of the accretion disc (Pringle et al. 1973; Lightman & Eardley 1974) which might produce clumpy structure (Day et al. 1990; George & Fabian 1991), that could further result in rapid flux variability through the relativistic motion of the clumpy medium and Doppler beaming (e.g. Abramowicz et al. 1991; Bao & Abramowicz 1996).

Other physical processes might imply rapid variable behavior, such as coronal magnetic flares (Chagelishvili et al. 1989; de Vries & Kuijpers 1992), vortices (Abramowicz et al. 1992), shock in the discs produced by tidal effects (Chakrabarti & Wiita 1993) or oscillations in the shock region (Chakrabarti & Titarchuk 1995). All of the mentioned are in principle able to produce short time variations with small amplitudes in both, radio quiet and radio loud AGNs.

1.3.4 Variability techniques

1.3.4.1 Reverberation mapping

It was established that the emission lines and the continuum variations are strongly correlated (e.g. Pogge & Peterson 1992). An increase of the luminosity in the BLR emission lines follows the increase of the luminosity of the continuum. The time lag between the emission line and continuum variations provides a simple estimate of the size of the BLR. The input signal for the reverberation is generated by the central continuum source, of the size of 10 - 100 gravitational radii in diameter. The response is a Doppler-shifted signal. There are several assumptions underlying the technique:

1. The continuum originates in a single central source. The size of the accretion disc is of the order of 10^{13-14} cm. The emission does not have to be isotropic.

2. The most important time scale is the light-travel time $\tau_{LT} = r/c$, which for luminous Seyfert galaxies ranges from days to weeks. Other time scale of a significant importance is the rapidity of the response of the individual clouds; the recombination time scale, which is the time for emission-line gas to re-establish photoionization. The typical time scale for a typical density of the medium is 1 hour or less. The dynamical time scale for the BLR gas is another important time scale, where $\tau_{dyn} \propto r/\Delta V$. For luminous Seyferts, this time scale is 3-5 years. Reverberation experiment should be kept shorter than this time scale to avoid smearing the light travel-time effects.

3. The relationship between the observed continuum (or UV) and the ionizing continuum, which drives the emission-line variation, is established. It is not necessarily linear. The observed

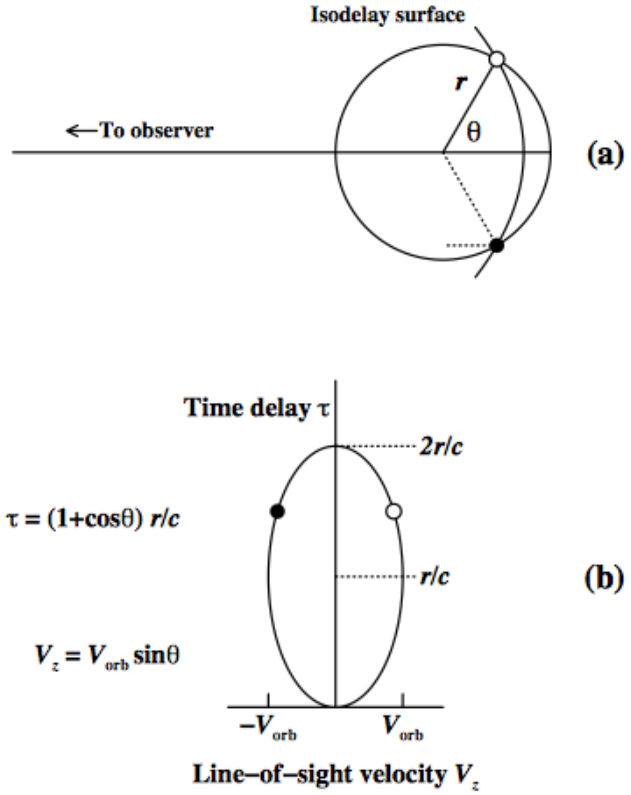

Figure 1.11: Diagrams demonstrating the reverberation mapping technique. The upper diagram pictures a ring containing emission-line clouds at a distance r from the central supermassive black hole. In response to an outburst from the central engine, the clouds seen by the distant observer at a time delay τ after detection of the continuum outburst will be those that lie along an isodelay surface, for which the time delay relative to the continuum signal will be $\tau = (1 + \cos\Theta)r/c$, the length of the dotted path shown. The lower diagram shows the circular orbit mapped into the line-of-sight velocity/time-delay plane. Adapted from Peterson (2001).

continuum must vary in phase with the ionizing continuum, driving the variations.

There are two observables which need to enter the reverberation mapping experiment, a continuum light curve, $L_c(t)$ and an emission line light curve $L_l(t)$. The aim of reverberation mapping is to find the relation between the two quantities. The standard method for doing so is via a transfer function. The basic equation is

$$L_l(v,t) = \int_{-\infty}^{\infty} \psi(v,\tau) L_c(t-\tau) d\tau, \tag{1.4}$$

where $\psi(v,\tau)$ is the transfer function, which depends on the BLR geometry, kinematics and properties of the gas reprocessing the continuum variations. The function is often called "velocity-delay map", the BLR responsivity mapped into the line of sight velocity/time-delay space.

To illustrate a simple example, let's consider edge-on ring of clouds in circular Keplerian orbits. Looking at Figures 1.11, we can generalize to radially extended geometry: a disc is a system of rings with different radii and a spherical shell is a system of rings with different inclinations, as seen in Figure 1.12. While inner orbits have a larger velocity range, they have shorter time delays and vice

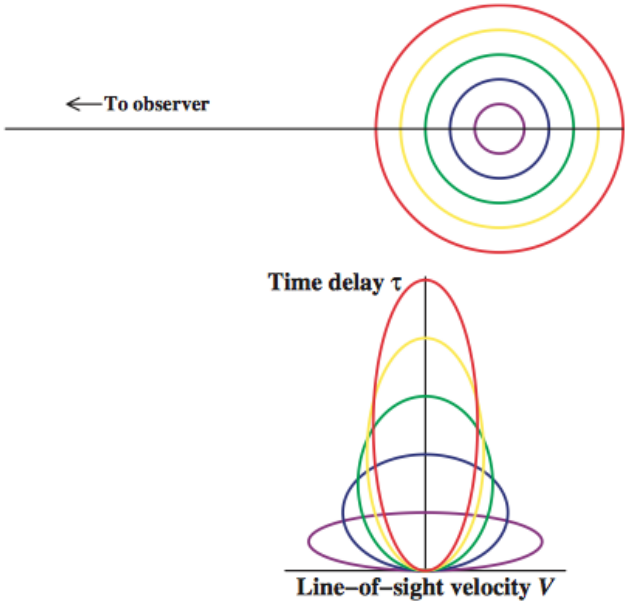

Figure 1.12: Demonstration of circular Keplerian orbits of different radii, mapped into the velocity-time delay plane. Inner orbits have a larger velocity range ($v \propto r^{-1/2}$) and shorter range of time delay ($\tau_{max} = 2r/c$), resulting in tapering of the map in velocity with increasing time delay, a general feature of gravitationally dominated systems. Adapted from Peterson (2006).

versa for the outer shells. This results in a typical "taper" in the velocity-delay map with increasing time delay.

In an ideal case, the two observables, the emission line light curve and the continuum light curve are observables sufficient to obtain the invert of the transfer equation and therefore recover the velocity-delay map $\psi(v, \tau)$.

The products of reverberation mapping campaigns are in a greater overview three: black hole masses, black hole scaling relationships and BLR geometry and kinematics. Below, the basic ideas behind obtaining results from the reverberation campaigns are described.

Black hole masses: the black hole mass can be derived under the assumption that the photoionized BLR gas motions are determined by the gravity and not by the radiation pressure. These conditions are probably not met by all of the emission lines, but most likely, they are satisfied for Hβ (e.g. Netzer 2009; Netzer & Marziani 2010). The most up to date catalog of black hole masses derived from reverberation mapping is Bentz & Katz (2015).

Black hole scaling relationships: there is a relationship between the time delay, and the luminosity of the central AGN at some particular wavelength (see Figure 1.13). The scaling relationship is expected from a simple photoionization argument. The power of the relation lies on the fact that instead of long term monitoring campaign, one can rely on the single spectra to estimate black hole mass. One of the most recent results in estimating the relationship is in Bentz et al. (2013).

BLR geometry and kinematics: in order to get more informations about the geometry and kinematics, one needs to solve transfer equation 1.4. This was almost impossible during the first campaigns. Resolving the time delays as a function of velocity across an emission line profile can give us constraints on the detailed geometry and kinematics of the BLR. Nevertheless obtaining

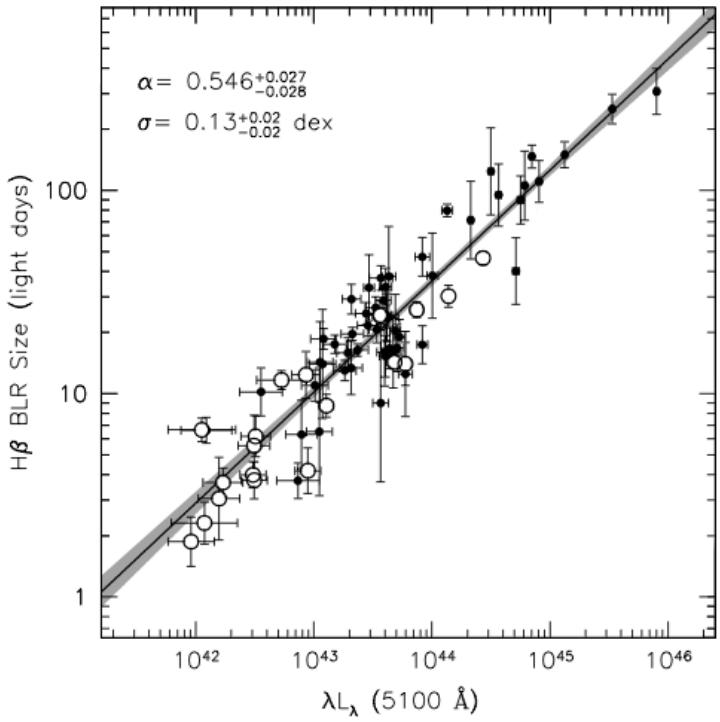

Figure 1.13: Black hole scaling relationships: the relationship between the Hβ time delay and the specific luminosity of the AGN at 5100 Å. Adapted from Bentz et al. (2013).

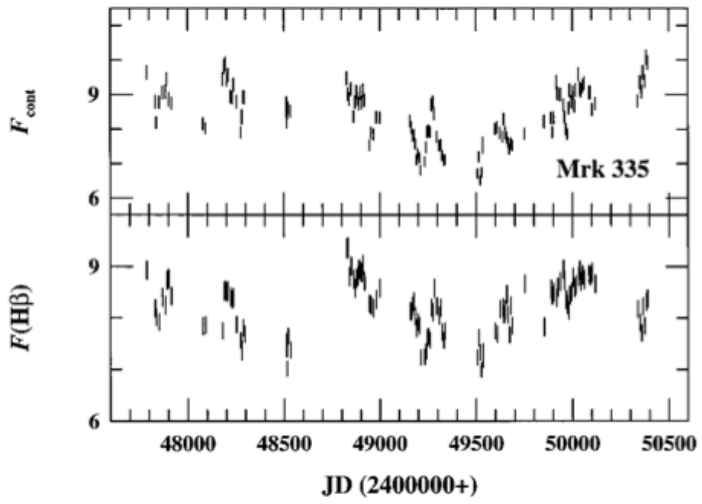

Figure 1.14: Light curves for Mrk 335. Upper panel shows continuum, centered at 5100 Å in the rest frame of the source, in units of 10^{-15} erg s^{-1} cm^{-2} Å^{-1}. Lower panel is the emission in Hβ in units of 10^{13} ergs s^{-1} cm^{-2}. The correlation is obvious in these light curves, nevertheless there is a shift of 15.6 days which significantly improve the linear correlation. Adapted from Peterson et al. (1998).

such information requires densely populated light curves.

1.3.4.2 Cross-Correlation Analysis

Cross-correlation analysis is mostly used in the cases where there are multiple time series available. The general task is to find out if two variable phenomena are correlated or not. Aside from actual correlation, by plotting both data sets against the time, one can see similarity (or lack of) in the profiles in the light curves, as seen in Figure 1.14. As a working example, one can imagine analyzing whether the variability of broad spectral lines is correlated with the variability of the continuum. The strength of the correlation is then given by the correlation coefficient

$$r = \frac{\sum_{i=1}^{N}(x_i - \bar{x})(y_i - \bar{y})}{\left(\sqrt{\sum_{i=1}^{N}(x_i - \bar{x})^2}\right)\left(\sqrt{\sum_{i=1}^{N}(y_i - \bar{y})^2}\right)}, \tag{1.5}$$

where there are N pairs of the values (x_i, y_i) and barred values are their means. Perfectly correlated values yield $r = 1$ and anticorrelated $r = -1$. Cross-correlation function is a set of correlation coefficients giving a measure of the correlation between the line and continuum light curves for certain time lags.

Figure 1.14 shows the two lightcurves entering our working example. Cross-correlation analysis requires that each point (from the upper light curve) is paired with a point in the other (lower) light curve. The cross-correlation is evaluated as a function of spacing between the data points δt using the pairs $[x(t_i), y(t_i + N\delta t)]$ for all integers N. In ideal case, the data are equally spaced. However there are only few real cases where the data are spaced so ideally. The simplest solution to that is an interpolation of the data. The interpolated data are then used to compute the cross-correlation function, CCF(τ). The correlation coefficient r is computed for every value of time lag τ. In principle, we are looking for the maximum of the correlation coefficient. Shifting the lagged data by a constant then increases the value of the correlation coefficient. For the data of Mrk 335

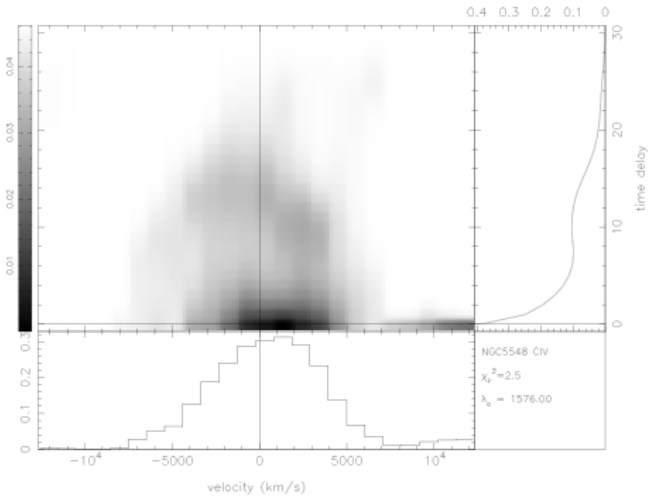

Figure 1.15: A transfer function for C IV λ1549 in NGC 5548. Observations obtained with Hubble Space Telescope over the course of 39 days. Plot adapted from Peterson (2001) .

from Peterson et al. (1998), such maximal value was 15.6 days. Another example of lag estimation is NGC 5548 (Peterson et al. 2002), where the lag varied between 6 and 26 days over a campaign lasting several years.

However even the interpolation might not solve the uneven distribution of the observation. An alternative to interpolating the data, one can use discrete correlation function (DCF Edelson & Krolik 1988). DCF binns the unevenly sampled data, so in contrast with the CCF(τ), where the contributing points are separated in time by an exact interval τ, we bin the data by pairing points with time separation in the range $\tau \pm \delta\tau/2$, where $\delta\tau$ represents width of the bin. The number of points in the bin might wary significantly and sometimes results in the underutilization of some data.

One of the challenges of the cross-correlation analysis is the estimation of uncertainities (Peterson et al. 1998; Shapovalova et al. 2012). Peterson et al. (1998) proposed a model independent Monte-Carlo method, which is used till present days (e.g. Peterson et al. 2013; Goad et al. 2016).

Time lags computed from the cross-correlation are then used to obtain transfer functions as the CCF relates to the transfer function as

$$CCF(\tau) = \int_{-\infty}^{\infty} L(t)C(t-\tau)dt \tag{1.6}$$

$$= \int_{-\infty}^{\infty} C(t-\tau)\int_{-\infty}^{\infty} \psi(\tau')C(t-\tau')d\tau'dt \tag{1.7}$$

$$= \int_{-\infty}^{\infty} \psi(\tau')\int_{-\infty}^{\infty} C(t-\tau')C(t-\tau)dtd\tau'. \tag{1.8}$$

Nevertheless the results can be ambiguous. As an example, the data in Figure 1.15 have been studied extensively in many works (e.g. Bottorff et al. 1997; Done & Krolik 1996; Wanders et al. 1995) without reaching a consensus on the results.

1.3.5 Multiwavelength variability

Multiwavelength or multi-frequency studies play a pivotal role especially, but not only, in observations of blazars as they are strong sources through the whole electromagnetic spectrum. Such observations naturally require a lot of resources. Aleksić et al. (2014) and Carnerero et al. (2015) are excellent examples of studies covering the electromagnetic spectrum from radio wavelengths all the way to very high energies observed by Cherenkov telescopes such as MAGIC (see for example Figure 1.16. The product of such studies is a multiwavelength light curve, which provides excellent constraints to the underlying physics. Carnerero et al. (2015) performed a cross-correlation analysis on the multiwavelength light curve of blazar OJ 248, discovering a complex radio - optical correlation and a delay of the optical variations after the gamma ray ones of about a month.

Apart from the cross-correlation analysis, multiwavelengths studies are extremely helpful for obtaining the SED of the sources, which provide another constraint to an underlying physical model. Carnerero et al. (2015) shows the change in SED of OJ 287 during three epochs with different brightness states (see Figure 1.17). Red curve corresponds to the peak of gamma-ray emission, black to the peak of X-ray emission and blue to the post burst epoch. Optical-UV emission, receiving contribution from the accretion disc radiation, is more evident in the post-burst SED.

Another great example of multiwavelength study of AGNs, is AGN watch project (Peterson 1999). The project was focused on obtaining multiwavelength light curves of Seyfert 1 galaxies. One of the conclusions of AGN watch is absence of time lag between the variations in the UV and optical, up until a precision of $\sim$ 1 day. Such observation goes against the assumption that the instabilities in the accretion disc propagate through the medium surrounding the central engine as the lag for that should be much longer than 1 day. There are indications that the UV and optical variations are rather driven by the area where the X-rays are emitted.

The models suggest that the fast X-ray variations are consistent with the reprocessing models built to explain the equivalent width of 6.4 keV Fe Kα line (e. g. Lightman & White 1988; George & Fabian 1991). It assumes that the thin accretion disc is irradiated by an X-ray source along the disc axis. In theory, the inner parts of the disc should respond at different times than the outer parts, which are cooler. Since the temperature is directly connected to the wavelengths through Wien's law ($\lambda \approx T^{-1} \approx r^{3/4}$), this results in wavelength dependent lags.

One of the successful campaigns dedicated to wavelength dependent lags measure was the observation of NGC 7496 (e. g. Wanders et al. 1997; Kriss et al. 2000), which was quite unique as the sampling rate was superior to any other observations and therefore it is hard to connect the positive results with other cases. Some marginal presence of a similar result was detected in (Peterson et al. 1998). Unfortunately there are not many targets which were observed densely enough to claim a universal phenomenological model, based on multi wavelength observations.

1.4 Statististics

The variations of AGNs can reach significant amplitudes over long time periods. However once the observer searches for photometric variations on a shorter time scales, the amplitude of the variations decreases and it becomes harder to detect by simple methods. The first reports of short time variations of 15 minutes in 3C 48 (type I quasar) (Matthews & Sandage 1963) were reported shortly after the discovery of quasars. The reported magnitude change was $\Delta mag_{\mathrm{v}} = 0.044$. Nevertheless due to the inaccessibility of a linear detecting medium, such reports were received with skepticism. The situation changed with the introduction of Charged Couples Device - CCD into astronomy. CCDs are linear mediums which allows us precise measurements which offer robust results, as long as instrumental effects are properly accounted for.

The common approach to study variability is to compare the differential light curve of the target with the differential curve of a non-variable star in the field. In the case of small variations, one must employ statistical methods to detect variations in the light curve of the target. In order to

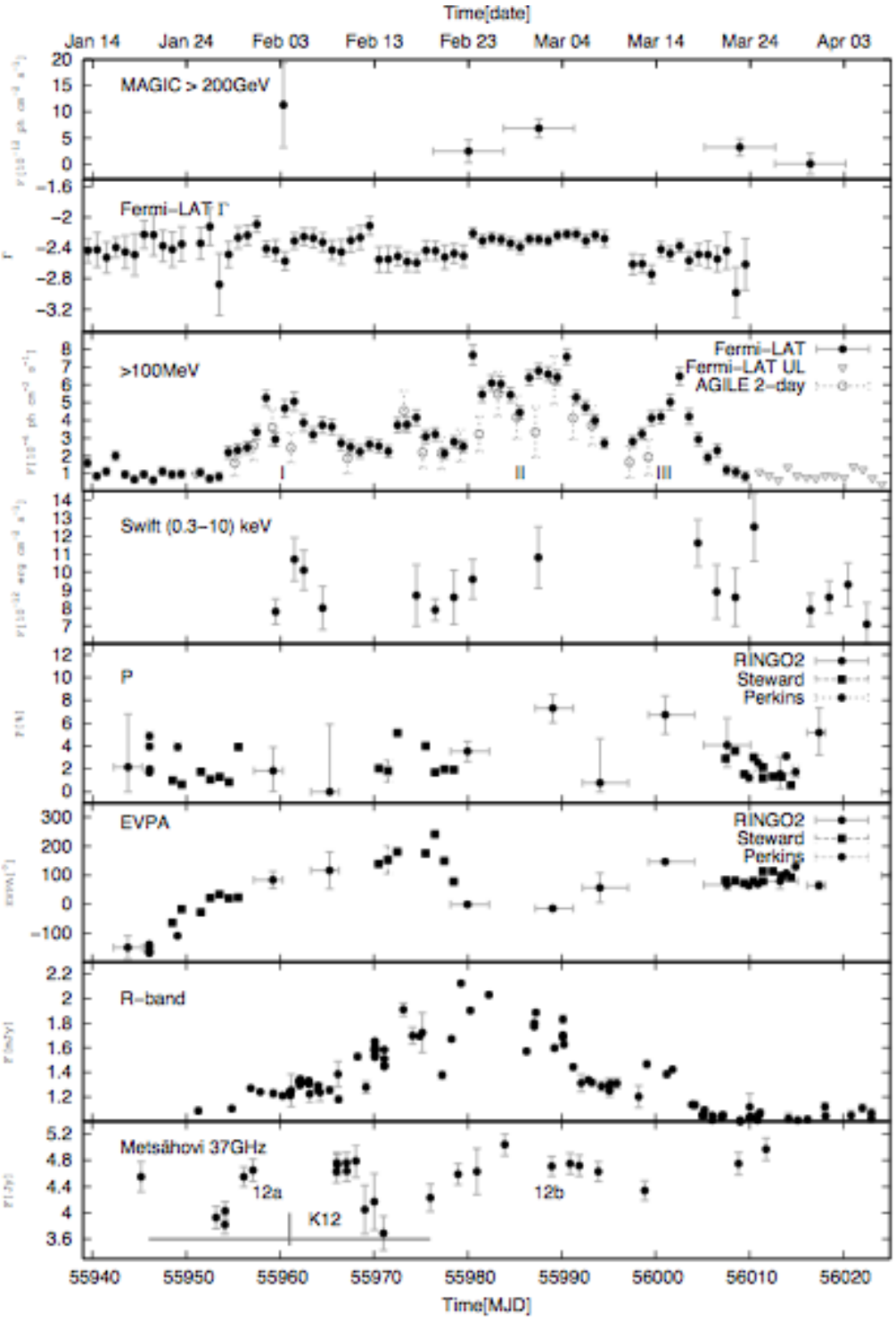

Figure 1.16: Multi-frequency light curve of blazar PKS 1510-089 from very high energies to radio, observed between February and April 2012. From upper panel down: ultra high energy observation, Fermi observations, Fermi and AGILE observations, Swift observations, polarization angle, electric vector position angle, optical observations in R band and radio observations on 37 GHz with marked outbursts (12a and 12b) and with marked new component K12, with an apparent speed of (16.23 ± 2.43)c. Plot adapted from Aleksić et al. (2014).

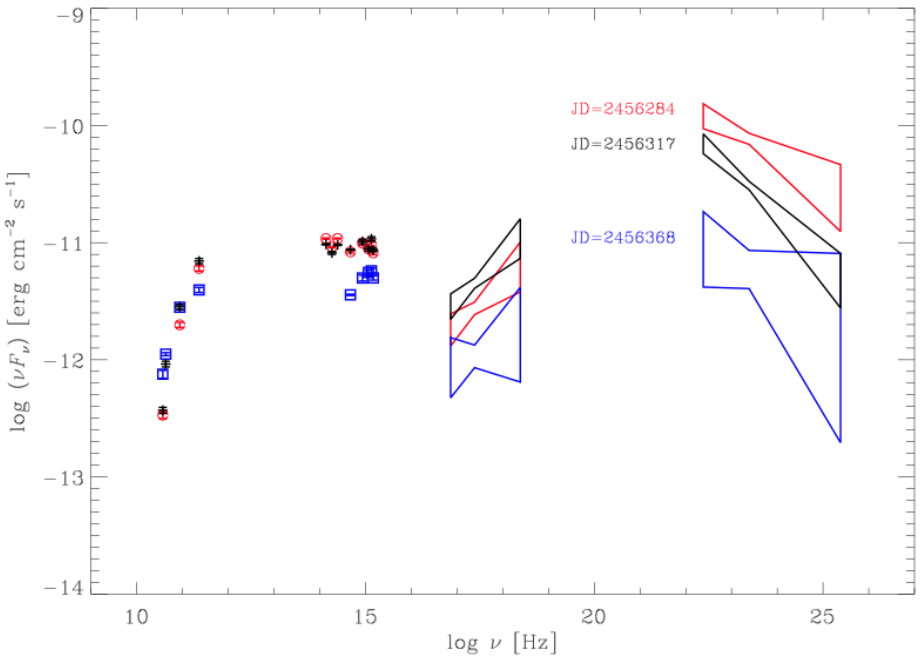

Figure 1.17: SED of OJ 248 from the radio to gamma ray frequencies during three epochs of different brightness. The radio data have smoother variability and hence are given a tolerance of few days. Plot adapted from Carnerero et al. (2015).

understand the statistical tests employed in the search for variations, it is needed to understand the statistical distributions as the assumption of normality is one of the basic ones to employ in the statistical testing.

1.4.1 Statistical distributions

1.4.1.1 Normal distribution and central limit theorem

The univariate (Gaussian) normal distribution has a form

$$P(X) = \frac{1}{\sigma\sqrt{2\pi}} exp\left[-\frac{1}{2\sigma^2}(X-\mu)^2\right], \tag{1.9}$$

where x is the variable with a mean μ and variance σ^2. The major importance of the normal distribution lies in the central limit theorem:

Let $\{X_1, \ldots X_n\}$ be a set of N independent random variates and each X_i have an arbitrary probability distribution $P(x_1, ..., x_N)$ with mean μ_i and a finite variance σ_i^2. Then the normal form variate

$$X_{norm} \equiv \frac{\sum_{i=1}^{N} x_i - \sum_{i=1}^{N} \mu_i}{\sqrt{\sum_{i=1}^{N} \sigma_i^2}} \tag{1.10}$$

has a limiting cumulative distribution function which approaches a normal distribution.

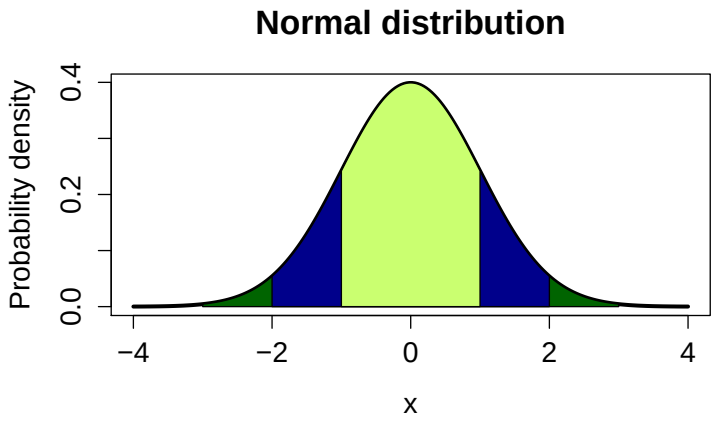

Figure 1.18: Normal (Gaussian) distribution $X \sim N(0,1)$. The total area under the curve is 1.0; the area between $\pm 1\sigma$ is 0.68 (light green), between $\pm 2\sigma$ is 0.95 (dark blue), and between $\pm 3\sigma$ 0.997 (green).

In other words, provided that the conditions are met, which in the majority of physical situation holds (as in majority of physical situations, we assume that the process is made up from many independent events), no matter what is the underlying distribution, averaging will produce a normal distribution. Therefore errors on averaged samples will always look Gaussian.

If a random variable X follows the normal distribution, we write

$$X \sim N(\mu, \sigma^2). \tag{1.11}$$

To interpret the "bell-shaped" function in the astronomical context, one can illustrate the chances of occurrence of the results, as illustrated in Figure 1.18. Given a range of 3σ, there's less than 1% probability that the result occurred just by chance.

1.4.1.2 Poisson distribution

The binomial distribution describes the distribution of two outcomes: success and failure.The Poisson distribution is a limiting case of the binomial distribution for very small number of success in a large number or trials. Therefore for

$$P(X=k)_{binomial} = \binom{N}{k} p^k (1-p)^{(N-k)} \xrightarrow{p\to 0, N\to\infty, Np\to\lambda} \frac{\lambda^k}{k!} e^{-\lambda} = P(X=k)_{Poisson}, \tag{1.12}$$

where N is the number of the trials, probability of success is p and k is the number of successes. The positive real number λ is equal to the expected value of X and also to its variance.

The Poisson distribution realistically captures the process of photons arriving onto the CCD during an integration. During the integration time, there is only a small amount of photon reaching the CCD (low number of successes). Therefore photons arriving at a rate x has a mean value of $\mu = xt$, fluctuating around $\sigma = \sqrt{\mu}$. If we increase the integration time, we eventually arrive at $\sigma \propto \sqrt{t}$ and signal $\propto t$. This leads us to the well used estimations of the signal - to - noise ratio. In the case of bright sources; $S/N \propto \sqrt{t}$, for sky-dominated (bright sky, faint source), $S/N \propto \sqrt{t/n_{pix}}$ where n_{pix} is the number of pixels. For read-out dominated (faint source, small background and dark), $S/N \propto 1/\sqrt{n_{pix}}$ and directly proportional to exposure time, so $S/N \propto t/\sqrt{n_{pix}}$.

For a large N, both distributions, binomial and Poisson converge to the normal distribution. Therefore the assumption of normality (essential for the statistical procedures used through the work) holds.

1.4.1.3 Lognormal distribution

The use of the lognormal distribution in astronomy comes naturally from the fact that the magnitude system is a logarithmic measurement of the optical brightness. Therefore the measurements are distributed lognormally rather than normally. The lognormal distribution is the probability distribution of a random variable whose logarithm is normally distributed. The probability density function in this case is

$$P(x) = \frac{1}{\sigma\sqrt{2\pi}} exp\left[-\frac{1}{2\sigma^2}(\ln X - \mu)^2\right], \tag{1.13}$$

which relates through the logarithmic transformation to the normal distribution (equation 1.11).

1.4.2 Statistical tests

Statistical hypothesis tests are a powerful tool when it comes to analyzing the light curves with differential photometry. Statistical hypothesis testing is a method of inference used for testing a statistical hypothesis H. The default position is the null hypothesis H_0, in the case of variability studies: H_0: the source is not variable. Null hypothesis is rejected for a level of significance given by a tester. If the null hypothesis is rejected, we can propose alternative hypothesis H_a. The robustness of the test is indicated by the occurrence of type I and type II errors. Type I errors occurs when the null hypothesis is incorrectly rejected while type II errors refer to the failure of rejecting a false null hypothesis. The hypotheses tests relevant to the presented work are discussed below.

1.4.2.1 χ^2 test for variances in a normal population

Kesteven et al. (1976) proposed a way to estimate the significance of the scatter of the magnitudes. Given a set of magnitudes m_i with an estimated standard error σ_i, we can compute the quantity

$$x^2 = \sum_{i=1}^{N} \frac{(m_i - \bar{m})^2}{\sigma_i^2}, \tag{1.14}$$

where

$$\bar{m} = \frac{\sum_{i=1}^{N} \frac{m_i}{\sigma_i^2}}{\sum_{i=1}^{N} \sigma_i^{-2}} \tag{1.15}$$

is the weighted mean magnitude, observed over the N observing period. For the case of random errors, x^2 should be distributed as χ^2 with $n-1$ degrees of freedom. Such approach was further used by Heidt & Wagner (e.g. 1996); Gopal-Krishna et al. (e.g. 2000); Andruchow et al. (e.g. 2005).

The possible problem of this approach lies in estimation of the σ_i. In this approach, it is the expected error, which arises from the photon noise of the source and the sky, the CCD readout noise and other non-systematic influences. But in practical cases, most of the influences are unknown in the quantitative sense (e.g. shutter timing errors in the case or very short exposures or sky gradients in CCD frames). Considering this, it is probable that the errors are underestimated. Therefore many authors who have used such test, proposed a multiplicative factor to account for this fact. For example, Bachev et al. (2005) uses a multiplicative factor of 1.3, Stalin et al. (2004) uses 1.5, Garcia et al. (1999) uses 1.73, etc.

The problem of correct error estimation is non-trivial. It is worth noting that this is affecting only the error estimation, not the measured brightness. Therefore the error effectively depends on the software used for its computation. To overcome such problem, the ideal solution is to estimate the error empirically. This sole problem undermines the reliability of χ^2 test for variability detection.

1.4.2.2 F-test and enhanced F-test

The F-test relies on the comparison between two sample variances. In general

$$F = \frac{s^2_{qso}}{s^2_{star}}, \tag{1.16}$$

where s^2_{qso} and s^2_{star} are the variances of the quasar and star light curve respectively. The number of degrees of freedom is ν_{qso} and ν_{star}, with respect to the number of measurements N, $\nu = N - 1$. The F-statistic is compared with the critical value $F^{(\alpha)}_{\nu_{qso},\nu_{star}}$ corresponding to the desired level of significance α.

The major caveat of such test lies in the fact that it is sensitive to non-normality. In other words, if the underlying distribution is not normal (or log-normal in the case of magnitudes), the test will not provide reliable results. Nevertheless a workaround was proposed by de Diego (2014) using many field stars, which increases the reliability of the test. It also deals with the changes proposed by Joshi et al. (2011), who incorporated scaling the photometrical error estimates in order to account for differences in brightness.

The proposal by de Diego (2014), based on simulations, takes into account the presence of other, likely non-variable stars in the field, observed along the quasars. Basically the strategy consists in increasing the number of degrees of freedom in the denominator of the F-distribution of reference for the null hypothesis with those field stars. For such procedure, we adopt the name 'enhanced F-test' through the work. The scaling enters this scheme in ideal case, all the stars accompanying the AGN in the field are of the same brightness. This requirement is of course not met in the real world. Following the approach by Howell et al. (1988) and Joshi et al. (2011), we introduce a scaling parameter ω to compensate for larger photometric errors of the dimmer objects. We can write:

$$s^2_{j,i} = \omega_j (m_{j,i} - \bar{m}_j)^2, \tag{1.17}$$

meaning that we are scaling the variance of $j-$th star to the level of the quasar q. By stacking all the variances $s_{i,j}$, we calculate the combined variance of the stars:

$$s^2_c = \frac{1}{(\sum_{j=1}^{k} N_j) - k} \sum_{j=1}^{k} \sum_{i=1}^{N_j} s^2_{i,j} \tag{1.18}$$

The combined variance is then directly compared with the variance of the light curve of the quasar. Resulting in the F statistic with $\mu_{qso} = N_q - 1$ degrees of freedom in the numerator and $\mu_{star} = (\sum_{j=1}^{k} N_j) - k$ degrees of freedom in denominator of equation 1.18. The increase of the number of degrees of freedom is the goal of the whole enhancement. Increasing the number of degrees of freedom, either in numerator or denominator yields an increase in the test power. In general, this means that the best way to achieve sensitive F-test is by having a well sampled light curve with a crowded field.

1.4.2.3 One-way analysis of variance - ANOVA and Nested ANOVA tests

The one-way analysis of variance (ANOVA hereafter) is a technique used to compare three or more samples. The null hypothesis of the ANOVA is that the samples in two or more groups are drawn

from populations with the same mean values. ANOVA is not sensitive to non-normality as no matter what the original distribution is, according to the central limit theorem, the sampling distribution of the mean converges to normal distribution. This fact makes ANOVA more robust than other statistical tests (in direct comparison with F-test for example). The mathematical description of the method follows a linear model describing every observation where $y_{i,j}$ is the i-th observation ($i = 1, 2 \dots n_j$) of the j-th group ($j = 1, 2 \dots k$), then

$$y_{i,j} = \bar{y} + g_j + \epsilon_{i,j}, \tag{1.19}$$

where $\bar{y}$ is the mean value of the whole dataset, $g_j = \bar{y_j} - \bar{y}$ is the deviation between groups and $\epsilon_{i,j} = y_{i,j} - \bar{y_j}$ is the deviation within the group (in other words, residual). The dataset contains $N = \sum_{j=1}^{k} n_j$ measurements, under the assumption that the number of the observations within the group is constant.

The total sample variation can be further described as a combination of variations between the groups and within the groups

$$\sum_{j=1}^{k}\sum_{i=1}^{n_j}(y_{i,j} - \bar{y})^2 = \sum_{j=1}^{k} n_j(\bar{y_j} - \bar{y})^2 + \sum_{j=1}^{k}\sum_{i=1}^{n_j}(y_{j,i} - \bar{y}_j)^2, \tag{1.20}$$

where the left side is the representation of the total variation. For the practical purposes, we can shorten the equation as

$$SS_T = SS_G + SS_R, \tag{1.21}$$

where index T marks the total sum of squares, index G and R stand for the sum of squares in the groups and residuals respectively. The samples are compared with a given level of significance α. If the samples have similar means (the null hypothesis cannot be rejected), then k groups of the data are normally distributed with mean μ and variance σ^2. Then we can write the F statistics

$$F = \frac{SS_G/(k-1)}{SS_R/(N-k)}. \tag{1.22}$$

with corresponding degrees of freedom $\nu_1 = k - 1$ and $\nu_2 = N - k$, where N is the number of observations. The null hypothesis is rejected when F exceeds the critical value for $F^{(\alpha)}_{\nu_1,\nu_2}$.

As well as in the case of the F-test, ANOVA can benefit from the presence of other stars in the field. The approach is called nested ANOVA and was developed by us. All bright stars in such case are used to build distinct differential light curves. The nested ANOVA studies the variances at the three different experimental levels. The levels being: the difference between the groups, which refers to proper variation of the source , the second level corresponds to the differences between the observations due to noise and sky subtraction and the third level corresponds to the variance between the tests caused by the different reference stars. The schema is described in Figure 1.19.

An example is provided in de Diego et al. (2015): assume a field which is observed 35 times. The observations can be divided into seven groups of five. The measured source is present in all the images along with field stars. Any given image is read n times (creating n pseudoreplicates), where the n is the number of the field stars. Hence we create $35n$ readings of the quasar differential photometry. As we use the same target in all images, the readings are not independent. An image is an experimental unit, therefore 35 images provide 34 degrees of freedom. We will loose six more degrees of freedom for every group of images. Hence in our experimental setting, we have $34-6 = 28$ degrees of freedom. Performing the replicate measurements on each image is improving the precision of the image.

Following the ANOVA notation, we can write the linear statistical model as (Montgomery 2013, chapter 14)

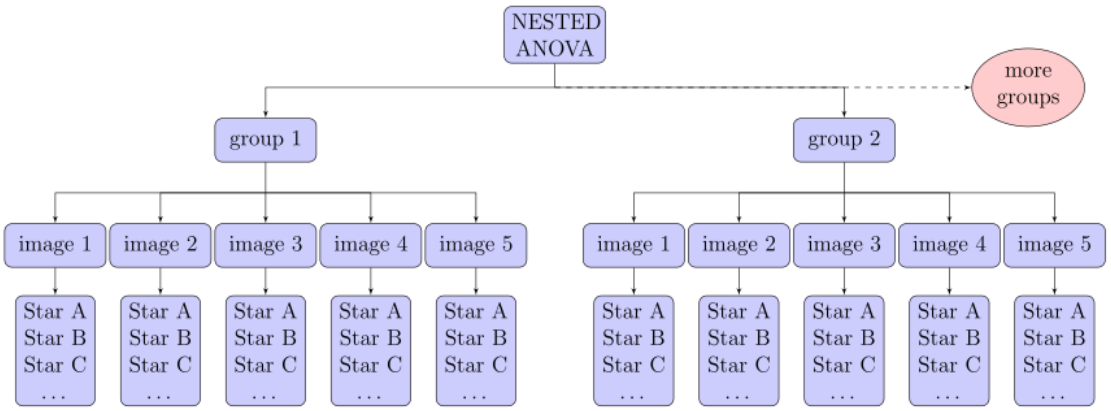

Figure 1.19: Nested ANOVA diagram. The final difference we are aiming for is the difference between the groups of the observations. In the presented scheme, each group contains five images (a scheme used in the observations). Adapted from de Diego et al. (2015).

$$y_{ijk} = \mu + \gamma_i + \omega_{j(i)} + \epsilon_{ijk} \tag{1.23}$$

where y_{ijk} corresponds to the measurement of the target's differential photometry using the reference stars indexed over $k = 1, 2, \ldots n$, located in the images $j = 1, 2, \ldots b$ of the $i = 1, 2, \ldots a$th group of observations. μ is the true mean and the deviation from the mean of the ith group is γ_i. Deviation on the jth image is in respect to the i th group is $\omega_{j(i)}$, where $j(i)$ denotes that the jth observation is nested under ith group. ϵ_{ijk} is the error term. If we follow the notation we have used above, for a simple one-way ANOVA, the sum of squares for the nested ANOVA is

$$\sum_{i=1}^{a}\sum_{j=1}^{b}\sum_{k=1}^{n}(y_{ijk} - \bar{y})^2 = bn\sum_{i=1}^{a}(\bar{y}_i - \bar{y})^2 + n\sum_{i=1}^{a}\sum_{j=1}^{b}(\bar{y}_{ij} - \bar{y}_i)^2 + \sum_{i=1}^{a}\sum_{j=1}^{b}\sum_{k=1}^{n}(y_{ijk} - \bar{y}_{ij})^2, \tag{1.24}$$

where the means are marked with the horizontal bars. As in the case of one-way ANOVA, we can write the symbolical equation

$$SS_T = SS_G + SS_{O(G)} + SS_E. \tag{1.25}$$

where SS_T is the total sum of squares, SS_G is sum of squares due to the groups, $SS_{O(G)}$ is the sum of squares due to the nested observations in groups and the SS_E are residuals. Considering the numbers of degrees of freedom for each of the square sums: $abn - 1$ for SS_T, $a - 1$ for SS_G, $a(b - 1)$ for $SS_{O(G)}$ and $ab(n - 1)$ for SS_E. Dividing the sum of squares by the respective degrees of freedom μ yields the mean square and such ratios are distributed as F.

Nested ANOVA as well as the enhanced F-test largely benefit from the increased number of degrees of freedom and are less prone to errors. A comparison is provided in Figure 1.20.

1.4.2.4 C-test

C-test is a parametric test which was proposed as a tool for search for variable behavior in the work of Jang & Miller (1997) and later was generalized by Romero et al. (1999). It is worth noting that the test is not a valid statistical procedure and therefore should be avoided (de Diego 2010). The test is included here purely as a historical note. The test parameter used is

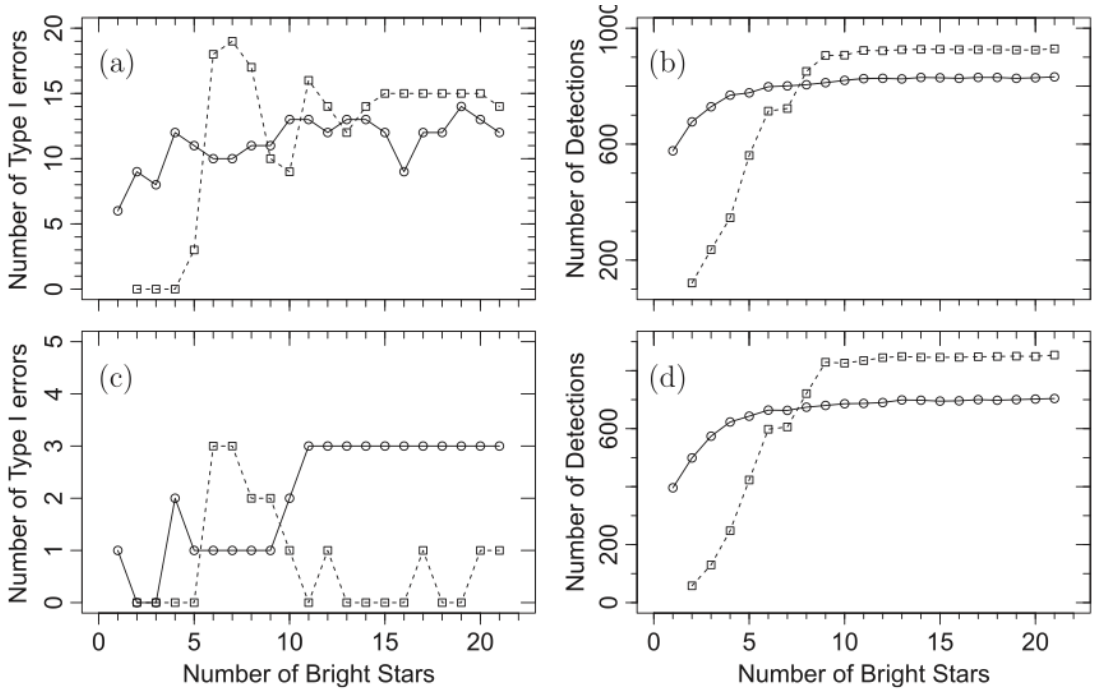

Figure 1.20: Results from enhanced F-test and ANOVA on a simulated dataset. F-test is marked by squares and ANOVA with circles. Panels a) and b) are showing the reliability of the test at $\alpha = 0.01$ level of significance, c) and d) for $\alpha = 0.001$. Panels a) and c) show the number of the type I errors (incorrectly rejected null hypothesis), whereas panels b) and d) show the number of the null hypothesis rejection. Adapted from de Diego et al. (2015).

$$C = \frac{\sigma_T}{\sigma}, \tag{1.26}$$

where σ_T and σ are the standard deviations of the quasar and the comparison star light curve, respectively. The positive or negative detection of the variations depends on the critical value. The commonly used critical value, corresponding to 1% significance level is C $\geq$ 2.576. Nevertheless this value is one of the problems the test has as a statistical procedure. The value stands for a two-tailed test, while in order to test for the variability, one needs a one-tailed test. This comes from the basic test design as we do not test whether the dispersion is smaller of larger than a critical value, rather we are testing only if it is larger. Using simulated light curves, de Diego (2010) showed that the C-test produced neither type I errors (incorrect rejection of null hypothesis) nor detections.

One of the biggest problems is that two standard deviations cannot be compared using a normal distribution. Standard deviations do not act as linear operators. Variances on the other hand do act as linear operators. Aside from this, C-test does not take into account the size of the sample and hence the number of degrees of freedom of the sample. In other words, it is possible to obtain the same result, whether the sample size is $N = 3$ or $N = 300$. The C does not reflect the real power of the test.

Nevertheless one can show the real power of the test, using F-statistic. Using the critical value 2.576: $2.576^2 = 6.636$. For $F_{(50,50)}$ degrees of freedom, the significance level of the test is 2.1×10^{-10}, which is less than the conservatively assumed value 10^{-2} (Jang & Miller 1997). As a result, the C-test is prone to type II errors (de Diego 2010).

1.4.2.5 Bartels test

Bartels test is a nonparametric test. All the tests mentioned above are parametric tests, meaning that the information about the population is completely known by means of its parameter. If we are missing information about the parameters (or the population), then nonparametric tests are used. On top of that, by using the non-parametric test, we do not make any assumption regarding the population and also the null hypothesis is free of parameters.

The Bartels test is a rank[2] version of von Newmann ratio test for randomness (RVN; Bartels 1982). The basis of the Bartels test is to search whether a sequence of n data occured in a random order or not. The test is based on the sum of squares of the rank differences between contiguous elements of a time sequence. We can write

$$RVN = \frac{\sum_{i=1}^{n-1}(R_i - R_{i+1})^2}{\sum_{i=1}^{n}(R_i - \bar{R})^2}, \tag{1.27}$$

where R_i is the rank of the ith observation and $\bar{R} = (n+1)/2$ is the rank mean. It is valid for large samples ($n > 10$). The RVN statistics will be normally distributed with mean μ and variance σ^2

$$\mu = 2 \tag{1.28}$$

$$\sigma^2 = \frac{4(n-2)(5n^2-2n-9)}{5n(n+1)(n-1)^2}. \tag{1.29}$$

Data trends in the time sequence will produce small values of the RVN statistic and therefore rejection of the randomness against the data trends (alternative hypothesis).

The mentioned tests are the most common ones when it comes to studying the variability in astronomical phenomena, notably quasars. Out of the five mentioned tests, three are viable and

[2]Statistical ranking refers to the data transfrmation, where the values are replaced by their rank when the data are sorted. Ranks are usually assigned in ascending order.

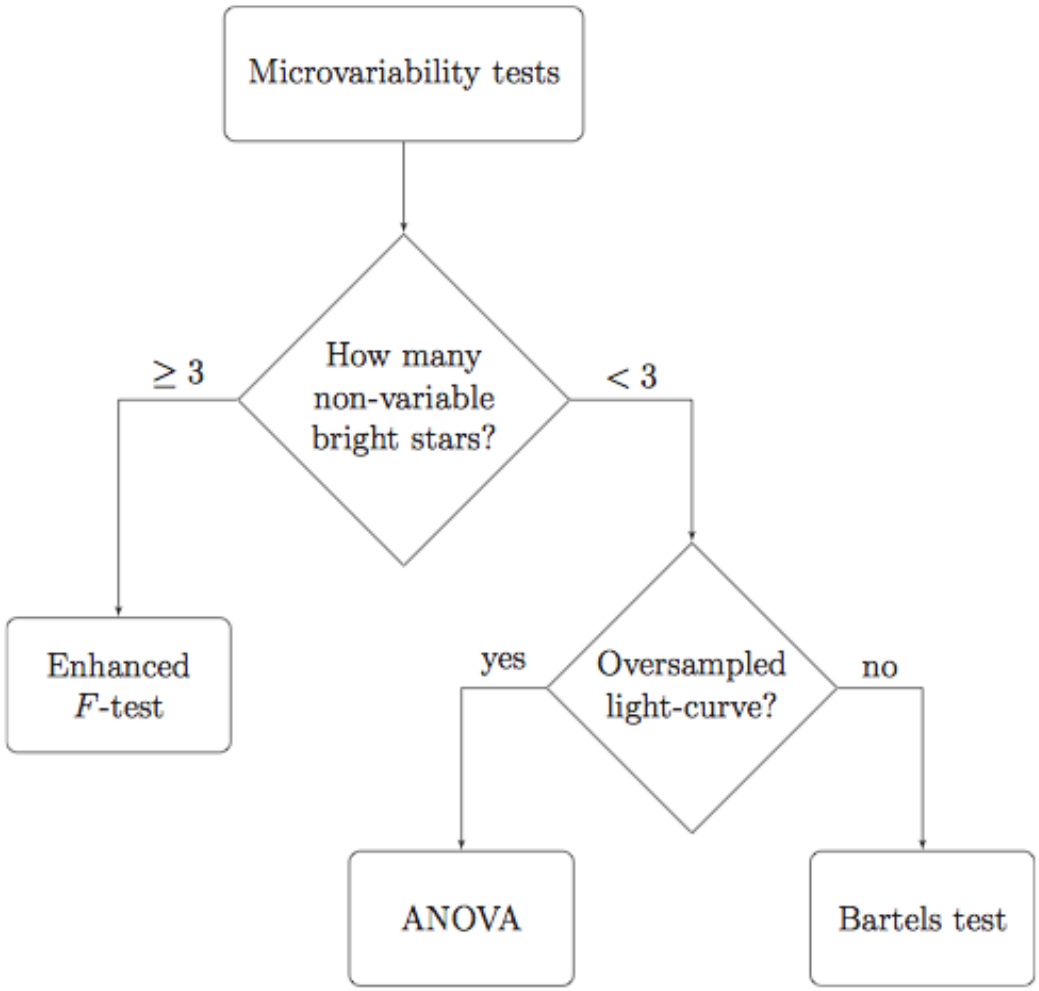

Figure 1.21: Decision flowchart for variability tests. If there is sufficient number of bright stars in the field, F-test is the most viable option. In the other case, ANOVA of Bartels test are better options. One has to take into account the general appearance of the data to make the final decision though. Adapted from de Diego (2014).

powerful enough to detect even small variations. The decision of which test is the most suitable one for the analysis can be guided by a simple flowchart depicted in Figure 1.21.

Chapter 2

San Pedro Mártir observations of microvariability in obscured quasars

This chapter describes the results of an initial campaign to search for microvariability in type 2 quasars which was conducted at San Pedro Mártir observatory in México. Type 2 quasars are observationally selected as targets with $L_{[OIII]} \gtrsim 10^{10} L_{\odot}$, which corresponds to an intrinsic UV luminosity of $M_{2500} \sim -28 mag$. We have chosen quasars instead of type 2 Seyferts as Seyfert galaxies have host galaxies more prominent than quasar. Avoiding subtraction of the host galaxy provides a major advantage for the photometry. The following results are summarized in Polednikova et al. (2015).

2.1 Sample

We aimed at obtaining a homogeneous set of obscured type 2 quasars, in order to avoid biases which might arise from observing sources with different attributes. We have chosen type 2 quasars instead of Seyfert 2 galaxies because of the host galaxy contamination. Studying type 2 quasars, which have relatively brighter nuclei than Seyfert 2 galaxies, helps to increase the nucleus contrast and alleviate this problem. The sample was selected on the basis of brightness and redshift. It was chosen from the catalog provided by Reyes et al. (2008), which is based on Sloan Digital Sky Survey Data Release 6 (Adelman-McCarthy et al. 2008). This catalog consists of 887 type 2 quasars selected based on [OIII] emission line luminosity. The limiting redshift of the catalog is $z = 0.83$. Up to the moment of this thesis writing, it is the largest catalog containing solely type 2 quasars. the catalog covers 80% of the SDSS DR6 spectroscopic database. Our targets were chosen to be bright ($g < 17$), to achieve accurate photometric measurements. There are four objects fulfilling our requirements in the catalog, all of them observable from the northern hemisphere. We were able to observe three targets out of them, since the fourth one collided with telescope pointing issues. A list of the observed targets can be found in Table 2.1, while finding charts can be found in Figure 2.2. The SDSS spectra of our selected targets are provided in Figure 2.1.

The targets we observed have similar redshifts. Even though the redshift was not the main drive for choosing the sample, thanks to the similarity, we can directly compare our sources without having to take into account effects like different rest frames and therefore different observed spectral regions and relativistic time dilatation which causes longer variability timescales in the rest frame of the observer.

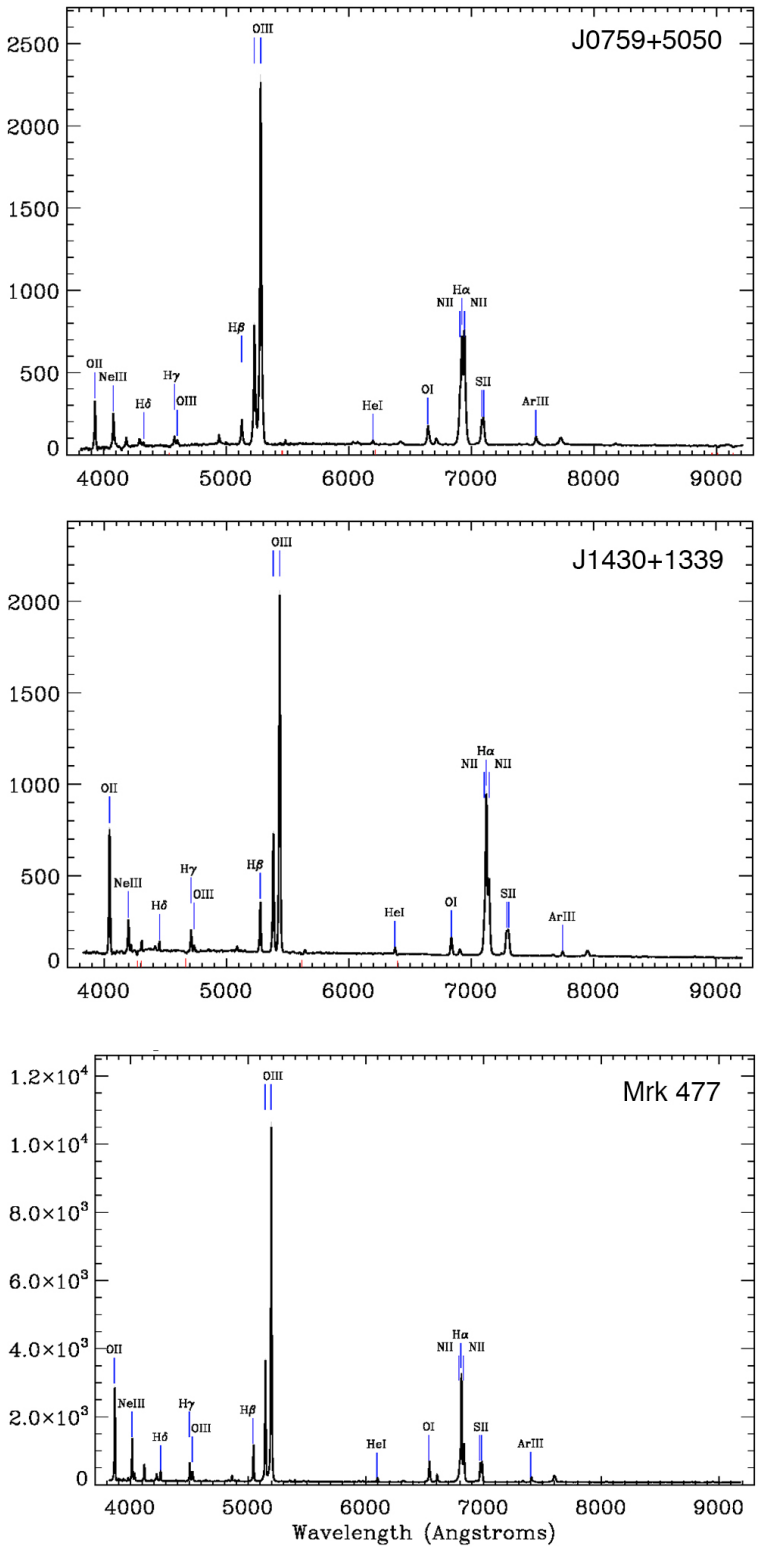

Figure 2.1: Optical spectra from SDSS Data Release 10, of the targets observed in the pilot project. From top to bottom: J0759+5050, J1430+1339, Mrk 477. x axis is wavelength in angström, y axis is flux in $10^{-}17$ erg/cm^2/s/Å.

Table 2.1: Properties of the observed targets from the Reyes et al. (2008) catalog. Right ascension and declination are in J2000.0. L[OIII] is in solar luminosities. Brightness in V filter was transformed from SDSS filters, values correspond to a catalogue of quasars and active nuclei: 13th edition (Véron-Cetty & Véron 2010).

Target	R.A.	dec	V_{mag}	z	$L_{[\mathrm{OIII}]}$
J0759+5050	07:59:40.96	+50:50:24.89	16.59 in	0.055	$10^{8.77}$
J1430+1339	14:30:29.88	+13:39:12.09	17.64	0.085	$10^{9.04}$
Mrk 477	14:40:38.09	+53:30:19.9	15.03	0.037	$10^{8.72}$

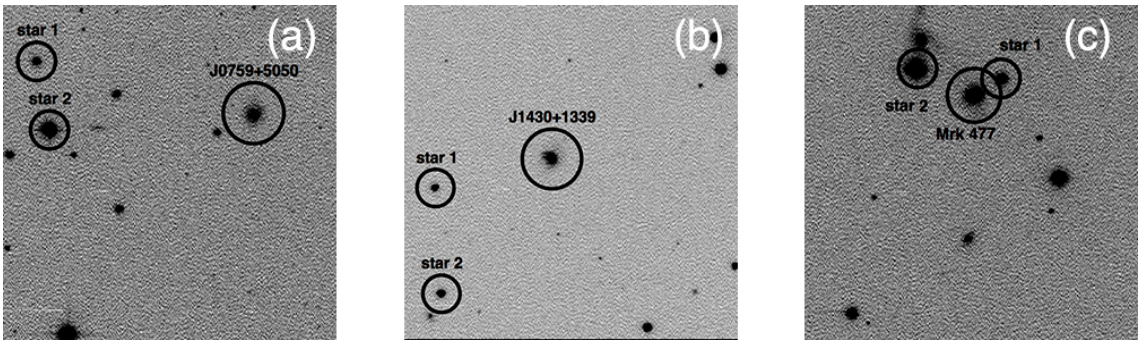

Figure 2.2: Sample images from our observing campaign, taken from the San Pedro Mártir observatory, Baja California, México. the field is 4x4 arcmin. North is up, east is right. Numbers next to stars correspond with numbers used in the differential light curves. the size of the circle mimics the size of the aperture used for the photometry.

2.1.1 Observation

Our sample was observed between March 28 and March 31, 2011 with the SITe 4 detector mounted on the Harold L. Johnson 1.5 m telescope located at Observatorio Astronómico Nacional in Sierra San Pedro Mártir, Baja California, México. The detector is 1024 x 1024 px, with 0.1581 arcsec/px. We employed the same observing strategy as in previous works (de Diego et al. 1998; Ramírez et al. 2009). All targets were observed in Johnson's V filter, as we expect that the variability, if originated near the central engine, is more prominent in blue bands. Johnson's V filter is a sensible choice, given that the sensitivity of U and B filters is significantly lower. Using Johnson's V filter provides a good compromise between the two. Exposure time for each target was set to 60 seconds, providing a signal to noise ratio, SNR > 100. J0759+5050 was observed for a total of 8 hours over three days, J1430+1339 was observed for 4 hours during two days and Mrk 477 was observed for a total of 5 hours over two days. This corresponds to a precision of 0.01 mag. The detector was binned (2x2) to allow fast readout with higher signal to noise. We have observed all the targets with airmass less than 1.3 and all of our observing nights were dark. We have checked the colors of the stars that we have used for the analysis, since Carini et al. (1992) and Stalin et al. (2004) proposed that the airmass effect is negligible as long as the color difference is $g - r < 1.5$. We provide the color information about our targets and stars in the Table 2.2.

Table 2.2: Colors of the targets, reference stars and comparison stars for every observed field. the values are adopted from the SDSS Data release 12 (Alam et al. 2015).

Field	star ID	g	$g-r$
J0759+5050		16.09	0.31
	star1	15.58	0.44
	star2	13.65	1.18
J1430+1339		15.80	0.37
	star1	16.68	1.1
	star2	15.01	1.21
Mrk477		14.84	0.14
	star1	15.01	0.60
	star2	13.23	-1.05

2.1.2 Data reduction

Bias subtraction and flat-fielding were performed using the standard tasks from the IRAF data reduction software[1]. Cosmic rays were removed using L.A.Cosmic[2] by van Dokkum (2001). Aperture photometry was performed using SExtractor 2.8.6[3] (Bertin & Arnouts 1996). We used fixed apertures for both the target and the stars in the field. We made sure to fully enclose the whole star and galaxy flux. In order to ensure the fitness of the chosen apertures, we created magnitude vs. aperture diameter graphs. One can clearly see when the magnitude (in our system where zero magnitude is 20 magnitudes) reaches relaxed value. We assumed the value gets relaxed when the aperture versus radius dispersion is similar or smaller than the photometric error (around 0.01 mag). Unfortunately the general rule of thumb of taking the $3\times$ FWHM, where FWHM values are obtained from SExtractor, does not apply here. The apertures estimated based on this assumption could be underestimated by as much as a factor of 2.

This is important because the contribution can be variable for bright galaxies as a result of intra-night fluctuations in the atmospheric seeing, as pointed out by Carini et al. (1992). According to Cellone et al. (2000), an aperture that would include the whole host galaxy can account for the seeing variations. For stars, we used apertures of 25 px (corresponding to 6.32 arcsec) diameter, while for the AGNs we used a 40 px (10.12 arcsec) diameter aperture. This is roughly four times the full width at half maximum (FWHM) of the objects. Hence we assume that with the apertures that we have chosen, the contribution of the host galaxy is constant over time and therefore is not causing any additional variations. Nevertheless including the galaxy itself increases the photon noise, so the detecter variations might be underestimated.

2.2 Analysis

We have taken advantage of the presence of field stars, which allowed us to perform differential photometry. We have used one star as a reference and another one for comparison, to assure the stability conditions (the properties of the stars are provided in table 2.2).

According to de Diego (2010), there are two statistical tests suitable to search for microvariability, namely F-test and one-way analysis of variance - ANOVA. ANOVA surpasses F- test in power in general, nevertheless enhanced F-test (de Diego 2014) can provide more statistical power than ANOVA. Unfortunately, the enhanced F-test takes advantage of the presence of many stars in

[1]Image Reduction and Analysis Facility (http://iraf.noao.edu/).
[2]Laplacian cosmic ray identification/ (http://www.astro.yale.edu/dokkum/lacosmic/).
[3]Source Extractor (http://www.astromatic.net/software/sextractor).

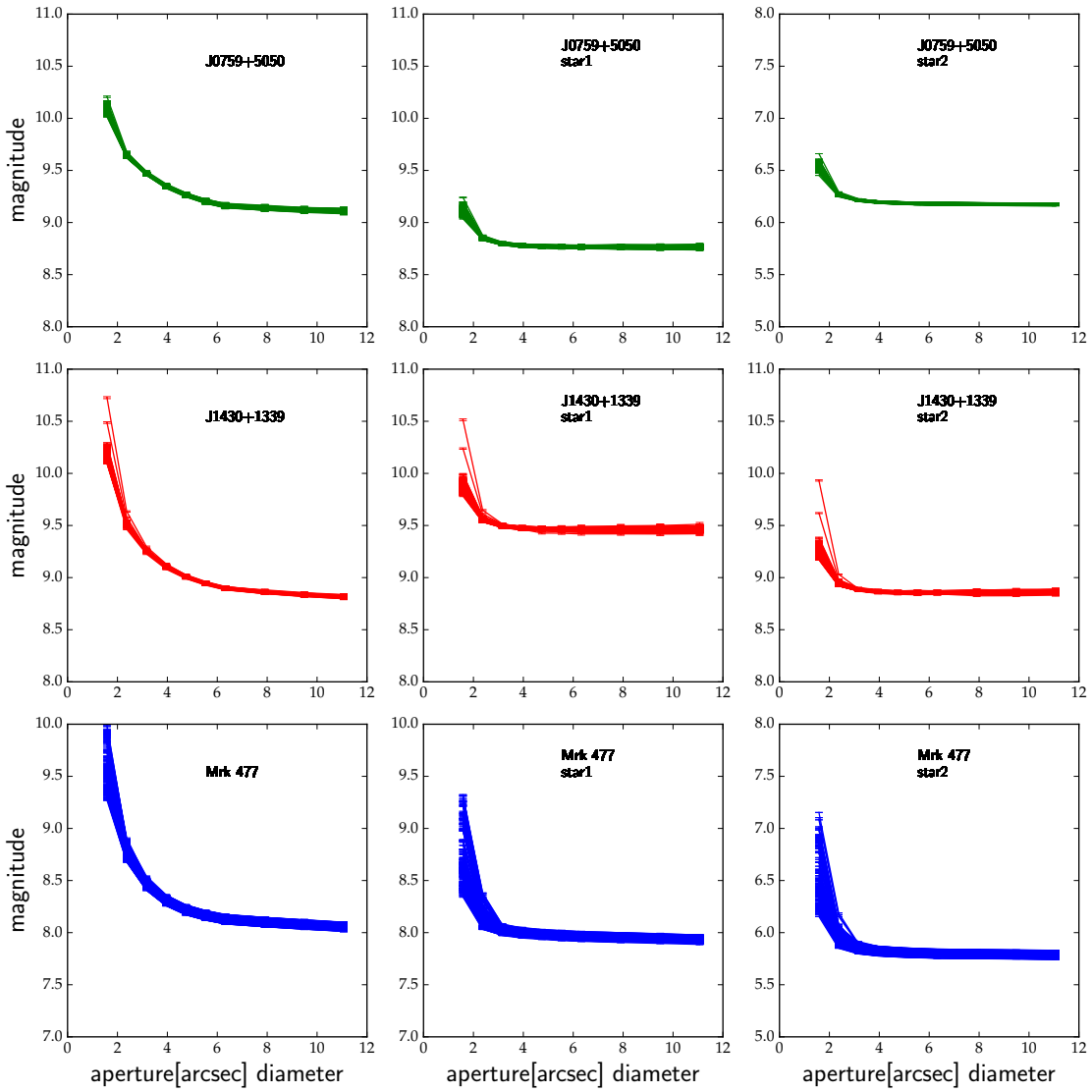

Figure 2.3: Evolution of magnitudes of the chosen field stars with increasing diameter of the aperture in SExtractor. Data for J0759+5050 and J1430+1339 are from March 28, 2011, for Mrk 477 from March 29, 2011. The first column corresponds to the quasar, while the other two columns to the field stars. It is clearly noticeable that the stars magnitudes reach the constant value earlier than the quasar.

Table 2.3: Results of microvariability in type 2 quasars. the second column describes which difference was used to create the differential light curve, where m_{QSO} stands for the target, m_{ref} stands for the reference star and m_{comp} stands for the comparison star used to control the stability of the stellar light curve. N stands for the number of groups used as an input for ANOVA. In the fifth column, we provide the probability of obtaining the result if null hypothesis is correct. the level of significance is $\alpha = 0.001$.

Target	DLC	Date	N	Probability	Microvariability
J0759+5050	$m_{QSO} - m_{ref}$	Mar 28 2011	30	0.0975	N
	$m_{comp} - m_{ref}$	Mar 28 2011	30	0.132	N
	$m_{QSO} - m_{ref}$	Mar 30 2011	20	0.073	N
	$m_{comp} - m_{ref}$	Mar 30 2011	20	0.146	N
	$m_{QSO} - m_{ref}$	Mar 31 2011	30	5.5E-04	Y
	$m_{comp} - m_{ref}$	Mar 31 2011	30	0.327	N
J1430+1339	$m_{QSO} - m_{ref}$	Mar 28 2011	25	0.0105	...
	$m_{comp} - m_{ref}$	Mar 28 2011	25	0.027	...
	$m_{QSO} - m_{ref}$	Mar 30 2011	12	0.391	N
	$m_{comp} - m_{ref}$	Mar 30 2011	12	0.436	N
Mrk 477	$m_{QSO} - m_{ref}$	Mar 29 2011	30	1E-04	Y
	$m_{comp} - m_{ref}$	Mar 29 2011	30	0.114	N
	$m_{QSO} - m_{ref}$	Mar 31 2011	20	4.95E-05	Y
	$m_{comp} - m_{ref}$	Mar 31 2011	20	0.102	N

the same field. As can be seen in Figure 2.2, there is only a handful of bright stars available on our fields. Taking guidance from Figure 1.21, ANOVA is the most suitable test for our needs.

For each object, we have divided the data from every night into groups of five data points, following the strategy of de Diego et al. (1998). We have computed the variance in each of the groups as well as the variance amongst the groups. We have largely benefited from the fact that ANOVA does not rely on the error estimation from the photometric software, which tends to underestimate or overestimate the photometric errors. The errors are computed from the standard deviation within each group of five observations. Light curves with error bars estimated from ANOVA for the sample nights for each target are provided in Figure 2.4.

2.3 Results

ANOVA was computed using Python package f-oneway[4]. The results are summarized in the table 2.3. N states that no microvariations were detected, while Y signifies the positive detection of microvariations. the case of target J1430+1339 unfortunately cannot be decided as the probabilities for the reference star are similar to the ones of the quasar. Due to lack of stable stars in the field, the conclusion for this target is not provided.

We have detected microvariability in two out of three targets that we have observed in the run. It has been shown that there is a strong evidence, at the $\alpha = 0.001$ level of significance, of variability in the light curves of 3 observations of type 2 quasars. Two of the variability detections were in the same target, one in another. Below, the results for the individual targets are discussed.The microvariable events are quantified as was proposed by Heidt & Wagner (1996):

$$Amp = \sqrt{(A_{max} - A_{min})^2 - 2\sigma^2}. \tag{2.1}$$

J0759+5050 was observed during three out of four nights. The observations from March 30, 2011 were disturbed by clouds, so it is not strictly continuous.

[4] `http://docs.scipy.org/doc/scipy-0.15.1/reference/generated /scipy.stats.f_oneway.html`.

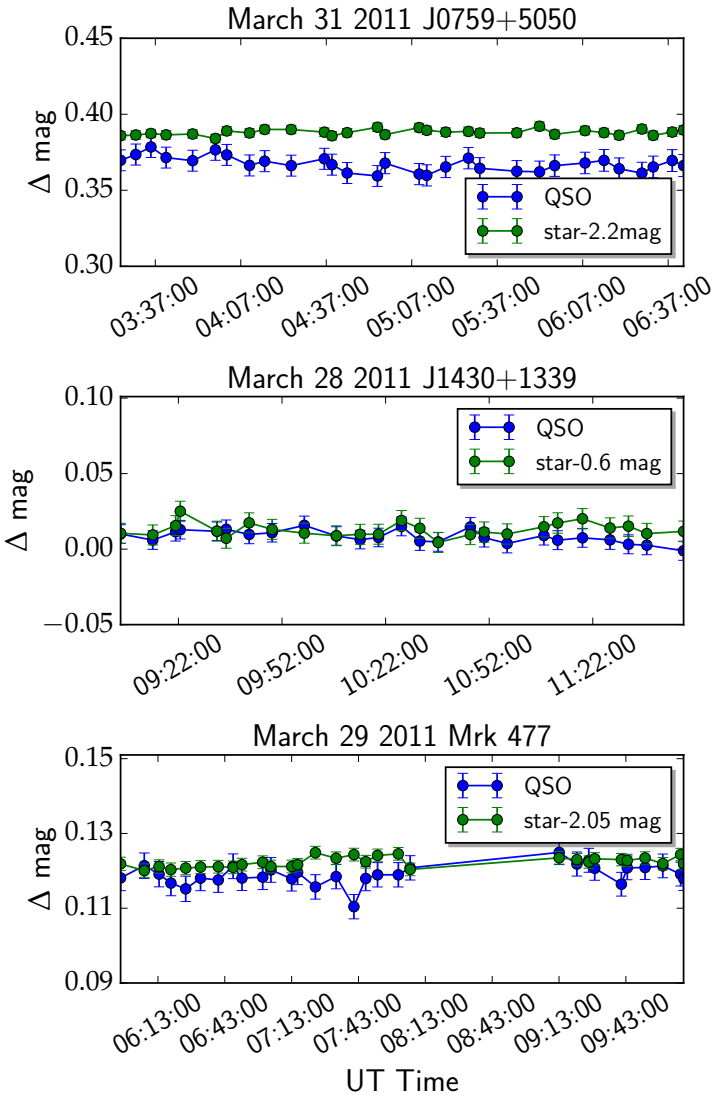

Figure 2.4: Differential light curves with errors computed as standard deviations withing the sets of five observations for the targets and comparison star. A constant is subtracted from the star to fit into one plot and provide direct comparison.

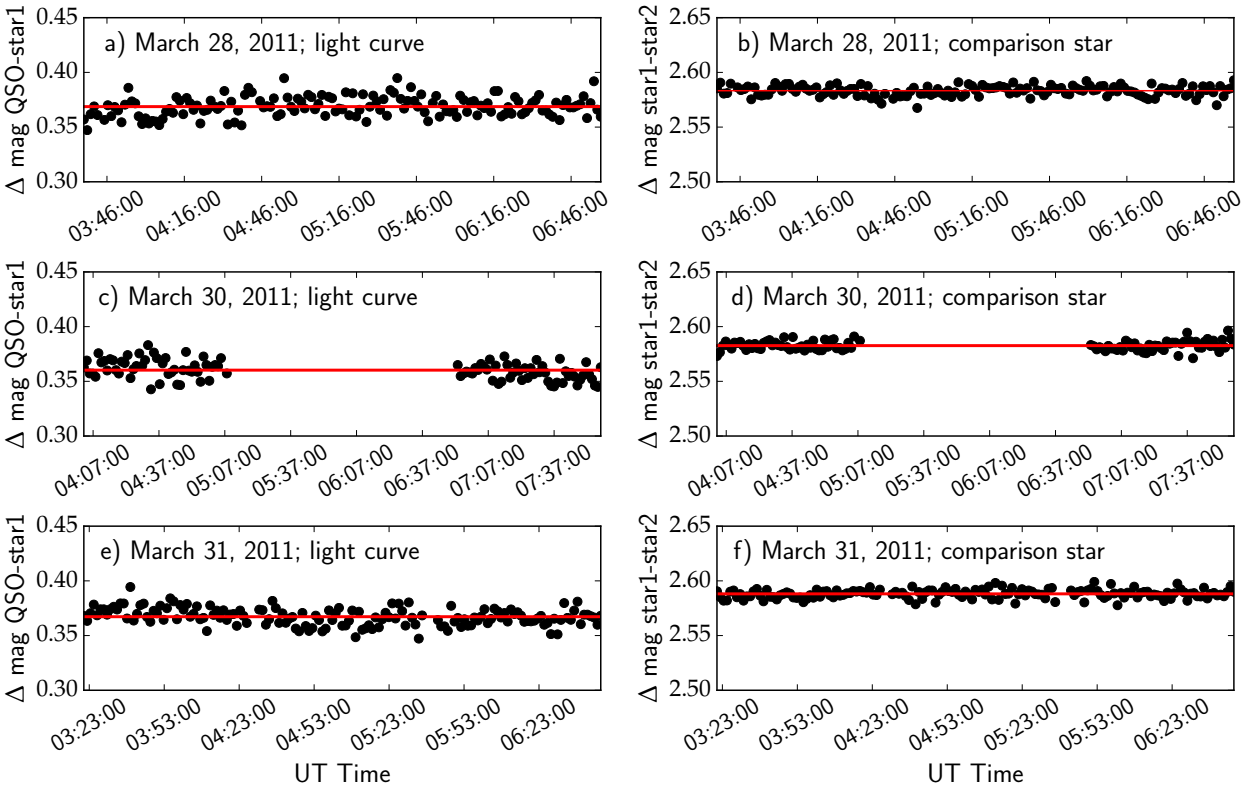

Figure 2.5: Differential light curves for J0759+5050. Panels a, c and e are representing $m_{QSO} - m_{ref}$, while panels b, d and f are $m_{comp} - m_{ref}$. Red lines represent mean values of the observations for every given night.

Microvariability was detected only during the observations carried on March 31st. The event was observed during the period between 3:21 and 5:42 UT. We can obtain the upper level of the amplitude which is 0.04 mag, well above our estimated precision set by the high SNR. The photometric variability amplitude is 4.6%. Contrary to the observations taken on March 31, 2011 the observations on March 28, 2011 and March 30, 2011 did not show any evidence of microvariability. We therefore conclude that the target is probably variable. The lightcurve for this source is plotted in Figure 2.5

J1430+1339 was observed on March 28 and March 30 2011. During the two observing nights, both the target and the comparison star exhibited very contradictory results from ANOVA. We were unable to find a comparison star which is not variable at $\alpha = 0.001$. The $p - values$ we obtained were of order of ~ 0.01 which is too low to accept the source as not variable and too high to accept it as variable. Unfortunately the field around this particular target limited the choice of comparison stars which we could have used for the ANOVA. As a conclusion, the results are too ambiguous to confirm or to disprove evidence of the presence of microvariability in this source. The resulting light curve is in Figure 2.6

Mrk 477 was observed during two nights, March 29 and March 31 2011. The gap between the observations on March 29, noticeable in the final light curve in Figure 2.7, is caused by a technical maintenance pause. Mrk 477 is the only target which has shown microvariability during both observing nights. The upper limit for variations is 0.027 between 5:55 UT and 7:02 UT and 0.023 mag between 8:46 UT and 10:02 UT (for the first and second observing night respectively). Computed

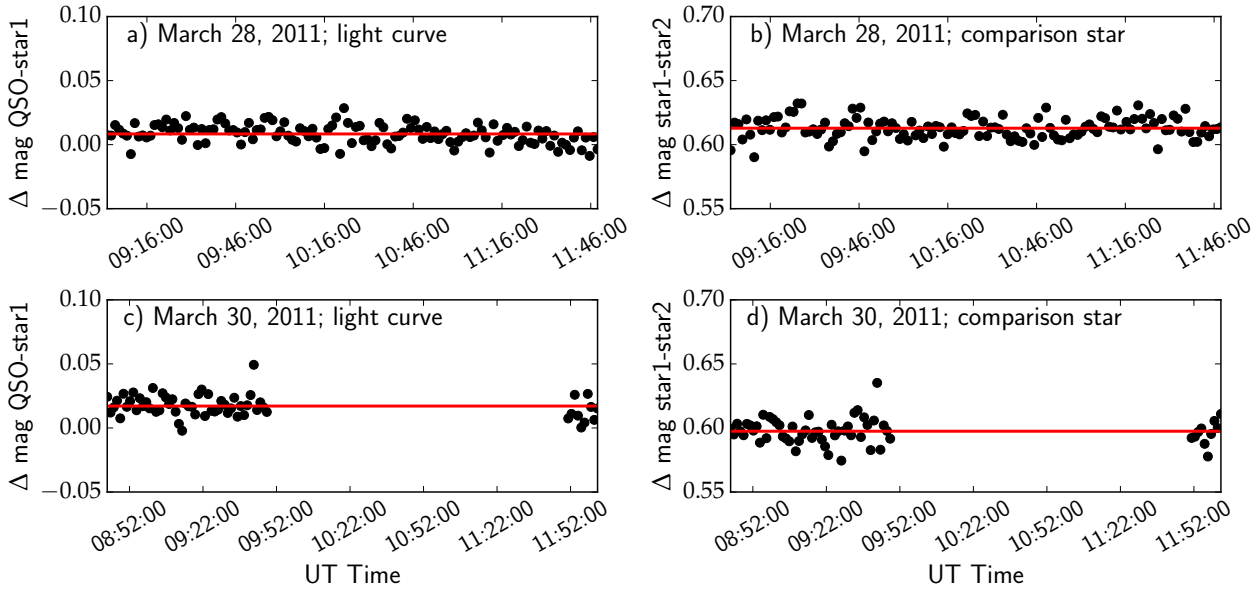

Figure 2.6: Differential light curves for J1430+1339. Panels a and c are representing $m_{QSO} - m_{ref}$, b and d are $m_{comp} - m_{ref}$. Light curves in both nights have very similar scatter along the mean value.

amplitudes of microvariability are 2.7% and 2.3% for the first and second observing night respectively. Based on our results, we conclude that Mrk 477 exhibits microvariations.

2.4 Discussion

We have detected microvariable events with a confidence level of $\alpha = 0.001$ during one night of observations of J0759+5050 and two nights of observations of Mrk 477. For J0759+5050 there was one positive detection in three observing nights, while for Mrk 477 there were two nights of microvariability detections out of two. As J0759+5050 microvariability detection was confirmed during only one out of three observing nights, we conclude that the target is probably variable, Mrk 477 is variable. In the case of J1430+1339, the ANOVA results proved too ambivalent to draw solid conclusions. It is highly unlikely that the systematics are affecting our measurements, as the possible effects would also affect the comparison stars, which we have detected as non variable. As we have been observing during dark nights, we can rule out any variations caused by significant change in the background level. We have also controlled the airmass of the observations. Since the airmass does not rise above 1.3 airmasses, it is highly unlikely that any of the variations would be based on the color change of the source. Given that the target detected as variable is in the vicinity of other sources on the image (see panel (c), Figure2.2), we have constructed check graphs with different aperture sizes to validate that there is no spurious light from other sources propagating into our measurements as seen in Figure 2.3. The apertures are sufficiently large so they are not affected by a change of the seeing.

Mrk 477, the brightest and closest of our sources, is the only one which was widely observed before our study. It was already reported to show optical microvariability by Jang (2001), although the report lacks details and comments on robustness of the result and the statistics used. Tran et al. (2000) reports detection of hidden broad line regions (HBLR) as a part of spectropolarimetric observations. the presence of HBLR might provide a clue about the mechanism behind the variability

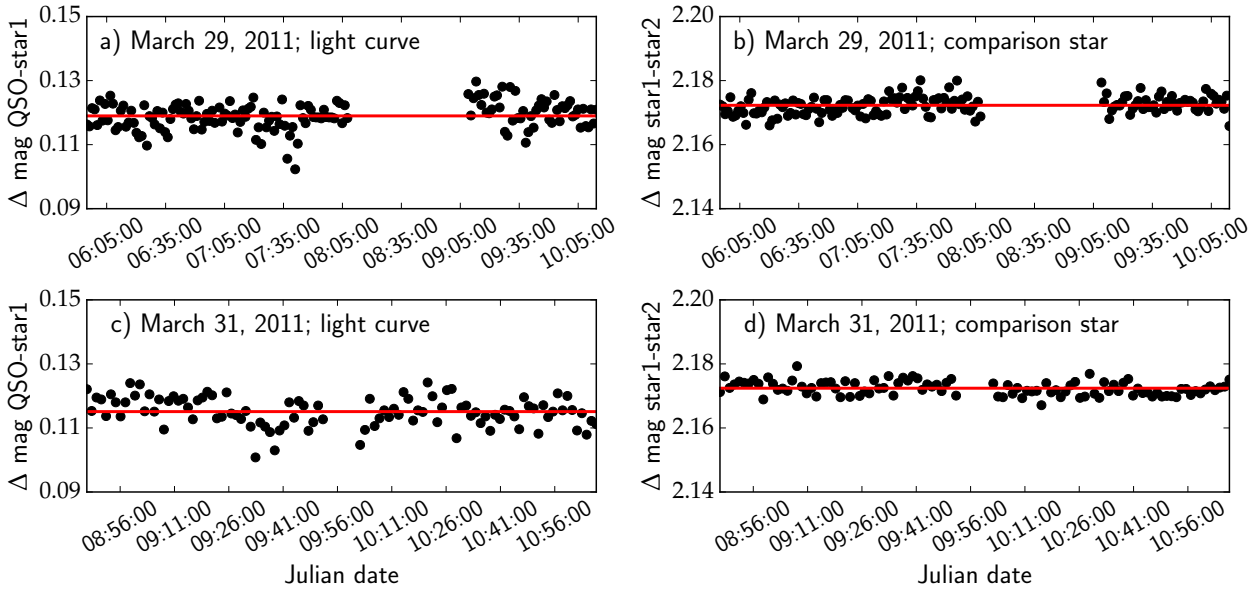

Figure 2.7: Differential light curves for Mrk 477. Panels a and c are representing $m_{QSO} - m_{ref}$, b and d are $m_{comp} - m_{ref}$. Each line represents one observing night. Red line represents mean values. Outlying points were not used for the ANOVA analysis. the target is variable during both nights.

of the source. Until now, almost all the sources that show optical microvariability are type 1 AGNs, i.e., they have a visible broad line region. It is likely that a part of the nuclear continuum is also visible in this case. Therefore is is possible that the variations come from partially visible continuum. Our detection of variability would therefore be consistent with the detection of the HBLR reported by Tran et al. (2000). The mechanism which allows us to detect the variability remains unclear, although there are possible explanations.

It is possible that the observed light is, in fact, originated close to the central engine and was reflected on the corona of charged particles above the dusty torus. Polarimetric observations would be needed to confirm such scenario. The variations we expect in the obscured sources should show small amplitudes, which is a scenario agreeing with our observations. Nevertheless we cannot confirm this statement as we would need to observe the source for an extended amount of time in polarized light.

Mrk 477 is also the only target out of our sample, which was detected also in X-rays. It was reported as a Compton thick source (Gilli et al. 2010). Recently, there have been reports of spectral variability in X-ray detected obscured sources (most notably Seyfert 1.8 galaxy NGC 1365; Risaliti et al. 2009; Brenneman et al. 2013) on short time scales. The variations are caused by alternate covering and uncovering of the X-ray source by clouds in the broad line region. Even though there are archival data of our source from XMM-Newton mission, the monitoring frequency of them is insufficient for performing a study of short term X-ray variations.

Another possible explanation lies within the structure in the dusty torus which could provide observational holes to observe the inner parts of the otherwise obscured AGNs. The original unified scenario introduced by Antonucci (1993), includes a geometrically thick obscuring rotating region known as torus. It is worth noticing that Krolik & Begelman (1988) suggest that such structure would be hard to maintain and introduces clumpy structure into the model of the torus. The model introduced by Nenkova et al. (2008) counts with no more than five or ten clouds, which is not suitable

for explaining high frequency variations. Considering orbital motion for the individual clouds in the dusty torus, variability is expected whenever these clouds, temporarily, do not completely hide the central engine. This may be the case for a few Seyfert galaxies that have shown spectral variations, changing from type II to type I AGNs. However, these variations happen in timescales of years and our data do not allow us to observe such a behavior.

Chapter 3

Detecting microvariability in type 2 quasars with the enhanced F-test

Based on the successful detection of microvariability in our pilot sample, described in the previous chapter, we decided to broaden our sample by four additional type 2 quasars, observable from the northern hemisphere, to see if the findings were serendipitous or could be backed up with more observations. We submitted a proposal to the Nordic Optical Telescope on La Palma, to further expand our sample and to look for a possible similarities between targets which are obscured and variable on short time scales. The observations were done in various filters in order to compare the variations at different wavelength ranges which provides more insights about their possible origin.

Following results were published in the Monthly Notices of Royal Astronomical Society paper by Polednikova et al. (2016).

3.1 Sample selection

Similarly to the sample described in Chapter 2, the NOT sample was chosen based on the catalog of type 2 quasars by Reyes et al. (2008). We have restricted the sources to be bright ($g' < 18$ mag) and with redshift $z < 0.1$. By constraining the redshift range, we are avoiding differences which might arise due to a change of the rest frame of the targets. This effect might result in an unnecessary bias of monitoring different physical regions. The spread over the redshifts of the chosen sample is 0.0367, which results in $\Delta\lambda \approx 144$Å. This difference is covered within one broad band filter (FWHM of the used filters g', r' and i' are 145, 148 and 171 nm respectively). The restriction placed on the brightness is based on the aim to obtain high quality data with signal to noise ratio > 100. There are 14 targets meeting our criteria. Three out of those targets were observed during the observing campaign on San Pedro Mártir Observatory in México, which is described in the previous chapter. We have not repeated the observations of these targets. The final sample was chosen based on the visibility during the observing nights. The properties of the selected targets are reported in table 3.1.

3.2 Observations

We have observed our targets on February 21 and February 22, 2014 with the 2.5 meter Nordic Optical Telescope on La Palma, equipped with the ALFOSC camera. ALFOSC (Andalucia Faint Object Spectrograph and Camera) is a back illuminated detector with a pixel scale 0.21 arcsec

Table 3.1: Overview of the sample observed with Nordic Optical Telescope on Roque de los Muchachos observatory, La Palma. Serendipitously, the sample included the galaxy J1316+4452b which is the neighbor of J1316+4452 which was observed in the same field as the targeted type 2 QSO J1316+4452.

Target	RA	Dec	z	gmag
J0802+2552	08 02 52	+25 52 55	0.0811	15.93
J0843+3549	08 43 45	+ 35 49 42	0.0539	15.28
J1258+5239	12 58 50	+52 39 12	0.0552	15.63
J1316+4452	13 16 39	+44 52 35	0.0906	15.98
J1316+4452b	13 16 36	+44 51 57	0.0602	16.17

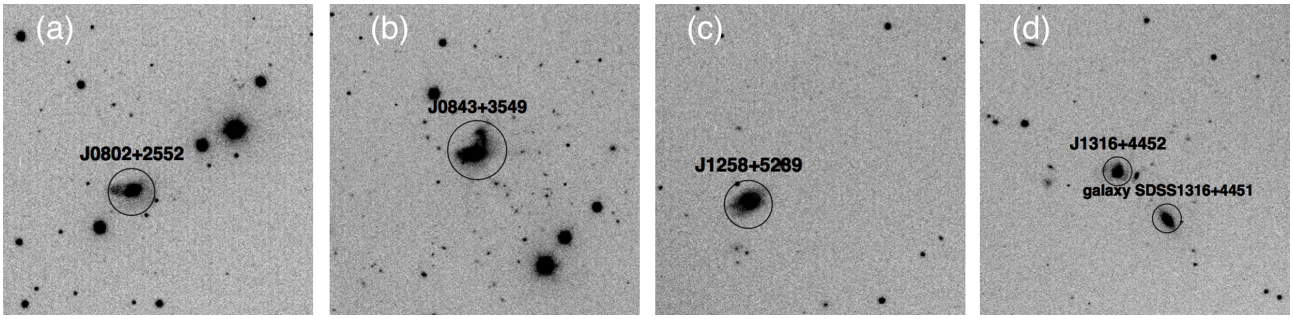

Figure 3.1: Targets observed in our observing campaign are marked with a circle, mimicking the size of the aperture used for the photometry. Panels (a) - (b) show targets with disturbed morphologies. J1316+4452 shows an accompanying galaxy of approximately the same brightness as the source itself J1316+4452b. North is up in all the images, east on the right.

px^{-1} and field of view 6.4×6.4 arcmin in imaging mode. Our observing strategy partly followed the works of de Diego et al. (1998) and Ramírez et al. (2004). During the first observing night, we were observing solely in the Sloan g' filter. During the second night, we were interchanging Sloan g', r' and i' filters. We have observed with 2×2 binning, in order to increase the signal to noise while maintaining the same exposure time as in the sample mentioned in previous chapter. We have reached a SNR > 100 in 60 seconds exposures in every filter. The targets were chosen to be close to each other, so that we could easily switch between them, every five exposures. Such setting allowed us to monitor the pairs on a longer time scale without long overheads. Previously detected microvariability events in quasars were reported to be of the time scales of ≈ 1.5 hours (Ramírez et al. 2004; de Diego et al. 1998). Based on this assumption, we have increased the chance of detecting any microvariations by setting the time on each of the targets to four hours per night.

Our monitoring resulted in roughly 70 points on the light curve per target during the first night, and 30 point per target per night in every filter during the second observing night.

3.3 Data reduction

Bias subtraction and flat-fielding were performed using the standard tasks in IRAF. Aperture photometry was performed using SExtractor 2.8.6 (Bertin & Arnouts 1996). We used a dithering pattern when obtaining the images, so we could remove fringing patterns, known to exist in i' filter. Therefore we needed to astrometrize the images. Astrometry on each image allowed us to compute the shifts of all the images with a high precision, which simplified further analysis. For this purpose we used SCAMP 2.0.4 (Bertin 2006)[1], which directly uses output from SExtractor. SCAMP matches the known pointing and SExtractor catalogs of the images with the chosen catalog (in our case USNO-B2.0 catalog). Resulting astrometric catalogs for every image were matched using TOPCAT (Taylor 2005)[2].

The ALFOSC i' images are affected by fringing which needed to be removed prior to photometry. The pattern proved to be time variable, therefore we grouped the i' filter observations in sets of five, following the observational pattern. The groups of five exposures were taken within 10 minutes, so we assume that over such time scale, the pattern remains stable. We have removed the pattern using procedures natively available in IRAF. We created a master fringe image by combining five images, obtaining a fringing pattern. We masked the objects on the images and removed the fringinb using the `rmfringe` method. This procedure was applied to all of the i' filter images.

We have used aperture photometry, even though our targets have resolved host galaxies. At the moment, there is no software which would allow us to decompose the galaxies which have complex irregular morphologies. Any attempt in decomposing our galaxies would most likely result in the introduction of additional errors. We have included the whole target in the aperture, including the non variable host galaxy, following the procedure mentioned in the previous chapter. Including non variable part would more likely underestimate the variation than enhance it. Besides the circular apertures, SExtractor offers also the option of elliptical apertures (AUTO and PETRO). Nevertheless the control of the size of the ellipse and its ellipticity is limited. On top of that, while the elliptical apertures might be more appropriate for galaxies, they are completely unjustified for stars. In order to obtain photometry as homogeneous as possible, we have used the same aperture diameter for the field stars. Unfortunately, the lack of precise photometric tools to measure heavily distorted galaxies such as the host of J0843+3549 prevents a reliable analysis of the variability for this object. For the details, see Section 4.

[1]Software for Calibrating AstroMetry and Photometry (`http://www.astromatic.net/software/scamp`).
[2]Tool for OPeration on Catalogues And Tables (`http://www.star.bris.ac.uk/ mbt/topcat/`).

3.4 Analysis

We have analyzed our data using the enhanced F-test introduced by de Diego (2014), applied to differential photometry light curves. We are testing the null hypothesis that the target is not variable. We fail to reject the null hypothesis when $p > 0.001$, meaning there is 99.9% chance the target is variable. If we reject the null hypothesis, we accept the alternative hypothesis that the target is variable. However there are several steps which need to be undertaken before the computation of the F statistics. We describe the procedure in the subsections below.

3.4.1 Estimating the error

SExtractor is a very convenient and fast tool for photometry, but the photometric errors provided by this software often seem to be underestimated. Since we compare variance of two samples, we must make sure the variances are estimated correctly. A similar issue was addressed by other authors (e.g. Goyal et al. 2013), who introduced multiplicative factor for errors in the APPHOT package in IRAF. To our knowledge, there is no study which would allow to reliably estimate possible multiplicative factors for SExtractor's photometric errors. There is no evidence such a factor would be universal, independent of the characteristics of the telescope, instruments or observed bands. Therefore to achieve the highest possible accuracy, we need to estimate the photometric errors independently of SExtractor.

In order to fully benefit from the enhanced F-test, we need to calibrate the brightness of stars in the field. To obtain the relation for the photometric error, depending on the brightness, we have constructed differential light curves for all the stars present in the field of the observed quasar. Out of those, we have chosen a constant comparison star for the differential photometry, based on the light curve obtained in the previous step. If the light curve did not show any significant trend or features, the star was considered constant at the first approximation. The comparison star is of roughly similar brightness as the studied target. We have computed the standard deviation of every light curve which serves as the estimated photometric error for a given star brightness. Stars with high errors are likely variable, hence we can exclude them from our calibration field. The quasars themselves were also excluded from the fitting as we assume they might be variable and would show up as outliers. Figures 3.2 - 3.4 show that the errors are following an exponential trend. As the precision decreases towards the faint end, we have decided to fit only a handful of comparatively bright stars. The error we can reach for an infinitely bright source gives us the maximal precision we can reach in our field, which is < 0.01 magnitudes in most cases.

3.4.2 Errors scaling

In the ideal case, our comparison field stars would be of the same brightness as the targeted quasar. As it is not the case, we have to employ a scaling factor, ω_j to scale the variance of the j-th star to the level of quasar q, where ω_j is determined based on the values obtained from the fits in Figures 3.2, 3.3 and 3.4. Howell et al. (1988) and Joshi et al. (2011) proposed different approaches to determine this scaling factor. As de Diego (2014) remarks, it is not necessary to have the same number of observations of all comparison stars. Let's assume k the number of stars observed in the field and N_j the number of the observations of the $j-$th star. Observations are indexed over i. We will estimate the pooled variance. We are using the scaled magnitudes of the stars, but this does not affect the estimation of pooled variance. For N_j stars, we can calculate the pooled (combined) variance as

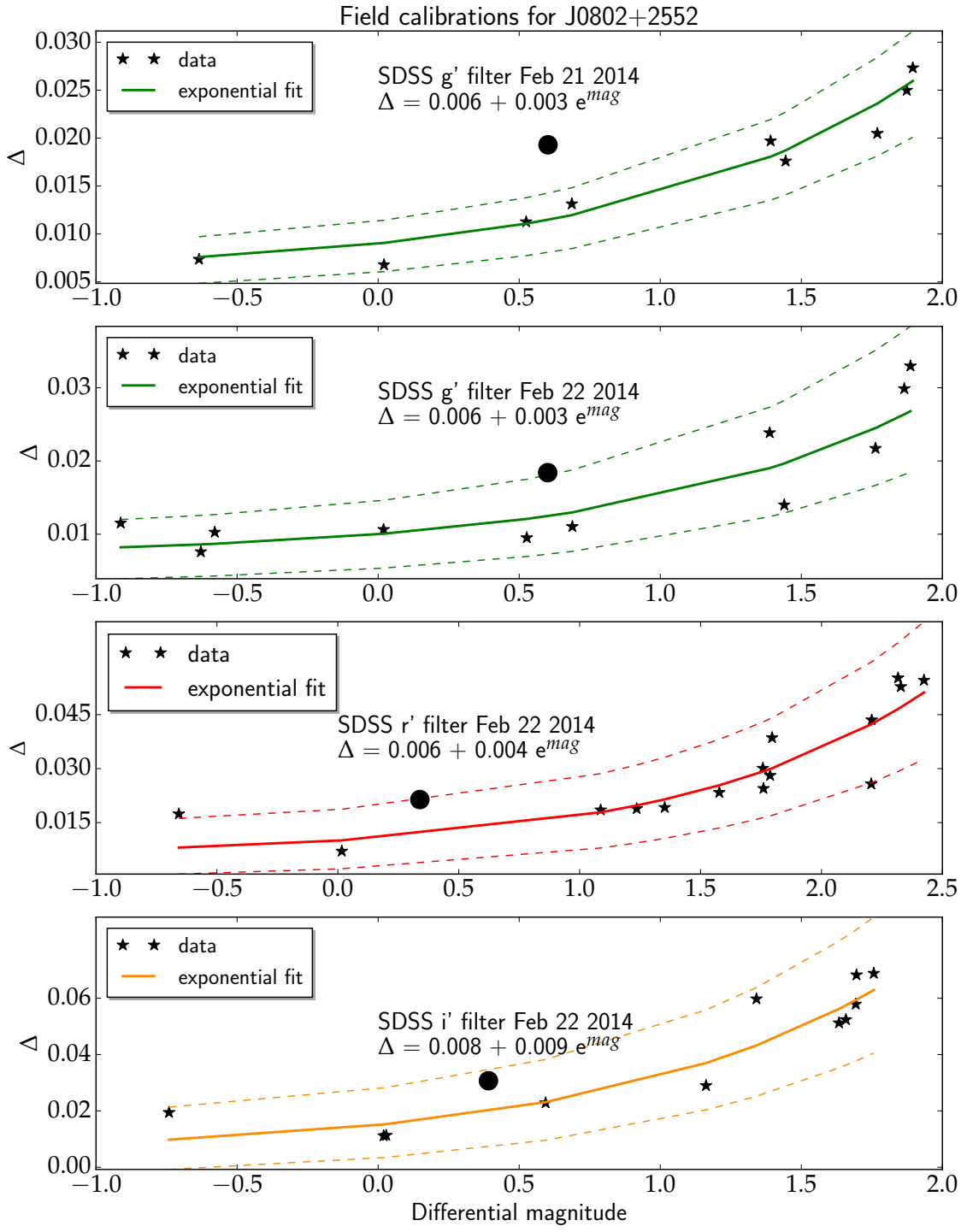

Figure 3.2: Calibration of the photometric error of the field stars around J0802+2552. The x axis marks the differential magnitudes of the field stars, y axis is the photometric error, Δ predicted from the exponential fit. The dashed line marks 95% confidence interval of the fit. The big black circle marks the position of the QSO (in all figures). First panel corresponds to February 21, 2014, when we observed solely in g' filter, the three following panels correspond to g',r' and i' filters observations on February 22, 2014. The graphs are color-coded, according to the filters (g' green, r' red and i' orange).

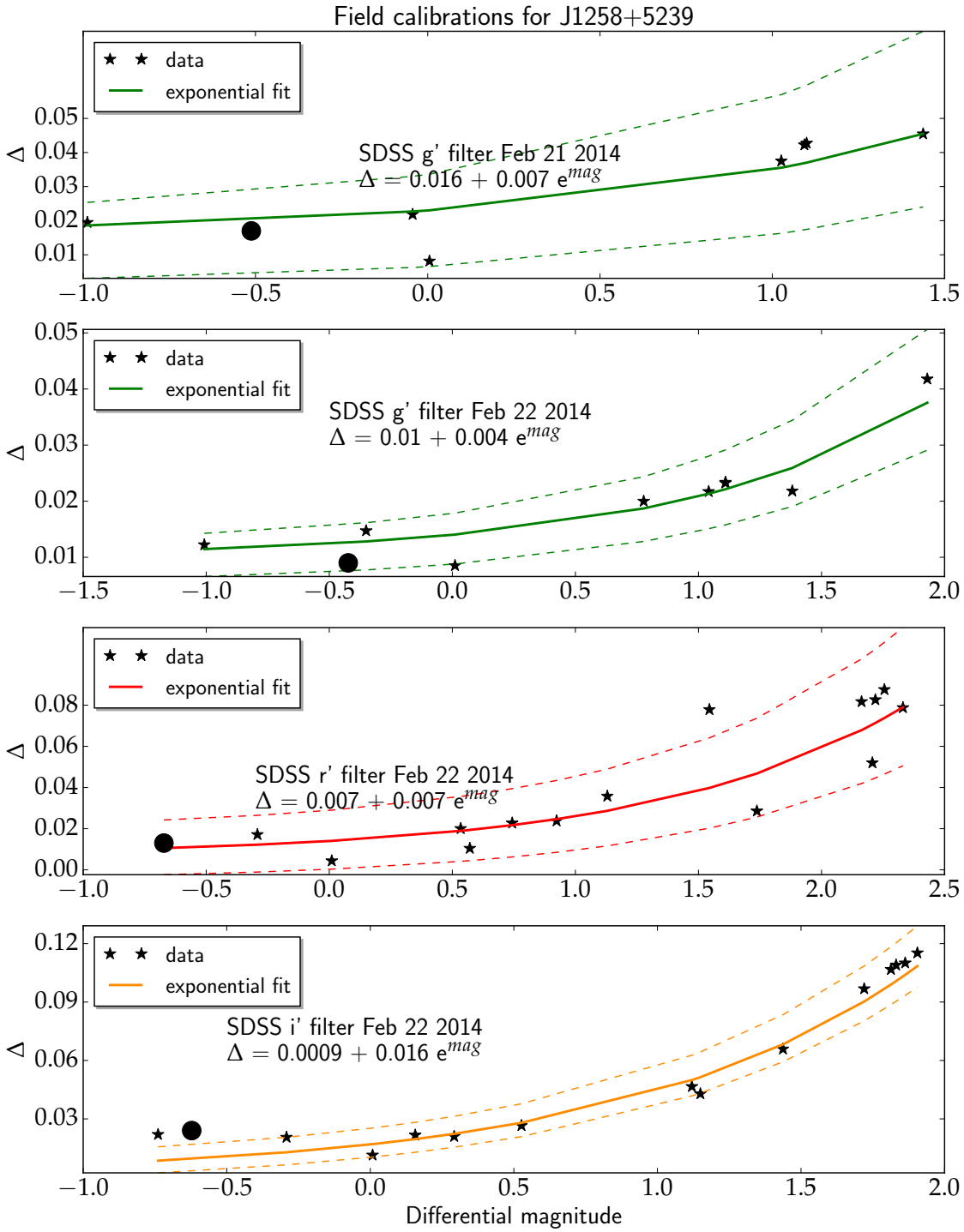

Figure 3.3: Calibration of the photometric error of the field stars around J1258+5239. The black circle marks the differential magnitude of the QSO with error Δ. The axes and color coding is adapted from the previous figure.

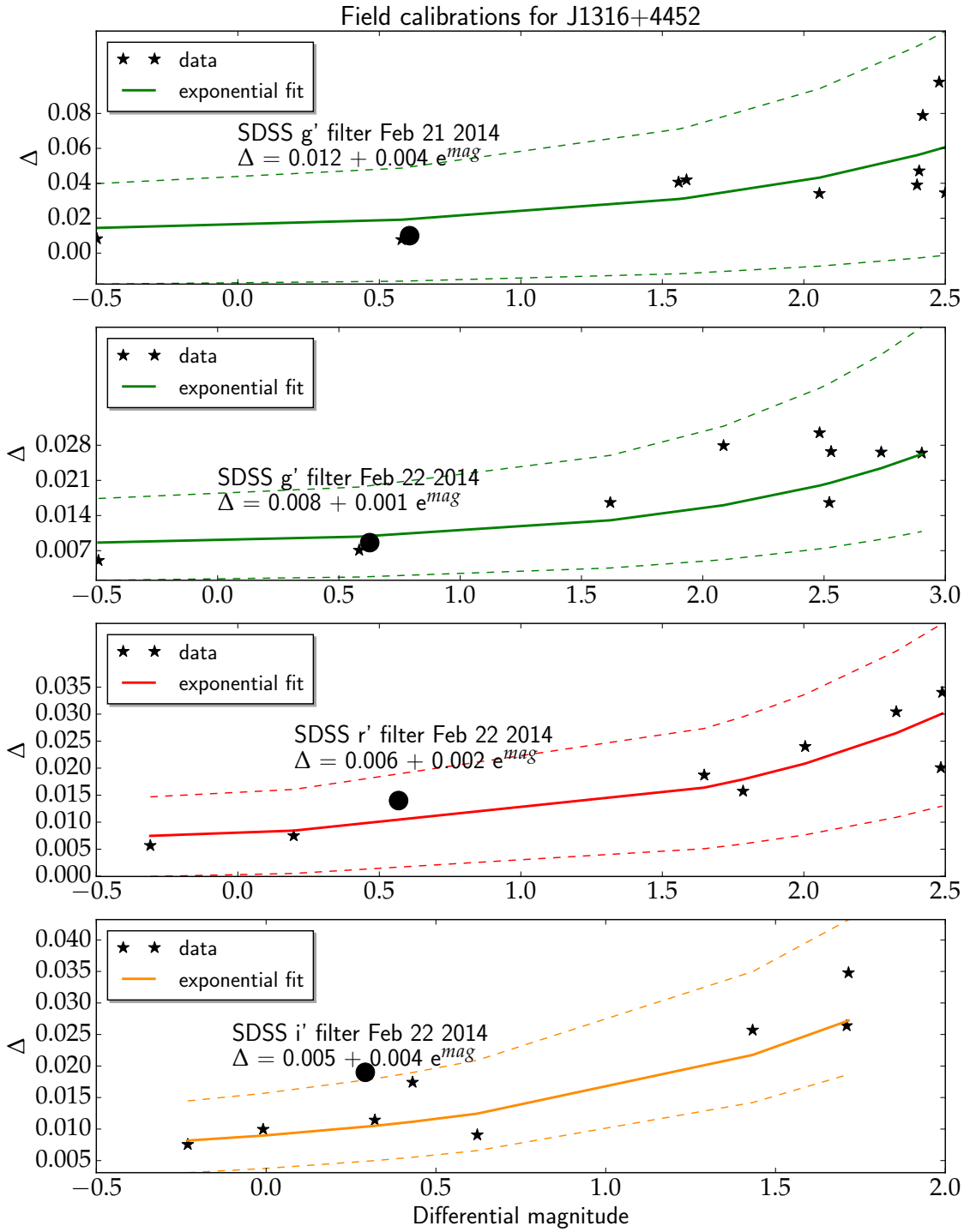

Figure 3.4: Calibration of the photometric error of the field stars around J1316+4452. The x axis marks the differential magnitudes of the field stars, y axis is the photometric error, Δ predicted from the exponential fit. The black circle marks the position of the QSO. Color-coding is following the same philosophy as in the previous figures. The field contains fewer stars bright enough to be fitted in comparison with the other targets, especially in i' filter.

$$\begin{aligned} s_c^2 &= \frac{\sum_{j=1}^{k}(N_j-1)s_j^2}{\sum_{j=1}^{k}(N_j-1)} \\ &= \frac{(N_1-1)s_1^2+(N_2-1)s_2^2+\cdots+(N_k-1)s_k^2}{(\sum_{j=1}^{k}N_j)-k}, \end{aligned} \tag{3.1}$$

where s_j^2 are the transformed light curve variance for the star j:

$$s_j^2 = \frac{\sum_{i=1}^{N_j}(x_{j,i}-\bar{x_j})^2}{N_j-1} \tag{3.2}$$

and the $(x_{j,i}-\bar{x_j})^2$ are the square deviations for the scaled data:

$$(x_{j,i}-\bar{x_j})^2 = \omega_j(m_{j,i}-\bar{m_j})^2 = s_{j,i}^2 \tag{3.3}$$

where m denotes the magnitudes of the observed stars and $\bar{m_j}$ is the mean magnitude of the light curve of each star.

Equations 3.2 and 3.3 yield:

$$\sum_{i=1}^{N_j} s_{j,i}^2 = (N_j-1)s_j^2, \tag{3.4}$$

which can be rearranged as

$$s_c^2 = \frac{1}{(\sum_{j=1}^{k}N_j)-k}\sum_{j=1}^{k}\sum_{i=1}^{N_j} s_{j,i}^2. \tag{3.5}$$

We have found that the empirical relation for the photometric errors, which for a non-variable object are distributed as the standard deviation of the light curve s, is in the form

$$s_{star} = s_j = a\ + b\, e^{\bar{m}}, \tag{3.6}$$

where s_{star} is the standard deviation of the given star light curve. In the case of non-variable quasar, the s_{qso} could be also fitted by equation (3.6). If the QSO is variable, it appears as an outlier from the fit. Fitting the dependence with a variable quasar results in a poor fit. We assume that the distribution of the observed magnitudes of non-variable comparison stars, is nearly normal, hence

$$\frac{m_{star,i}-\bar{m}_{star}}{s_{star}} \sim \frac{m_{qso,i}-\bar{m}_{qso}}{s_{qso}} \sim \mathcal{N}(0,1), \tag{3.7}$$

Taking into account equation (3.7), we can isolate $m_{t,star,i}$ as

$$m_{t,star,i} = (m_{qso,i}-\bar{m}_{qso})\frac{s_{qso}}{s_{star}} + \bar{m}_{star}, \tag{3.8}$$

where s_{qso} is the standard deviation of the quasar based on the fits, and the index t denotes the transformed magnitudes. Taking into account the transformed magnitudes, we can rewrite equation 3.3 as:

$$(x_{j,i}-\bar{x_j}) = (m_{t,j,i}-\bar{m_{t,j}})^2 = s_{j,i}^2. \tag{3.9}$$

Table 3.2: Results from enhanced F-test on sample in g' filter on February 21. Y marks variability at the 0.1% ($\alpha = 0.001$) significance level by default. $F_{\alpha=0.01}$ and $F_{\alpha=0.001}$ mark the cutoff values for claiming the variability, given the degrees of freedom used. Column marked 'star' provides F test for a check star from the same field, measured with the same method as the quasars.

Target	F_{obs}	$F_{\alpha=0.01}$	$F_{\alpha=0.001}$	var?	star	p-value
J0802+2552	2.93	1.52	1.74	Y	1.19	1.54e-10
J1258+5239	1.02	1.44	1.62	N	1.16	0.43
J1316+4452	0.31	1.44	1.61	N	0.16	0.58
J1316+4452b	0.25	1.44	1.61	N	0.16	0.99

3.4.3 F-test

The F-test compares the variances of two samples. In our case we are testing whether our sample of stars with transformed magnitudes has similar variance as the quasar. Therefore

$$F = \frac{s^2_{qso}}{s^2_c}, \tag{3.10}$$

where the variance s^2_{qso} is obtained directly from the photometry. As we have scaled all the observations of all suitable field stars, we can greatly benefit from the high number of degrees of freedom which enhances the power of the F-test. Assuming k is the total number of the scaled down stars and N_{qso} is the total number of observations of the quasar, we have $\nu_1 = N_{qso} - 1$ degrees of freedom in the numerator and $\nu_2 = \sum_{j=1}^{k}(N_j - 1)$ in the denominator, where N_j is the number of observations of the i-th star. We are loosing two additional degrees of freedom due to the fitting of two parameters in equation (3.6). As we are scaling the stars to the brightness of the quasar, we can see that it is not necessary to observe all the calibrating field stars on every image. This allows us to dither images. The only star which needs to be present in all the images is the comparison star we are subtracting from all the field stars in order to obtain differential magnitudes. To determine variability, we have computed the F test as in equation (3.10). To determine the success of the detection, we have computed cutoff levels for two levels of significance; $\alpha = 0.01$ and $\alpha = 0.001$. Cutoff levels values are different for each target as we had different number of images and different number of field stars in every case. We have used the R-code[3] (R core team 2013) to determine the values.

3.5 Results

The overall results for the separate filters are contained in the tables 3.2, 3.3, 3.4 and 3.5. We provide overview of the numbers of degrees of freedom used for the enhanced F-test in Table 3.6. We do not necessarily expect similar behavior in all filters, therefore we do not search for similar trends in color (de Diego et al. 1997; Ramírez et al. 2009).

J0802+2552 was observed during the first half of the night in both nights. As we were observing just before the last quarter, the Moon had not risen and therefore it was not affecting our observations. The data from the first observing night, February 21 2014, were calibrated using 9 stars from the field. The omitted stars were either too faint or too bright or even saturated (e.g. north-eastern part of Figure 3.1). Using them would introduce imprecisions. We have obtained 60 exposures of the target in g' band. We have used apertures of 34.4 arcsec (90 px). The seeing fluctuated between 1-1.5". Not all the calibration stars were available in all the images, therefore the total number of calibration stars from the set of 60 images is 504 instead of 540. All of these

[3] `http://www.r-project.org`

Table 3.3: Results from enhanced F-test on sample in g' filter on February 22. Y marks variability at the 0.1% ($\alpha = 0.001$) significance level by default. $F_{\alpha=0.01}$ and $F_{\alpha=0.001}$ mark the cutoff values for claiming the variability, given the degrees of freedom used. Column marked 'star' provides F test for a check star from the same field, measured with the same method as the quasars.

Target	F_{obs}	$F_{\alpha=0.01}$	$F_{\alpha=0.001}$	var?	star	p-value
J0802+2552	2.07	1.77	2.11	$Y_{\alpha=0.01}$	1.41	2.0e-3
J1258+5239	0.56	1.81	2.17	N	1.00	0.96
J1316+4452	0.58	1.81	2.17	N	0.31	0.99
J1316+4452b	0.55	1.80	2.17	N	0.40	0.99

Table 3.4: Results from the observations taken on February 22, 2014 in r' filter. The columns follow the same arrangement as in the previous table.

Target	F_{obs}	$F_{\alpha=0.01}$	$F_{\alpha=0.001}$	var?	star	p-value
J0802+2552	2.45	1.76	2.10	Y	0.59	7.0e-05
J1258+5239	1.30	1.78	2.12	N	0.89	0.14
J1316+4452	2.36	1.83	2.21	Y	0.77	3.8e-4
J1316+4452b	4.03	1.83	2.21	Y	0.77	6.3e-09

Table 3.5: Results from the observations taken on February 22, 2014 in i' filter. The columns follow the same arrangement as in the previous tables for g' and i' filters.

Target	F_{obs}	$F_{\alpha=0.01}$	$F_{\alpha=0.001}$	var?	star	p-value
J0802+2552	3.04	1.78	2.12	Y	1.49	1.1e-06
J1258+5239	4.96	1.76	2.11	N	0.64	1.1e-11
J1316+4452	2.87	1.85	2.25	Y	1.01	2.2e-05
J1316+4452b	3.73	1.85	2.25	Y	1.01	1.1e-07

Table 3.6: Numbers of degreed of freedom $df1$ and $df2$ used for the enhanced F-test. The number of degrees of freedom of the star ($df2$) does not correspond to the expected number based on multiplication of the exposures by the number of stars used. This is caused by a slight shift in the observations. It does not affect the results. .

Source	Date	Filter	$df1$	$df2$
J0802+2552	2014/02/21	g'	59	504
	2014/02/22	g'	29	313
	2014/02/22	r'	29	402
	2014/02/22	i'	29	305
J1258+5239	2014/02/21	g'	84	479
	2014/02/22	g'	29	202
	2014/02/22	r'	29	293
	2014/02/22	i'	29	351
J1316+4452	2014/02/21	g'	83	553
	2014/02/22	g'	29	202
	2014/02/22	r'	29	163
	2014/02/22	i'	29	135

stars were used as a reference to detect variability. We have detected variability at a significance level $\alpha = 0.001$ during this observing night.

During the second night of the run, we have observed in three filters (g', r' and i'). We have obtained only 30 exposures per filter, therefore reducing the number of reference star data points and number of degrees of freedom. Nevertheless we had better quality observations and we were able to use more field stars per filter (11 in g', 15 in r' and 11 in i'), hence the reduction in the number of exposures in a given filter with respect to the first night was partially compensated by the increase in the number of comparison stars. However the test lost some power, which is a possible reason why the target does not appear variable at the significance level $\alpha = 0.001$ on every filter. The overall variability is detected at the $\alpha = 0.01$ level of significance. It is detected as variable at the significance level $\alpha = 0.001$ in the r' and i' which both have higher number of field stars and therefore higher number of degrees of freedom. The aperture used for photometry was the same as during the first observing night.

The light curves are displayed in Figure 3.5. Overall we conclude that there is a positive detection of variability.

J0843+3549 is a target with highly disturbed morphology. This irregular morphology poses a problem for the aperture photometry, which we are using in all the other cases. The target is quite extended, therefore to include it completely within the aperture is not feasible. Aperture diameter containing this target is approximately 45.6 arcsec (120 px). Such a big aperture is unsuitable for the stars. However the target, as shown in Figure 3.1, seems to be a composite of two merging targets. We focus on the brighter (southern) target. SExtractor treats the whole source as two, the tail (in north-south direction) and the quasar itself, therefore it seem sensible to use a smaller aperture enclosing only one of the targets

The aperture photometry used by SExtractor counts the pixels above the detection threshold in the given aperture. The fainter tail is above the threshold level and as the seeing varied slightly over the first half of the night, we cannot control the propagation of the light from the tail into the target we are interested in. The varying propagation of the light would introduce a higher variation of the target, which is not of physical origin.

We have tried to constrain the threshold more strictly to avoid detection of the tail. The number of pixels above the threshold was increased to discard the tail. There are numerous caveats in this approach. We are severely lowering the number of stars which SExtractor detects. On the other hand, the bright stars are saturated. Therefore we fit only three stars which are roughly comparable with the brightness of the quasar with this criteria. The aperture used in this case was 83 pixels (31.54 arcsec). To obtain the error estimate, we are fitting only three stars, which is the minimum number of stars to perform the F-test as pointed out by de Diego (2014). The asymptotic error is high in comparison with that of other targets.

As a conclusion, the resulting F statistic is very high ($F > 20$), providing very unlikely results. Comparing with the positive detections we have obtained in the other cases ($F \approx 3$) it is highly possible that there is a fluctuation caused by light propagating into the aperture, which is not of a physical origin. Therefore we refrain from drawing conclusions about this target. Due to difficulties in performing accurate photometry, the results for the second observing night are also inconclusive.

J1258+5239 was always observed during the second part of the night, when the Moon had already risen.

We have obtained 85 observations in g' filter during the first night. The aperture photometry was performed with a diameter of 34.2 arcsec (90 px). We have used seven stars from the field. Considering the number of exposures and the number of field stars, taking into account that not all of them might be present on all the images due to the dithering pattern, we have obtained in total 535 scaled down star observations used for analysis of the variability. The statistical analysis

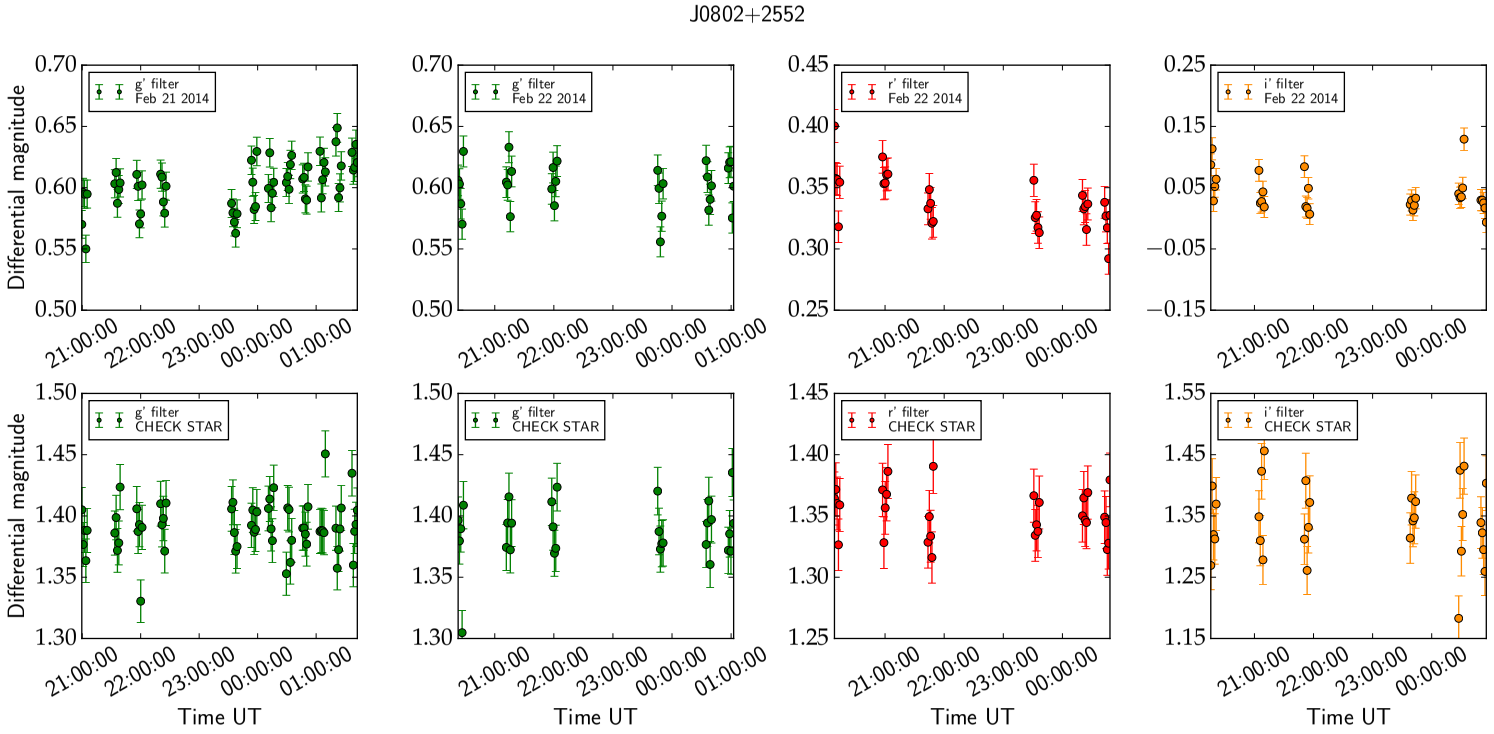

Figure 3.5: Light curve for J0802+2552 during both nights in all available filters. There is a noticeable increase in the brightness in g' filter during the first night. During the second observing night, there is a decrease in brightness in both, r' and i' filters while g' appears to be non variable. Color-coding is adopted from previous figures.

results in negative detection of variability. The asymptote of the fit has a higher value compared with other days (≈ 0.01 mag for an infinitely bright source) which reduces our ability to detect microvariability. It borders the limit we set up for a sensible analysis.

The seeing improved slightly during the second observing night, therefore we have reduced the size of the aperture to 28.5 arcsec (75 px). We have obtained 30 images in all filters. Accounting for this change with respect to the first night, following the strategy for J0802+2552, we have used more field stars (8 in g', 11 in r' and 14 in i'). The variability is detected only in i' filter, at the significance level of $\alpha = 0.001$.

Considering that the variability was detected only during one night in one filter, we conclude that there is not enough evidence to confirm variable behavior in the source. Light curves for both observing nights of J1258+5239 are shown in the figure 3.6. Although the light curve for the r' filter on the night of February 22 seems to exhibit variable behavior, a similar pattern is present in the light curve of the check star (shown in the same figure) and then, there is not enough evidence for microvariations during our observations.

The presence of the Moon during the observations might have affected the sensitivity of the test. As moving towards the red part of the spectrum, the sensitivity of the filter to the Moon decreases, and then the lack of detections in g' and r' filters might be due to the moonshine. As it can be seen from the fits, the asymptote in both filters is significantly higher in comparison with the Moon-less observations of J0802+2552. The variability can be therefore lost due to the lack of sensitivity.

J1316+4452 was observed during the second half of the nights, with the same conditions of lunar illumination as J1258+5239. Aside from our targeted source, there is a galaxy present in the field of view, southeast from the target (as seen in Figure 3.1). It is of roughly similar brightness as our target. It is classified as a broad line galaxy in SDSS-III (Eisenstein et al. 2011). We have applied the same statistical tests on the galaxy as on the target, to see if the galaxy is also variable on the short time scale or not.

During the first observing night, we have obtained 84 images of the field (hence 84 observations of both, targeted type 2 quasar and accompanying galaxy) in g' filter. We used 9 stars in the field for scaling. The total number of stars we have used for scaling was 580. Aperture photometry was measured within a diameter of 22.8 arcsec (60 px). The enhanced F-test on both, accompanying galaxy (J1316+4452b) and J1316+4452 itself results in negative detection of microvariability.

We have followed the same strategy as for the other targets and during the second observing night, we were circulating g', r' and i' filters. We have obtained 30 exposures of the target in each filter. In general there are not many comparison stars accompanying the quasar and the galaxy. However in this case, we were able to use 9 stars in g', 8 in r' and 9 in i' filters. As the seeing improved compared to the first night, we have used an aperture of diameter 20.8 arcsec (55 px). The statistical analysis result in detection of variability at the significance level $\alpha = 0.001$ in both, broad-line galaxy and the type 2 quasar. Broad line galaxies were previously detected as variable sources on small scales (e. g. de Diego et al. 1998). Both light curves are displayed in figures 3.7 and 3.8 (respectively).

As in the case of J1258+5239, the observations were carried out in the presence of the Moon. As the only filter where we fail to detect variability is g', which is sensivite to the Moon shine, it is possible that the sources are indeed variable and the variability is not prominent enough to be detectable in g' filter. Therefore we conclude that the source is probably variable as well as the accompanying broad-line galaxy.

3.6 Discussion

In this campaign, we have observed four type 2 quasars during two nights in February 2014 with the Nordic Optical Telescope located at the Roque de Los Muchachos observatory on La Palma,

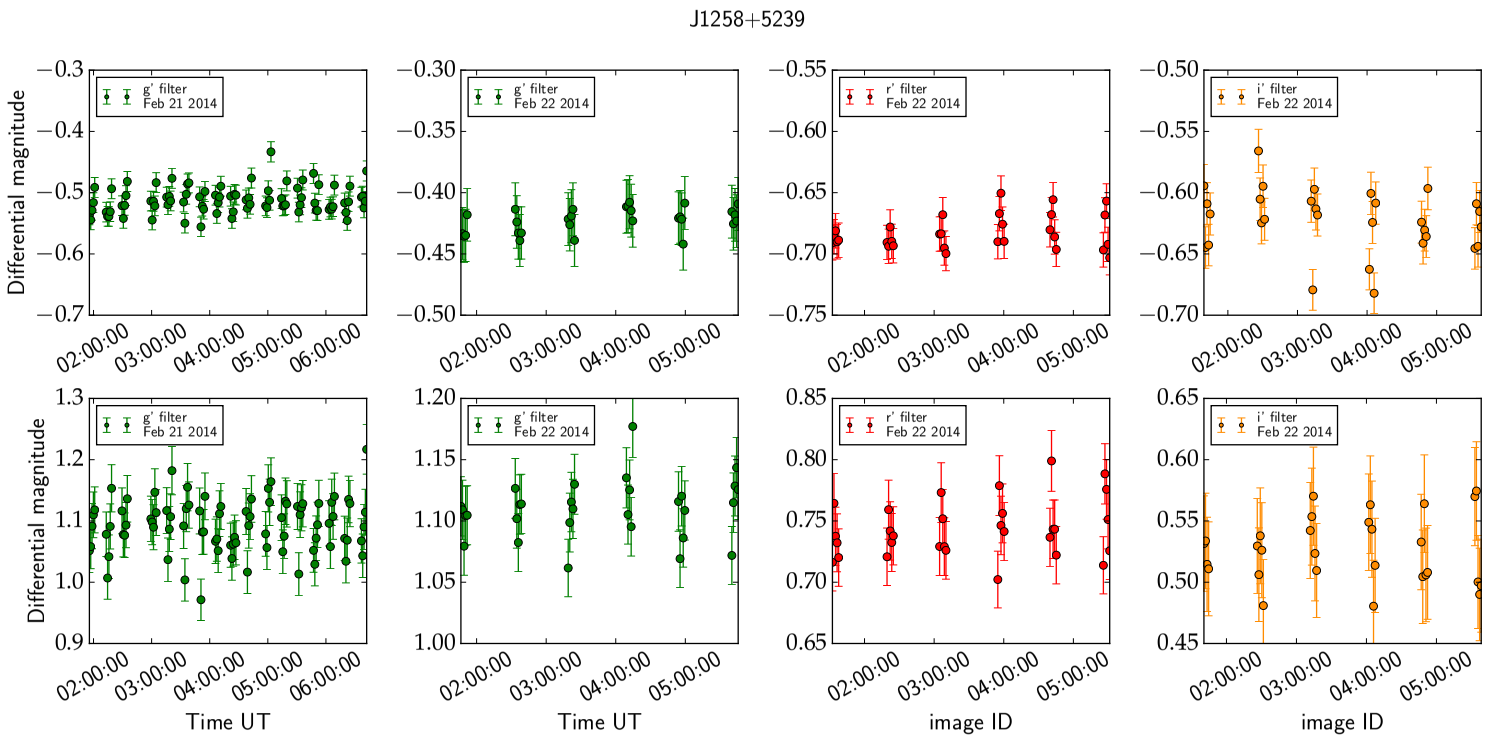

Figure 3.6: Light curve for J1258+5239 during both nights in all available filters. Variations were reported for February 21 with 1% significance level. The seemingly variable behavior in the r' filter is present in all the sources during the given night, independent on the comparison star used for differential photometry, therefore we can conclude it is not a real variation, which is indeed confirmed by the F-test.

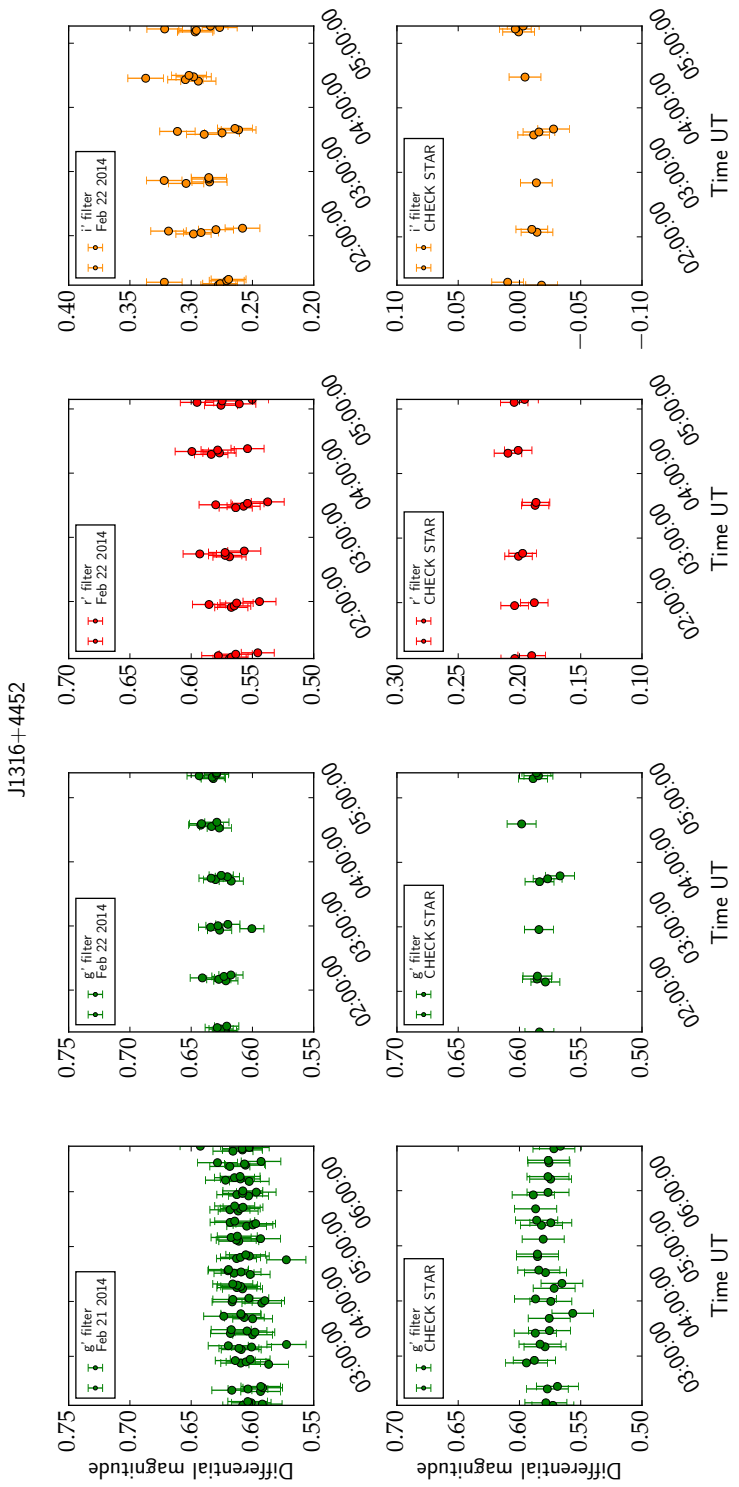

Figure 3.7: Light curve for J1316+4452 during both nights in all available filters. We have detected microvariations at the 1% significance level in the i' filter. There are fewer observations of the check star, which is the result of the dithering pattern in combination with few stars in the field.

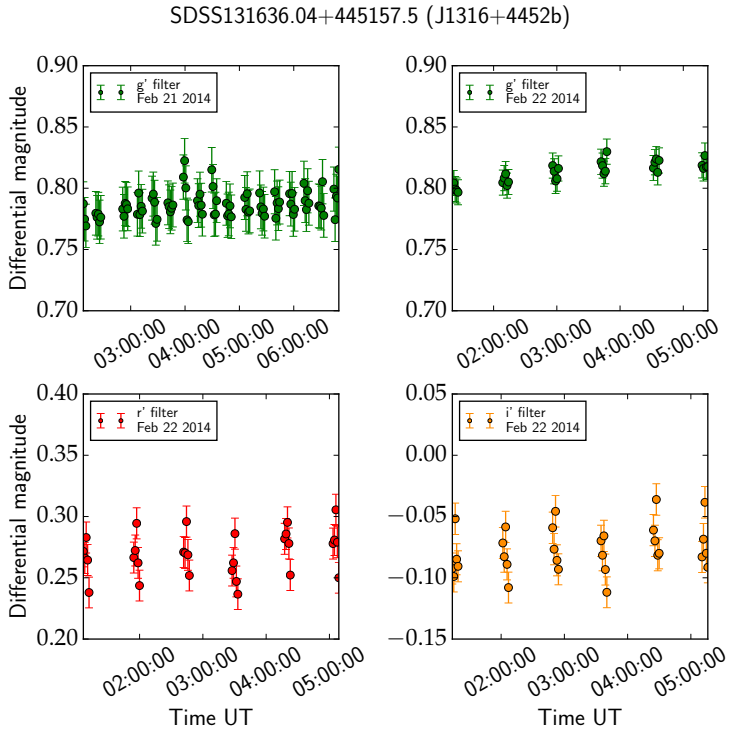

Figure 3.8: Light curve for the broadline galaxy J1316+4452b. The galaxy was observed in all the images obtained for the target, regardless of the dithering. There were no statistically significant variations detected during any of the nights or in any filter. The check star figures are the same as in the previous figure.

Canary Islands. Although we have not initially focused on the morphology, it should be noticed that two of our targets have highly disturbed morphologies (Figure 3.1 Panels a and b), pointing towards recent merging events. We have detected microvariability on a time scale less than 4 hours in one target (J0802+2552) in all filters at the 0.001 significance level during both observing nights, in J1258+5239 (in i' filter) and J1316+4452 (in r' and i' filter) with 0.001 significance level only in the second observing night. In the cases of J1258+5239 and J1316+4452, the Moon was present during the observations, which probably resulted in lessening the sensitivity of the g' and possibly r' filter. As the phenomenon we are detecting is very fine, the smallest contribution from the Moon are likely affecting the observations.

J1258+5939 was detected as variable only in one filter and therefore we conclude there is not enough evidence for microvariability, J1316+4452 was detected as variable with a level of significance 0.01 in two filters, the negative detection is consistent in g' filter which is affected by the Moon more than the i' and r'. Therefore we conclude the target is probably variable. We are not drawing conclusions on one of the targets (J0843+3549) since the analysis was impossible due to the complex morphology of its host galaxy.

Optical microvariability in type 2 quasars is a phenomenon previously unaccounted for. It is hard to observe short time scale variability in this kind of objects since our view to the central engine is supposed to be blocked by the dusty obscuring torus.

A possible explanation of this phenomenon might lie in the misclassification of the targets, caused by the insufficient quality of the spectra used for analysis. Such misclassification can be addressed by infrared data as studied by Chen & Shan (2009). They suggested that the population of type 2 quasars might be divided into a group of true type 2 quasars without any underlying broad line regions and heavily obscured type 1 quasars, based on the infrared color-color diagram. the study by Chen & Shan (2009) showed that 43% of type 2 quasars are dominated by a thermal spectrum, while the rest is following a power law, pointing out a non-thermal origin of the emission, which bears a similarity with type 1 quasars. Out of our studied sample, one target (J13116+4452) falls into the power law group. This target is detected as probably variable which is consistent with the results of microvariability detections in type 1 sources (e. g. Fitch et al. 1967; Paliya et al. 2013). Such result hints that the belonging to the power law group, based on the infrared color, might have an effect on microvariability detection. Drawing conclusion based on one source is however not reliable and we would need a larger sample to confirm the hypothesis.

The only target in which we have detected microvariability during both nights in all filters stands out in the sample at first sight because of its morphology. Since all our targets are selected based on the SDSS catalog, we were able to check the morphology types based on citizen science projects Galaxy ZOO and Galaxy ZOO2 (Lintott et al. 2011; Willett et al. 2013). All our targets have been classified by more than 30 Galaxy ZOO users. In the first iteration, J1258+5239 is the only one which reaches the reliability threshold for the classification. It is classified as spiral galaxy, while the other two (J0802+2552 and J1316+4452) are uncertain. the second iteration of the morphology classification marked J1316+4452 as a spiral with a bulge and medium winded arms with notable irregularity, while J0802+2552 was marked as an irregular elliptical with many votes in favor of a merging state. However since our sample is very small, it would be premature to draw conclusions on a relation between the detection of microvariability and the morphology.

The physical processes lying behind the microvariations are difficult to determine as there are not many reports of similar phenomena to this date. Recent studies dedicated to rapid variations are directed mostly on local AGNs in X-ray (Risaliti et al. 2005, 2009). Risaliti et al. (2009) observe changes on the time scales of hours in NGC 1365, a Seyfert 1.8 galaxy. They report a transition from the reflection dominated source to increase in the 7-10 keV emission in $\sim$ 10 hours. The authors propose that the variations are due to the rapid changes in the absorbing column density along the line of sight. Although we cannot confirm such behavior in our target, as we have no X-ray data available, we cannot rule out the possibility of a similar behavior in our case. Detected microvariations in the optical regime would fall into the gaps where there is no Compton-thick clouds

obscuration. We can assume that such change would be reflected in the optical spectra, although to the best of our knowledge, there was no rapid optical spectroscopic follow-up performed on NGC 1365. Changes in the spectrum were not reported in our microvariable target either. In such case, the variability is not necessarily intrinsic.

On the other hand, microvariability is common in the unobscured targets. If it is intrinsic to the source itself, it is visible when the central engine is visible along our line of sight. Given the orientation of obscured sources, we would see the central engine only if the obscuring medium is clumpy as proposed by e. g. Nenkova et al. (2008). Nevertheless we do not have enought data to test whether the variations are intrinsic and might favor the clumpy scenario or not.

Chapter 4

Comparative study of optical variability in radio loud and radio quiet quasars

Based on the study published by de Diego et al. (1998), we have revisited the sample of type 1 AGNs previously studied for microvariability. The sample was studied extensively, but never on the basis of variability in the observations with weekly cadence. In fact, comparing variability in radio loud versus radio quiet sources was not previously done on a weekly time scales, therefore this is the first project taking it into account. In the present study, the sample was observed during two semestral campaigns in 2013 - 2014.

4.1 Sample selection

Selection of the sample for the monthly variation campaign was based on the previously published works by de Diego et al. (1998) and Ramírez et al. (2004), which were focused on the differences between the core dominated radio loud quasars (CRLQ) and radio quiet quasars (RQQ) on short time scales (microvariability). CRLQs were chosen since they are a more homogeneous subset than radio loud quasars due to assumed orientation and if the variations arise from the jet, CRLQs will present boosted variations which would be easier to detect than in 'lobe-cominated' radio quasars. Moreover all the observed quasars are $mag_{\mathrm{V}} \leq 17$, so that the desirable signal to noise ratio can be reached. The sample was chosen, so the targets form CRLQ - RQQ pairs. The pairs share approximately the same redshift and brightness to avoid selection effects which might bring an undesirable bias. The most notable effect arising from observing targets of different redshifts is a correlation between the amplitude variations and redshift (e.g. Nair 1997) which can be accounted for observing different spectral regions in the rest frames of the quasars. An anti-correlation between the amplitude and the luminosity of the objects (Netzer et al. 1996) is also reported. Therefore by pairing targets with similar properties, we are avoiding the most obvious sources of bias known. For the presented study, a subsample of 10 pairs from the de Diego et al. (1998) is chosen. Four of the chosen quasars are variable on short time scales, one is possibly variable and one has a dubious variability detection. The sample and its basic properties, along with the information about the microvariability, are described in table 4.1.

4.1.1 Observations

The sample was observed during two semesters, 2013B and 2014A (July 2013 - June 2014, with a short winter break), for 90 hours within each. The observations were realized using the RATIR

Table 4.1: Overview of the pairs of RQQs and CRLQs observed for the two semesters long campaign on San Pedro Mártir observatory in México. The pair IDs are following the IDs set up by de Diego et al. (1998).The informations about microvariability come from de Diego et al. (1998); Joshi et al. (2012); Goyal et al. (2013). RQQs are the first elements of each pair.

Pair ID	Target	RA [hh mm ss]	Dec [hh mm ss]	Vmag	z	microvariability
6	US 737	09 35 02	+43 31 12	16.3	0.456	Y
...	PKS 1103-006	11 06 31	-00 52 52	16.4	0.426	Y
8	CSO233	09 39 35	+36 40 01	17.0	2.030	N
...	PKS 1022-102	10 24 56	-10 31 44	17.0	2.000	N
9	CSO21	09 50 45	+30 25 19	17.0	1.190	N
...	PKS 1127-14	11 30 07	-14 49 27	16.9	1.187	N
10	TON 156	13 21 16	+28 47 19	16.6	0.549	Dubious
...	PKS 1327-21	13 30 07	-21 42 04	16.7	0.528	N
11	TON 133	12 51 00	+30 25 42	17.0	0.650	Possible
...	3C 281	13 07 53	+06 42 13	17.0	0.599	N
13	E 0111+388	01 13 54	+39 07 45	16.6	0.234	Y
...	PKS 2247+14	22 50 25	+14 19 50	16.9	0.237	N
14	Mrk 1014	01 59 50	+00 23 41	15.6	0.163	N
...	PKS 2349-01	23 51 56	-01 09 13	15.3	0.173	Y
15	Q0050-253	00 52 44	-25 06 51	16.1	0.626	N
...	PKS 2243-123	22 46 18	-12 06 51	16.4	0.630	N
16	US 3150	02 46 51	-00 59 31	16.8	0.467	N
...	PKS 0003+15	00 05 59	+16 09 49	16.4	0.450	Y
17	US 3472	02 59 38	+00 37 36	16.6	0.532	Y
...	PKS 0122-042	01 24 34	-04 01 05	17.0	0.561	N

Table 4.2: Number of observations in separate filters, observed during the total of 180 hours of observation campaign in San Pedro Mártir

	Number of observations		
Target	g' filter	r' filter	i' filter
US 737	6	5	6
PKS 1103-006	5	5	6
CSO 233	5	5	5
PKS 1022-102	4	4	4
CSO 21	5	5	n/a
TON 156	17	15	17
PKS 1327-21	5	4	4
TON 133	6	8	8
3C 281	4	4	4
E 0111+388	13	13	13
PKS 2247+14	10	11	10
Mrk 1014	10	11	12
PKS 2349-01	13	15	16
PKS 2243-123	12	12	12
US 3150	10	11	11
PKS 0003+15	8	8	8
US 3472	7	7	6
PKS 0122-042	8	8	7

instrument mounted on the Harold L. Johnson 1.5 m telescope located at Observatorio Astronómico Nacional in Sierra San Pedro Mártir, Baja California, México. The RATIR instrument consists of four detectors, two optical and two near-infrared, which are observing the targets simultaneously (see Figure 4.1). The telescope is described in a greater detail in Butler et al. (2012). C0 and C1 detectors are Fairchild 3041 CCDs with a field of view of 5.4 arcmin^2. By default, the detectors are used in 2x2 binning, which gives 0.32 arsec pixels. C2 and C3 are HAWAII-2RG detectors. C2 has a 1.7 μm cut-off, pixel scale 0.30 arcsec and a field of view of about 10 arcmin^2. There is a split filter installed on the detector in a N-S direction, splitting the image between WFCAM Z and Y filters. C3 is of a similar design, with a cut-off at 2.5 μm. The split filter close to the focal plane images the eastern half of the detector in MKO J and the western half in MKO H. Nevertheless given the fact that the C3 detector, covering J and H channels provided only partial functionality, we have not used the near-infrared observations. We have analyzed the data from the optical detectors C0 and C1. C0 observes the targets in SDSS u', g' and r' filters, while C1 is dedicated solely to SDSS i' filter observations. Unfortunately the sensitivity of the u' filter is poor and therefore we refrain from using the u' filter data.

For each given night, the targets were observed five times in each of the u', g', r' filters. The i' filter was observed simultaneously, hence yielding in 20 observations in i filter for the given target per night. The i' filter showed a significant shift after each set of 10 exposures, resulting in target being no longer in the field, therefore only 10 images per i' filter were on target and hence useful for our campaign. The exposure time for each target was set to 80 seconds. The overview of the final number of observations in each filter is provided in 4.2.

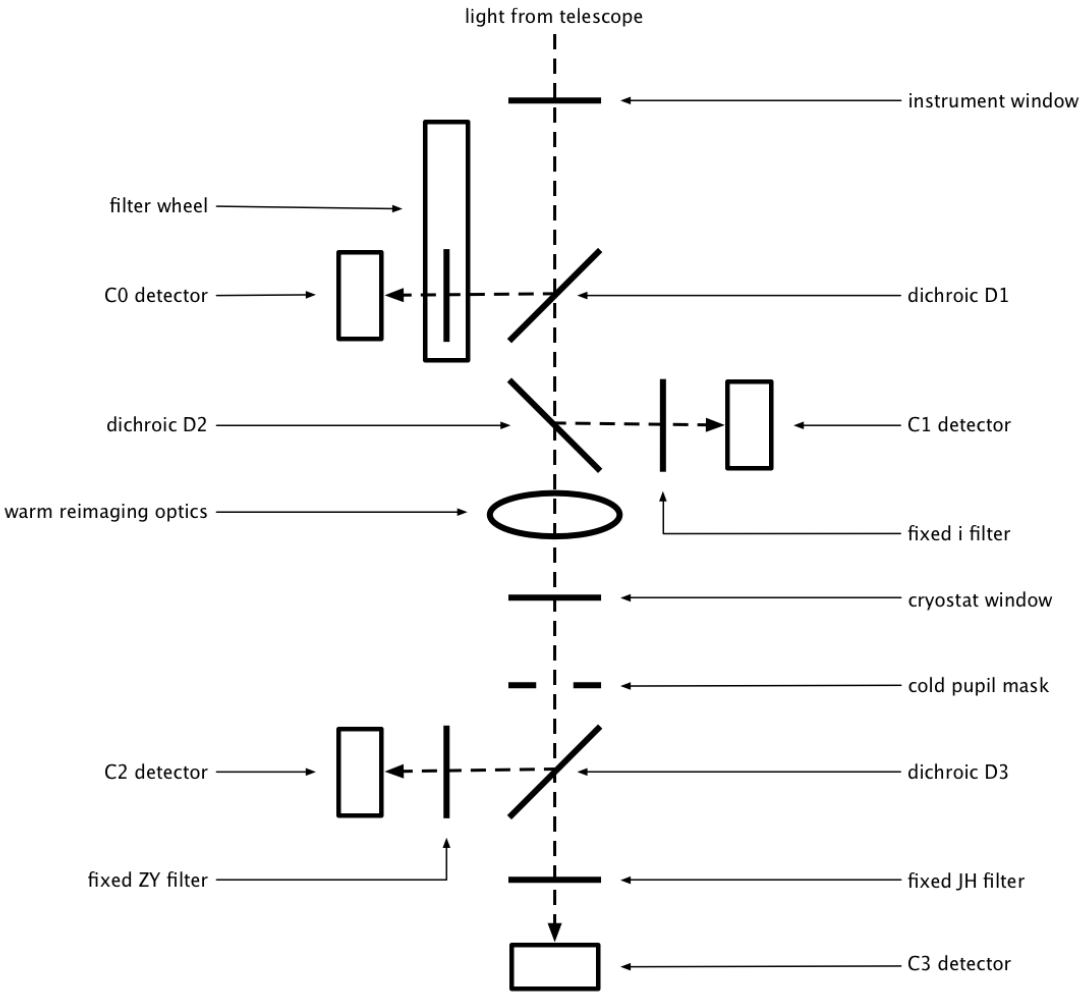

Figure 4.1: The schematic of the RATIR instrument mounted on OAN/SPM 1.5-meter Johnson robotic telescope.

4.1.2 Data reduction

The bias subtraction and flat-fielding was performed using standard procedures in IRAF. There is an unexpectedly high dark current in the C0 detector, which resulted in a pattern over the fields, therefore we had to subtract also the dark frames, which was done also via the standard IRAF tasks. The telescope itself, even though it is a robotic one, meets with some pointing problems, mainly the slight shift in right ascension during the observations. On top of that, the obtained fits files lacked the astrometry information in the header. In order to solve this, we have used astrometry.net[1] (Lang et al. 2010) software on all of our images, matching the positions of the targets with the USNO-B1.0 catalog. As a result, we obtained images with correct headers which could further be stacked using the SWarp software[2] (Bertin et al. 2002) which automatically computes the shifts, based on the information provided in the header, modified by the astrometry.net software. We stacked astrometrized images for each night, hence each stacked image consists of five images (ten in the case of $i'filter$) taken during one night.

The stacked fields were not centered at the same position, so the targets did not appear on the same positions on every image. We decided to follow the approach from the NOT campaign, where we have used the Astromatic softwares SExtractor (Bertin & Arnouts 1996) version 2.8.6 and SCAMP 2.0.4 (Bertin 2006), which directly uses output from SExtractor. At first, we run SExtractor to find an ideal aperture for all the fields, so during the first run of SExtractor, we have computed photometry for different apertures, ranging from 3.2 to 22.4 arcsec (10 to 70 pixels). We have plotted the evolution of the brightness of several brightest stars on the image in every day. The aim was to use a uniform aperture on all the fields. In most cases, an aperture of 30 px captures all the light. The cases where we would need larger apertures are flagged and not used for further analysis as they frequently coincide with very low quality images or increased full width half maximum (FWHM). A sample is shown in Figure 4.2.

In order to obtain a catalog for each field, we used SCAMP. SCAMP takes an input from SExtractor, with one chosen aperture and provides a catalog with the positions of the stars in every field, which allowed us to align the images for further analysis. We have matched the images using USNO-B2.0 catalog. Resulting catalogs were matched using TOPCAT (Taylor 2005)[3].

In most cases, TOPCAT matches the catalogs without problem, with a maximum offset of 0.001 pixels in Cartesian coordinates. However the matched catalog needs supervision as in some cases the astrometry of the field is not precise and therefore needs to be added manually.

4.1.3 Analysis

The light curves we obtained during the campaign consist of 4 to 17 data points per light curve. Even though the images were stacked to gain higher signal-to-noise ratio, the majority of the detected stars are very faint, especially in g' filter. There are rarely more than 3 stars to compare with the quasar. We have taken the lead from the Figure 1.21, which suggests that in such case, the Bartels test is the best option for analysis. As already mentioned in Section 1.3.2.4, Bartels test is used to examine whether a sequence of n data occurred in random order or not. Given the small number of observations, we cannot assume anything about the underlying distribution. Bartels test is a non-parametric test which suits our needs in this case. However when computing the test statistic

$$RVN = \frac{\sum_{i=1}^{n-1}(R_i - R_{i+1})^2}{\sum_{i=1}^{n}(R_i - \bar{R})^2}, \tag{4.1}$$

[1] Available at `http://astrometry.net`.
[2] `http://www.astromatic.net/software/swarp`.
[3] Tool for OPeration on Catalogues And Tables (`http://www.star.bris.ac.uk/ mbt/topcat/`).

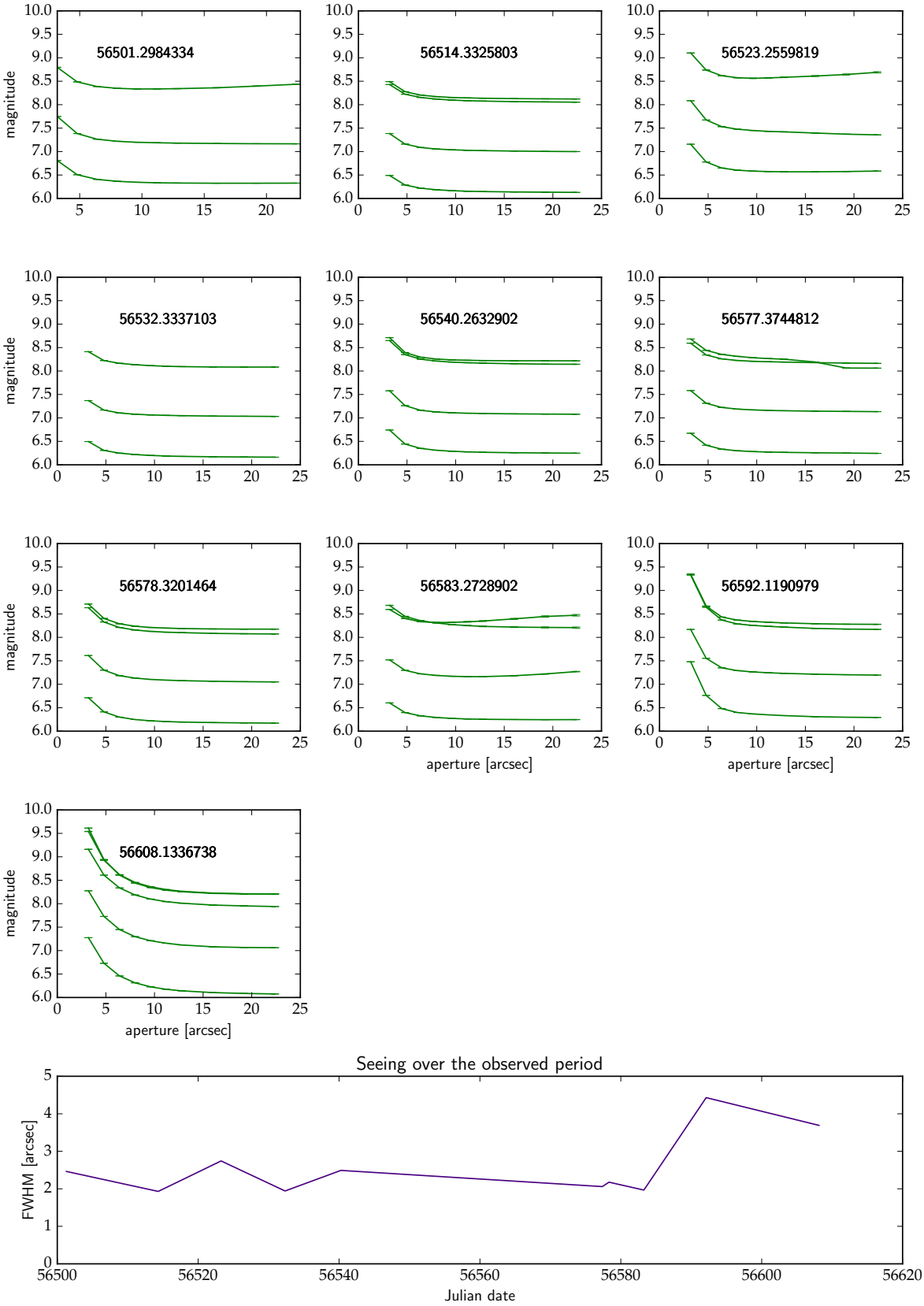

Figure 4.2: Check plots for PKS 0003+15 in g' filter, with modified Julian date. At 9.6 arcsec aperture, the brightness gets relaxed. In this case, the last image MJD=56608.1336738 was flagged as the quality of the image is noticeably lower and we would need a bigger aperture to include all the light from the stars. In the lower panel, we plotted the evolution of the FWHM during the campaign.

the assumption is such that the sample is large, with a number of observations $n > 10$. We are using R code (R core team 2013) to analyze the light curves. Bartels test is a part of R package 'lawstat'. The R native version of the Bartels test assumes large sample. For a smaller sample the probablilities have discreet value depending on the sample size and their order. RVN is normally distributed with mean 2 and variance

$$\sigma^2 = \frac{4(n-2)(5n^2-2n-9)}{5n(n+1)(n-1)^2}. \tag{4.2}$$

Then RVN $\overset{H_0}{\sim} N(2, \sigma^2)$ so the normal statistic is computed as

$$z = \frac{RVN - 2}{\sigma}. \tag{4.3}$$

The original R package for Bartels test computes statistic as $\sqrt{n}(RVN-2)/2$. Given equation 4.2 and 4.3, we made adjustments to the native function in R and used the normal statistic. We have cross checked the observed fields with the 2MASS catalog of extended sources as well as with AAVSO's 'The International Variable Star Index' VSX database to avoid extended sources and variable stars in differential photometry. Excluding the extended sources and variable stars, we have chosen the three brightest stars present on the fields during all observations. We performed all possible combinations of differential photometry using the three stars and choose the final comparison star based on the difference between the extreme points of the stars' light curve. We selected the stars whose difference was smallest. The chosen star was then used for the differential photometry of the quasar.

Using this method, we were able to reveal low quality images as they appeared as outliers, which were too extreme to be of physical origin. The occurrence of these outliers usually corresponds to less than 4 images combined with SWarp.

We have observations in three filters available and it is highly unlikely that the phenomenon would be constrained only to one filter. We are testing the null hypothesis three times, one for each filter. In such cases, the problem of multiplicity arises from the fact that as we increase the number of hypotheses being tested, we are then increasing the likelihood of type I errors (incorrect rejection of the null hypothesis). Such problem is solved by using Bonferroni correction. The Bonferroni correction is addressing the problem of testing N hypotheses, while maintaining the family wise error rate (the probability of making one or more false discoveries, or type I errors, among all the hypotheses when performing multiple hypotheses tests). It tests each individual hypothesis at a statistical significance level of $1/N$ times instead of N times, which is required by an individual testing.

4.2 Results

In all but one case, we obtained observations in three filters, therefore the level of significance is $\alpha' = \alpha/3$. The probability that k of N tests yields a rejection of the null hypothesis at the significance level of α' under the assumption that the null hypothesis holds, is

$$\alpha' C(N,k) p_c^k (1-p_c)^{N-k}, \tag{4.4}$$

where

$$C(N,k) = \frac{N!}{[k!(n-k)!]} \tag{4.5}$$

is the combination of k elements from a set of N elements. In our case $k \in \{0,1,2,3\}$ and $C(3,k) = 1,3,3,1$. Given the size of our sample, it is needed to compute the discrete p-value. The computation

Table 4.3: Results of the Bartels test.

		g' filter		r' filter		i' filter		
Pair	Target	p-value	Var?	p-value	Var?	p-value	Var?	Radio loudness
6	US 737	0.5	N	0.56	N	0.59	N	RQQ
...	PKS 1103-006	0.61	N	0.95	N	0.68	N	CRLQ
8	CSO233	0.24	N	0.14	N	0.25	N	RQQ
...	PKS 1022-102	0.03	probably	0.39	N	0.85	N	CRLQ
9	CSO21	0.04	probably	0.39	N	n/a	n/a	RQQ
...	PKS 1127-14	n/a	n/a	n/a	n/a	n/a	n/a	CRLQ
10	TON 156	0.12	N	0.47	N	0.007	Y	RQQ
...	PKS 1327-21	0.5	N	0.61	N	0.39	N	CRLQ
11	TON 133	0.09	N	0.56	N	0.31	N	RQQ
...	3C 281	0.61	N	0.86	N	0.39	N	CRLQ
13	E 0111+388	0.01	probably	5e-05	Y	3e-04	Y	RQQ
...	PKS 2247+14	0.11	N	0.78	N	0.06	N	CRLQ
14	Mrk 1014	5e-03	Y	7e-03	Y	0.01	probably	RQQ
...	PKS 2349-01	0.02	probably	3e-04	Y	2e-03	Y	CRLQ
15	Q0050-253	n/a	n/a	n/a	n/a	n/a	n/a	RQQ
...	PKS 2243-123	0.06	N	0.06	N	0.05	probably	CRLQ
16	US 3150	0.36	N	0.02	probably	0.34	N	RQQ
...	PKS 0003+15	0.03	probably	0.06	N	0.03	probably	CRLQ
17	US 3472	0.09	N	0.37	N	0.31	N	RQQ
...	PKS 0122-042	0.79	N	0.05	probably	0.31	N	CRLQ

Table 4.4: Contingency table for the results of variability of the quasars.

	RQQ	CRLQ	Sum
Variable	2	3	5
Not variable	7	6	13
Sum	9	9	18

of the discrete critical p-value p_c can be done using the R function *uniroot* (R core team 2013). The critical values for the level of significance $\alpha = 0.001$ for 1, 2 and 3 detections are $p_c = \{1e-04, 0.011, 0.069\}$ respectively.

The results from analysis of the final light curves are summarized in Table 4.3, while the light curves are plotted in the Figures 4.3 - 4.7.

Given the p-values from the Bartels test, using the Bonferroni correction at the significance level $\alpha = 0.001$ we see that all three p-values are below the critical value in five cases; E 0111+388, Mrk 1014, PKS 2349-01, PKS 2243-123 and PKS 0003+15. Based on the radio loudness of the target, we can write down the results into a contingency table (see Table 4.4). Two targets out of the sample had too few observations (PKS 1127-14 and Q0050-253) and therefore were excluded from the further analysis. That reduces the number of the targets in the final sample to 18.

In order to analyze the contingency table, we used Fisher's exact test, which is designed especially for small samples. Although it is possible to compute Fisher for a $2x2$ matrix by hand, there is a R routine *fisher.test* which allowed us to compute the exact p value, for two tailed case. With the result $p \sim 1$, the association between groups and outcomes is not statistically significant.

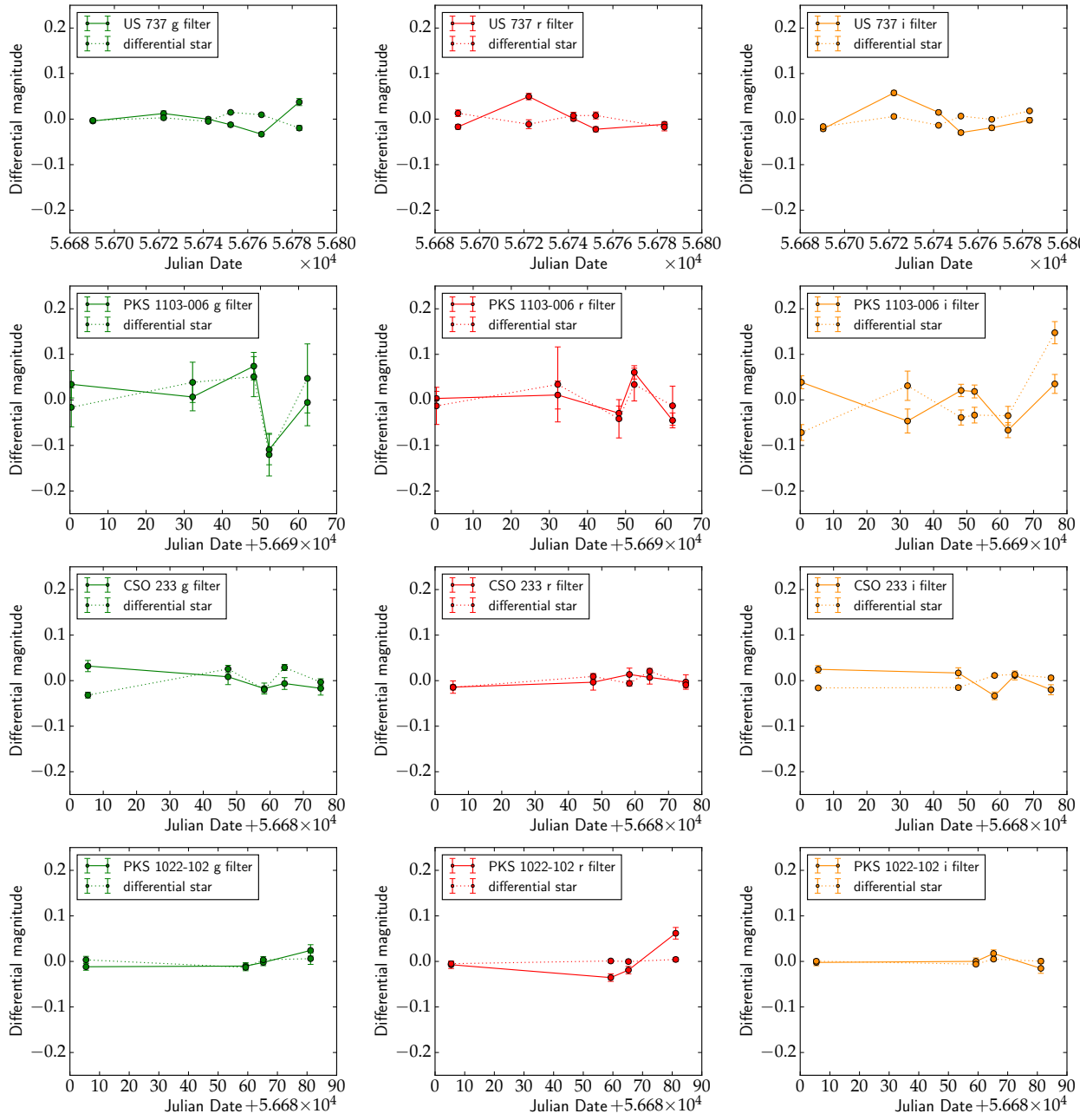

Figure 4.3: Light curves observed in the year long RATIR campaign with optical filters. The colors correspond to g' green, r' red and i' orange. The differential magnitude was adjusted by a constant to fit the star and the AGN in the same plot for a direct comparison. The differential magnitude interval was adjusted to 0.5 mag for a direct comparison.

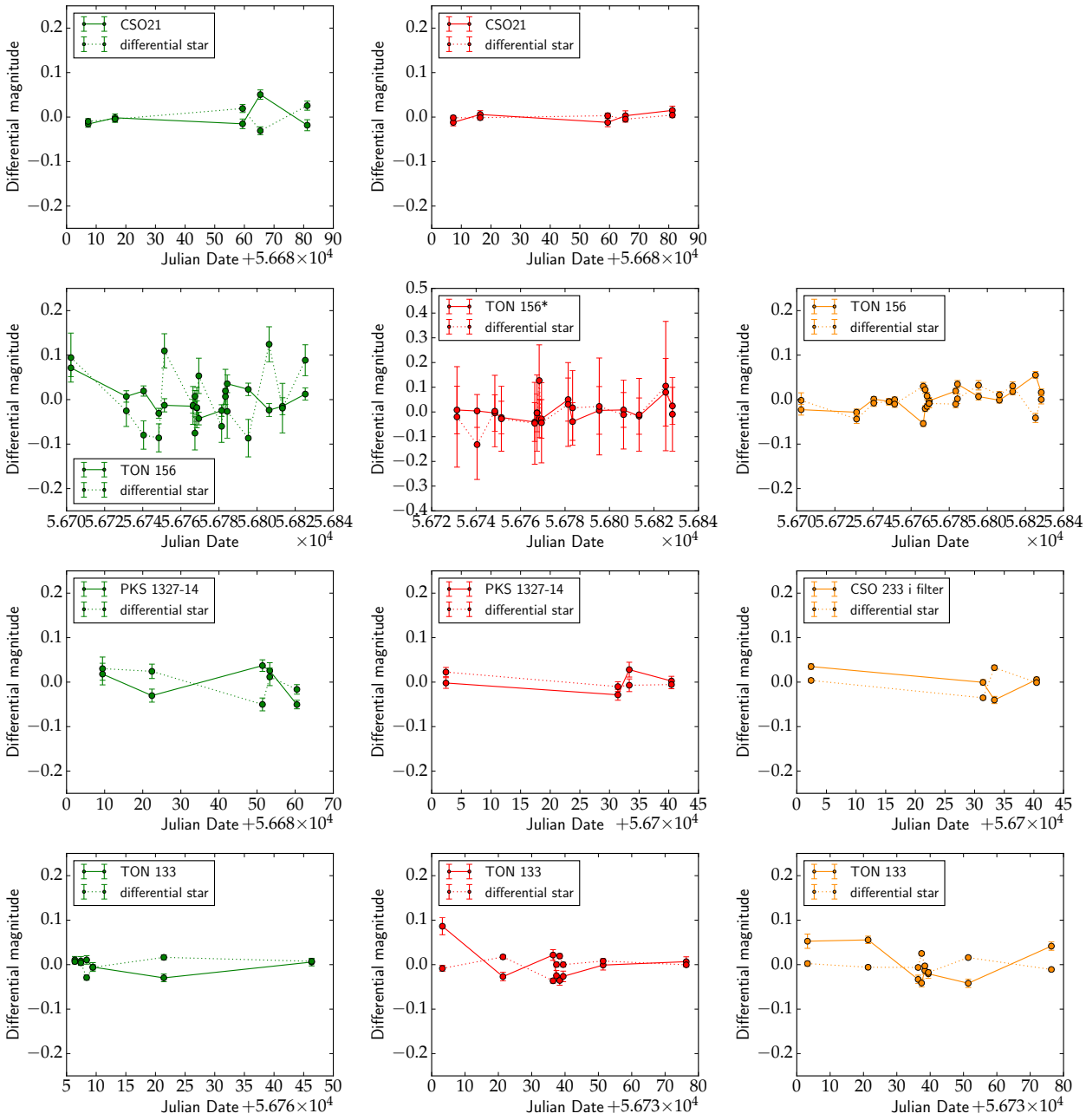

Figure 4.4: Light curves observed in the year long RATIR campaign with optical filters. The colors correspond to g' green, r' red and i' orange. The differential magnitude was adjusted by a constant to fit the star and the AGN in the same plot for a direct comparison. The differential magnitude interval was adjusted to 0.5 mag for a direct comparison. CS021 does not have enough data points for a light curve in i' filter and therefore the light curve is missing. r' filter of TON 156 observation spreads over 0.9 mag to capture the errors of photometry which are unusually large in this case.

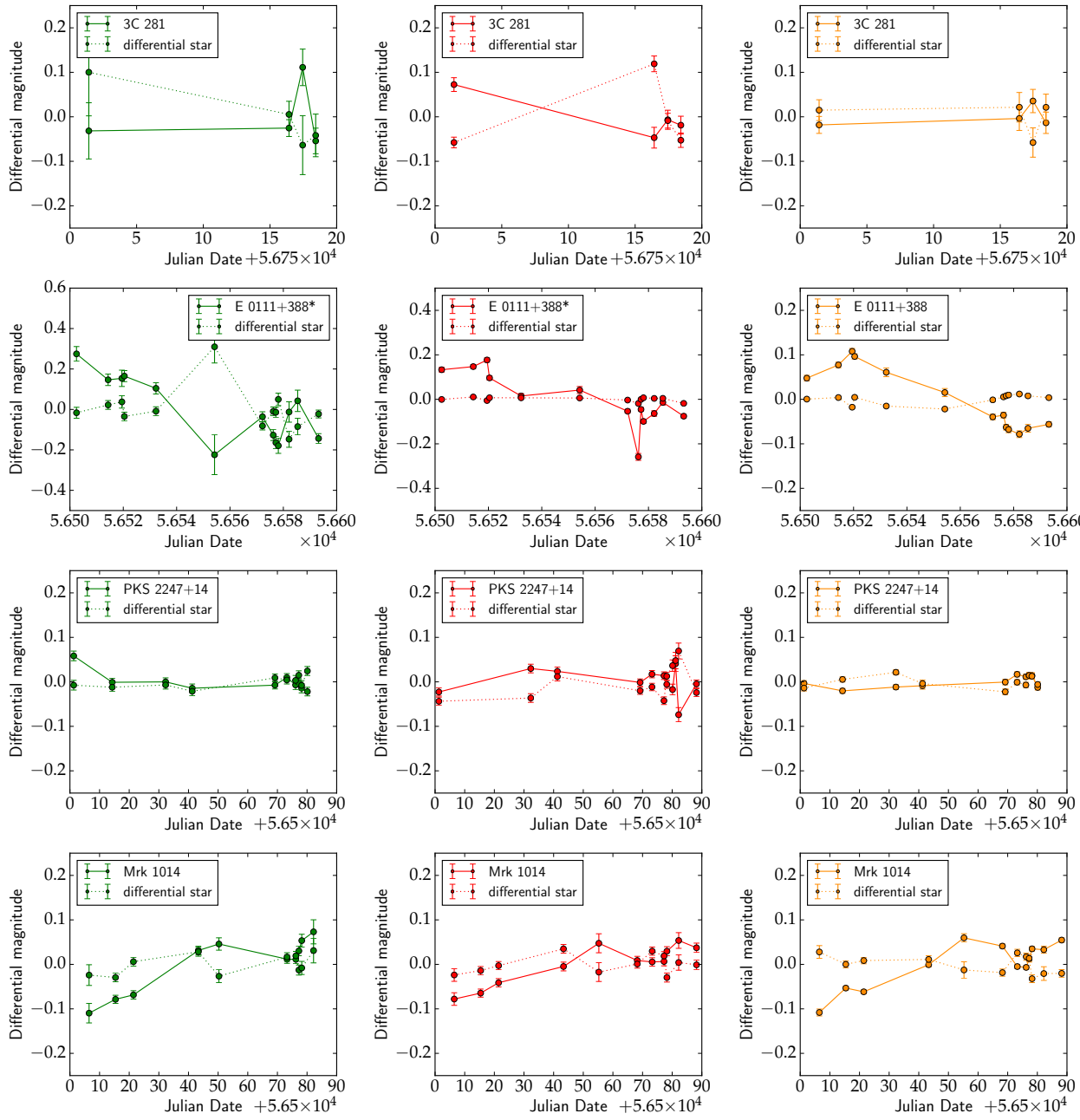

Figure 4.5: Light curves observed in the year long RATIR campaign with optical filters. The colors correspond to g' green, r' red and i' orange. The differential magnitude was adjusted by a constant to fit the star and the AGN in the same plot for a direct comparison. The differential magnitude interval was adjusted to 0.5 mag for a direct comparison. E 0111+388 and Mrk 1014 are variable sources. * g' and r' filters in E 0111+388 are plotted in differential magnitude interval of 1.1 and 1 mag respectively due to the noticeable change of brightness.

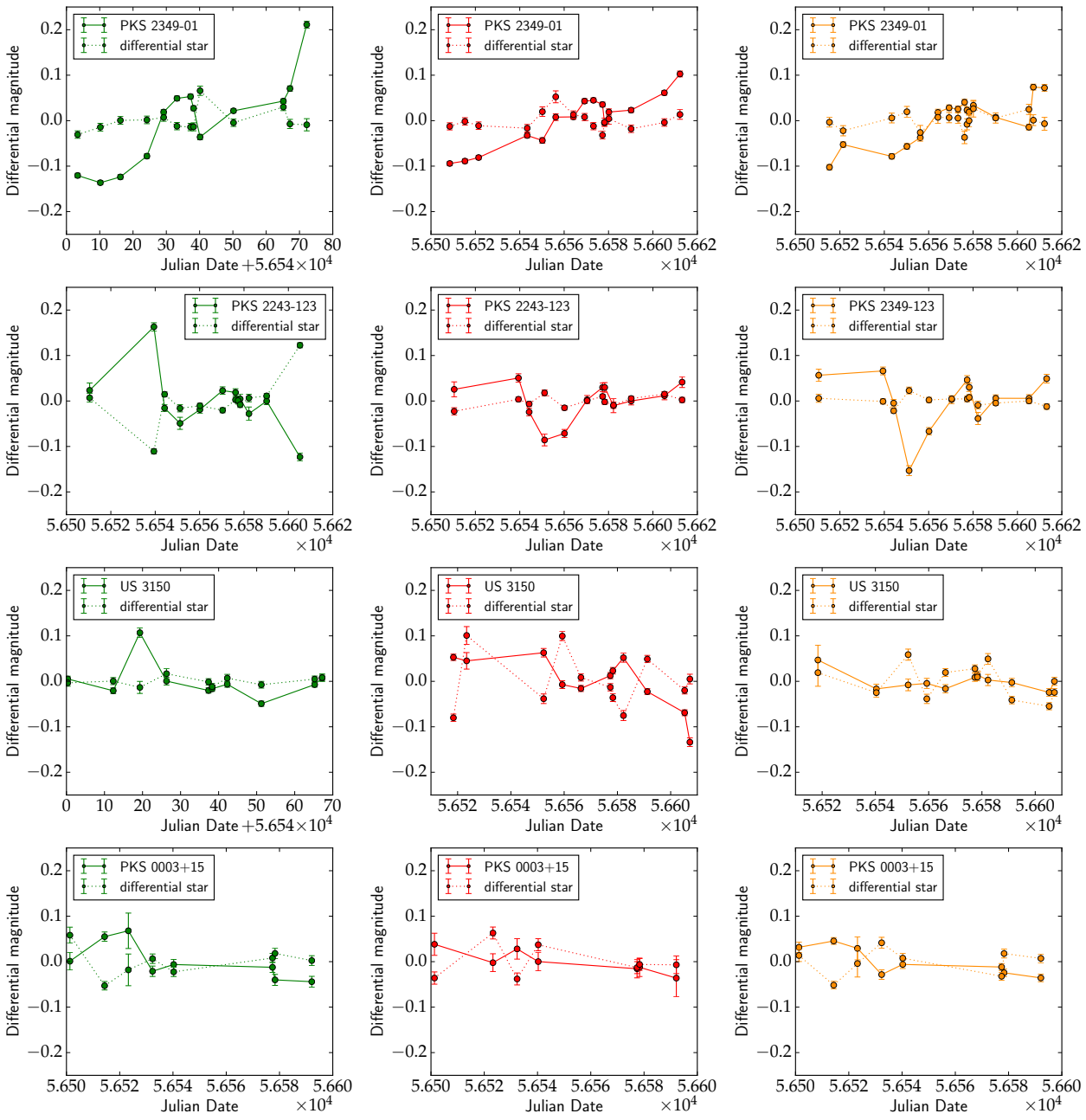

Figure 4.6: Light curves observed in the year long RATIR campaign with optical filters. The colors correspond to g' green, r' red and i' orange. The differential magnitude was adjusted by a constant to fit the star and the AGN in the same plot for a direct comparison. The differential magnitude interval was adjusted to 0.5 mag for a direct comparison. Targets PKS 2359-01, PKS 2349-123 and PKS 0003+15 are detected as variable.

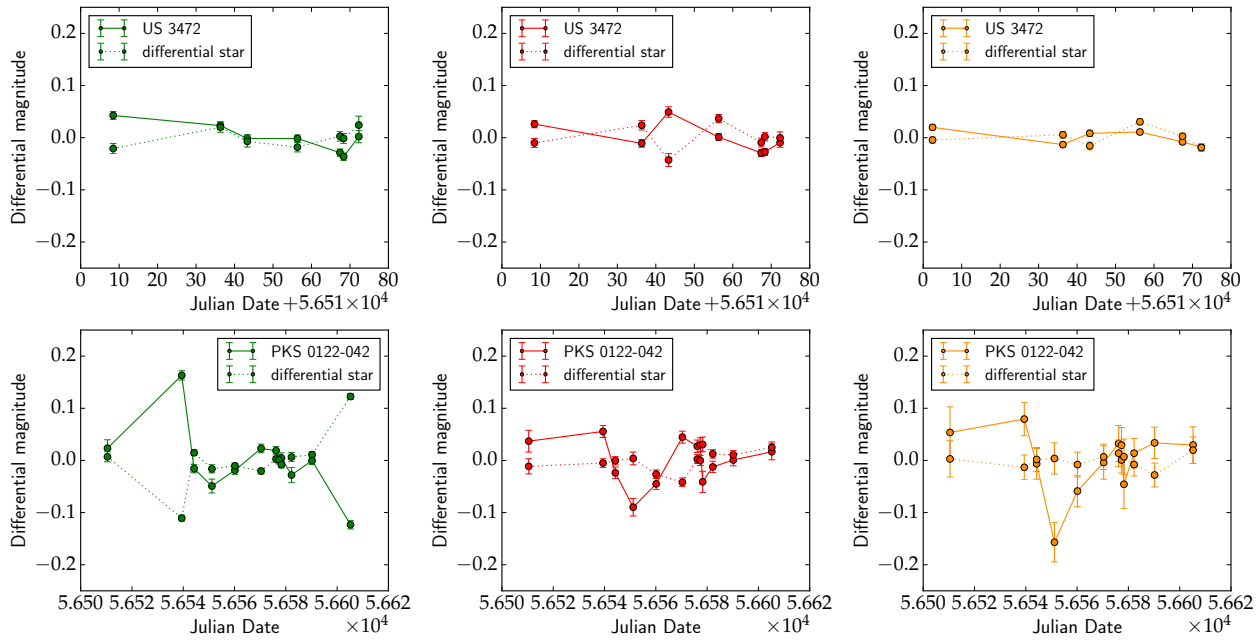

Figure 4.7: Light curves observed in the year long RATIR campaign with optical filters. The colors correspond to g' green, r' red and i' orange. The differential magnitude was adjusted by a constant to fit the star and the AGN in the same plot for a direct comparison. The differential magnitude interval was adjusted to 0.5 mag for a direct comparison.

Table 4.5: Estimated intrinsic variability of the variable AGNs from the sample.

Target	$V_r(g')$	$V_r(r')$	$V_r(i')$
E 0111+388	2.30E-02	1.30E-02	4.00E-03
Mrk 1014	2.30E-03	1.70E-03	2.40E-03
PKS 2243-123	4.00E-03	1.60E-03	3.30E-03
PKS 2349-01	8.70E-03	3.00E-03	2.50E-03
PKS 0003+15	1.30E-03	4.00E-04	7.00E-04

In order to verify the detections, we have computed also the estimated intrinsic variance, which takes into account the photometric errors of the measurements. Note that the errors were not necessary in the Bartels test. In general, it is not feasible to rely on the error estimations (Goyal et al. 2013) as they tend to be underestimated. In order to get an estimation of the error, we have computed the standard deviation of the background and compared it with the noise. Based on this approach, we have estimated errors of $\sim 2\%$ at maximum. While SExtractor underestimates the errors, IRAF procedure `qphot` agrees with the empirical measurements we have obtained, therefore we have computed errors using the `qphot` procedure. The intrinsic variability, or part of the observed variance not accounted for the errors, is

$$V_r = V_0 - \frac{e^2}{N} \geq 0, \tag{4.6}$$

where N is the number of observations. The restriction of $V_r \geq 0$ arises from physical considerations. The results of the estimated intrinsic variance are summarized in Table 4.4. We consider AGNs as variable when $V_r > 10^{-3}$, sources which are of order of 10^{-3} are bordering the detection level.

With the exception of E 0111+388, V_r of all the sources borders detection level of the variability in the given data set. Also, considering Table 4.2, we notice that in the majority of the cases, variability was detected only in one filter. In such cases, we marked the sources as probably variable. Moreover several light curves, noticeably those with few data points, show variations also in the case of the differential star. We do not draw conclusions on those targets.

4.3 Discussion

Based on the results of the Fisher's test, we conclude that there is no difference between the detection of variability in the core-dominated radio loud quasars and radio quiet quasars. Such result is in agreement with the results by de Diego et al. (1998) who have studied a sample of CRLQs and RQQs, of which the sample presented here is a subsample, for the detection of microvariability. Nevertheless the present study deals with many issues which have to be taken into account. The original sample had in total 40 targets. The presented study focuses on 50% of the original sample. Moreover, we lost one more target due to the low quality of the observations, which can be probably attributed to the high airmasses.

We searched for variability using a statistical test. The use of a statistical test naturally penalizes the targets which have not been observed many times as the power of the test decreases. 8 out of 18 sources were observed less than 8 times and none of them are marked as variable. In other words, the variation would have to be extremely prominent to be picked up by Bartels test in the case of few observations. All the variable sources have been observed at least 8 times. The median number of observations in the case of not variable sources is 6, while for variable sources, the median is 12.There is a possibility that such discrepancy plays a role in the variability detection. The overview of the number of observations is provided in table 4.2.

Table 4.6: Contingency table for the results of variability of the quasars from the campaign, with connection to X-ray detection.

	X-ray detection	no X-ray detection	Sum
Variable	4	1	5
Not variable	7	6	13
Sum	11	7	18

Nevertheless adjusting the contingency table for 10 sources which were observed for the longer periods does not affect the result of the study.

The lack of high quality light curves also affected the possibility to follow the path set up by the previous comparison study by de Diego et al. (1998), who directly compared detected microvariability within the pairs matched by redshift and brightness. The insufficient image quality was caused by the highly variable conditions, especially in terms of airmass. The low quality of the images prevented us from estimating the error of the measurement precisely. In terms of paired targets, both of the sources are detected variable in the pair #14. The radio quiet source exhibits larger amplitudes, based on the estimation of the intrinsic variability, but one pair is not a statistical sample.

Aside from the variability, we have addressed the X-ray detection of the sample, examining the possibility that the variability detection can be linked with the X-ray brightness of the data. As in the case of the radio loudness, we have used contingency table and subsequent Fisher's test to look if the X-ray brightness can be attributed to only one of the groups. Given that except Mrk 1014, which was observed by XMM-Newton (Piconcelli et al. 2005) and Chandra (Teng et al. 2005; Kelly et al. 2007) satellites, the only consistent X-ray data come from the ROSAT all sky survey (Voges et al. 1999), thus we have searched through the ROSAT catalogue to obtain information about the X-ray properties.

Based on the contingency table 4.6, the resulting $p-value = 0.59$, and therefore we fail to reject the null hypothesis, stating that there are no differences between the X-ray properties of the samples.

It is worth to check the microvariability properties of the variability sources. de Diego et al. (1998) detect microvariability in PKS 2349-01 and PKS 0003+15, Joshi et al. (2012) detect microvariability also in the case of E 0111+388. For the rest of the variable sources, there are no reports of microvariability. On the other hand, some of the sources that we do not detect as variable exhibit microvariable behavior (de Diego et al. 1998). However as some of them fall into the subset of the data which does not seem to have enough data points observed, it is unreliable to draw any conclusion.

Chapter 5

Conclusions

This thesis explores the subject of variability in quasars. We have taken into account short time scale variability known as microvariability and weekly variations. Below is the summarization of the result we obtained.

5.1 Microvariability of type 2 quasars

Microvariation in type 2 quasars is a phenomenon previously unaccounted for. From our observing campaign at San Pedro Mártir Observatory in México, we reported a detection of one variable (Mrk 477) and one not confirmed variable type 2 quasar (J0759+5050) that were detected as variable during one observing block shorter than two hours. Both results were obtained using a statistical method, namely a one-way analysis of variance, ANOVA, which previously proved to be a powerful test for the detection of microvariations in AGN light curves. Given the observation history of the variable object Mrk 477, we discussed the possible causes of the variations, which include structure in the dusty torus and clouds in the broad line region, a situation observed in some of the obscured AGNs in X-ray. Our observing campaign was limited to one filter in the optical regime, therefore we cannot confirm any of our hypotheses by observational evidence. Because of the possible importance of microvariability to the study of the physics of the type 2 quasars and their obscured regions, it is worth investigating whether this is a ubiquitous phenomenon in this class of AGNs.

Based on the success of the pilot sample, we proposed new observations with the Nordic Optical Telescope to broaden the sample by four more type 2 quasars. We have detected microvariability on a time scale less than 4 hours in one target (J0802+2552) in all filters at the 0.001 significance level during both observing nights, in J1258+5239 (in i' filter) and J1316+4452 (in r' and i' filter) with 0.001 significance level only in the second observing night. We have tested a newly proposed method for detecting variability/microvariability: the enhanced F-test (de Diego 2014). The test shows sensible results and provides enough power to search for variability. But as the power of the test relies on the sample size, it is desirable to have as many observations as possible, and a high number of stars in the field observed. We discussed a possible connection of morphology of the type 2 quasar to variable behavior. We have noticed that variable sources tend to have disturbed morphologies. Such statement would be in concordance with the first study where we detected microvariations in Mrk 477, which seem to be in a merging state. However the disturbed morphologies tend to have more powerful AGNs, which are more probe to exhibit variability. The sample is to small to draw conclusion, but it is worth investigating in the future.

We have documented the limitations for the method, posed by the nature of the targets we have observed. As long as the target is only moderately extended without irregularities, the aperture

photometry works reasonably well. Irregular targets are problematic as, at the moment, there is no routine available which would be able to separate the quasar from its host galaxy. Including the presumably steady host galaxy, increases the noise in the data, which results in a possible underestimation of the amplitude of the variation. We have shown that in the case of significantly extended host galaxies (as in some interacting systems), the variability detection is hampered due to the problems with aperture photometry. Alternative photometry available in SExtractor (e.g. isocor photometry or elliptical photometries using Kron radius) might introduce inhomogeneities into the dataset, due to different aperture sizes for the stars in the field and the quasars, therefore we are not focusing on them. We have tried to limit the threshold to account for light propagating into the main target from the fainter tail of the source. Such adjustment severely reduces the number of stars that can be used for differential photometry and, therefore, diminishes the main advantage of the F-test, which is to increase the number of degrees of freedom based on using as many field stars as possible. We have shown that the brightness of the sky might play a role in the reliability of the test as we were unable to achieve similar photometric precisions for targets observed when the sky was partially illuminated by the Moon.

5.2 Radio loud versus radio quiet quasars

Following previous studies (de Diego et al. 1998; Ramírez et al. 2009), we have focused on comparing the variability behavior of a pair of radio quiet and core-dominated radio loud sources, matched in redshift and brightness. However the campaign met with many technical problems. Out of the initial sample of 20 sources, we have lost two sources as there were not enough observation and the ones obtained were of a low quality, possibly caused by the fact that both sources were observed in high airmasses. Additional data loss was caused by the imprecise astrometric solutions. Out of the 18 sources used for the final analysis, 8 were observed very few times and resulted in severely under sampled light curves, which given the fact that we employed statistical methods to detect variability, had a negative effect on the power of the test. On the other hand, we have detected variability in 5 out of 10 quasars which had densely populated light curves. Unfortunately such a low number of useful data prevents us from obtaining solid conclusion. Nevertheless applying Fisher's exact test, we find no difference between the occurrence of variable phenomenon in radio quiet versus core-dominated radio loud quasars.

Furthermore, we have explosed the datased based on the X-ray detection of the sample from the ROSAT all sky survey. The energy coverage of the survey is 0.04 – 0.2 keV. We have found no indication of significant difference of the variable and not variable subsets of the sample in terms of X-ray brightness.

The present results are in concordance with works by de Diego et al. (1998); Ramírez et al. (2009) who reported similar result from the microvariability point of view, however in the present moment, the observed sample is not statistically significant and therefore we refrain from drawing solid conclusions from the sample.

5.3 Methods

All the obtained data sets were calibrated for photometric errors and when needed, astrometrized. The data sets differ in quality. We have employed different statistical tests to search for variability. The pilot sample for microvariability of obscured quasars was analyzed using one way analysis of variance, ANOVA, as there were enough data points, but few stars accompanying the sources in the observed field. The initial sample was extended with the sample from Nordic Optical Telescope, which provided a test set for the enhanced version of the F-test, developed by de Diego (2014). The enhanced F-test requires a number of stars in the observed field along with the source itself and significant number of observations. As both conditions were fulfilled, the enhanced F-test,

more powerful than simple ANOVA, was used to analyze the data set. The last data set contained undersampled light curves and few field stars. Given these conditions, we decided to use Bartels test, which is not as powerful as ANOVA or enhanced F-test, but more suitable for the situation. We have shown that the Bartels test can indeed be used in such conditions.

5.4 Conclusion overview

The main conclusions of this work are:

- We report the first robust proof of microvariability of type 2 quasars at optical wavelengths.
- We attempt to link the detection of microvariability in type 2 quasar to a physical origin. The plausible scenarios include structure in the dusty torus, clouds in the broad line region (connected with X-ray variability) or reflected light from the central engine. However given the restrictions of our purely photometric dataset, we can conclude that there is no evidence of a conection between X-ray and microvariability.
- We made an attempt to link microvariability to the disturbed morphology. Given the small sample, there is prima facie evidence for such a link, althought more evidence is needed for deriving conclusive results.
- We studied the feasibility of statistical tests in search for microvariability. The two tests we used, one-way analysis of variance (ANOVA) and the enhanced F-test resulted to be powerful enough for detection of the microvariability. The choice of the test depends on presence of other stars in the field. With more stars in the field, the enhanced F-test is more powerful, ANOVA proves reliable in the cases with few stars in the field. We showed also the feasibility of Bartels test, a nonparametric statistical test which looks for trends in the data, thus pointing to variable events. Bartels test is extremely useful in cases where the data sets are small and we cannot assume anything about the underlying distribution. By further examination, we have determined that the scarcely populated light curves are insufficient for the analysis. Nevertheless removing those from our sample did not affect the result, which is in concordance with previous studies.
- Even for a moderatelly extended source, aperture photometry is a useful choice. We have demonstrated that aperture photometry using SExtractor is an excellent tool to search for variability, although the photometric errors must be estimated using other means. The only exception are significantly extended or morphologically disturbed targets.
- We have not found differences in weekly variability behaviour between CRLQ and RQQ. This result allows extending that of de Diego et al. (1998) and Ramírez et al. (2009) on intranight variability (microvariability).

5.5 Future plans

The data obtained during RATIR campaign will be submitted to a refereed journal, reporting confirmation of the results reported by de Diego et al. (1998); Ramírez et al. (2009), who reached the same result, but using long term variability.

Mrk 477 seems to be a very peculiar source which is microvariable and has hidden broad lines in the polarized light. On top of that, there seem to be a merger with the accompanying galaxy I Zw 92. We have obtained spectroscopic observations during our NOT run and we are expecting data from integral field unit (IFU) mounted on Calar Alto. We plan on analyzing the stellar and

gas content and the velocity field of the two interacting galaxies. We expect I Zw 92 to be a feeding channel of the AGN in Mrk 477.

We are planning to ask for time for a spectropolarimetric campaign, observing the sources we have detected as microvariable, in order to provide the possible link between the hidden broad line region and microvariability. Linking these two might provide a 'low-cost' way to distinguish between the true type 2 AGNs and those with hidden broad lines. Such distinction is nowadays addressed in time consuming spectropolarimetric observations.

We are planning to broaden the sample of type 2 quasars with an emphasis on different morphologies, to establish whether there is a connection between the disturbed morphologies and microvariable events.

We plan to revisit the RATIR sample with better sampling. We plan to obtain more populated light curves in order to be able to analyze not only the presence of variability, but also the differences in the amplitudes.

We are planning on carrying out a project focused on the search for type changing AGNs in the photometric surveys with the J-PAS collaboration. J-PAS will survey the sky in 56 narrow band filters in optical and hence will provide us with 'low resolution' spectra. We plan follow up of the positive detections, including microvariability campaigns. Such campaign is extremely valuable as it might link obscured and unobscured AGNs together in an evolutionary scenario.

References

Abramowicz, M. A., Bao, G., Lanza, A., & Zhang, X.-H. 1991, A&A, 245, 454

Abramowicz, M. A., Lanza, A., Spiegel, E. A., & Szuszkiewicz, E. 1992, Nature, 356, 41

Ackermann, M., Ajello, M., Albert, A., et al. 2015, ApJ, 813, L41

Adelman-McCarthy, J. K., Agüeros, M. A., Allam, S. S., et al. 2008, ApJS, 175, 297

Alam, S., Albareti, F. D., Allende Prieto, C., et al. 2015, ArXiv e-prints

Aleksić, J., Ansoldi, S., Antonelli, L. A., et al. 2014, A&A, 569, A46

Andrillat, Y. & Souffrin, S. 1968, Astrophys. Lett., 1, 111

Andruchow, I., Romero, G. E., & Cellone, S. A. 2005, A&A, 442, 97

Antokhin, I. I. & Bochkarev, N. G. 1983, Soviet Ast., 27, 261

Antonucci, R. 1993, ARA&A, 31, 473

Antonucci, R., Barvainis, R., & Alloin, D. 1990, ApJ, 353, 416

Antonucci, R. R. J. & Miller, J. S. 1985, ApJ, 297, 621

Aretxaga, I. & Terlevich, R. 1994, MNRAS, 269, 462

Arévalo, P., Uttley, P., Kaspi, S., et al. 2008, MNRAS, 389, 1479

Bachev, R., Strigachev, A., & Semkov, E. 2005, MNRAS, 358, 774

Bahcall, J. N., Kozlovsky, B.-Z., & Salpeter, E. E. 1972, ApJ, 171, 467

Baldwin, J. A., Phillips, M. M., & Terlevich, R. 1981, PASP, 93, 5

Bao, G. & Abramowicz, M. A. 1996, ApJ, 465, 646

Bartels, R. 1982, Journal of the American Statistical Asociation, 77, 40

Bauer, A., Baltay, C., Coppi, P., et al. 2009, ApJ, 705, 46

Bentz, M. C., Denney, K. D., Grier, C. J., et al. 2013, ApJ, 767, 149

Bentz, M. C. & Katz, S. 2015, PASP, 127, 67

Bertin, E. 2006, in Astronomical Society of the Pacific Conference Series, Vol. 351, Astronomical Data Analysis Software and Systems XV, ed. C. Gabriel, C. Arviset, D. Ponz, & S. Enrique, 112

Bertin, E. & Arnouts, S. 1996, A&AS, 117, 393

Bertin, E., Mellier, Y., Radovich, M., et al. 2002, in Astronomical Society of the Pacific Conference Series, Vol. 281, Astronomical Data Analysis Software and Systems XI, ed. D. A. Bohlender, D. Durand, & T. H. Handley, 228

Bignall, H. E., Jauncey, D. L., Lovell, J. E. J., et al. 2003, ApJ, 585, 653

Blandford, R. D. & Königl, A. 1979, ApJ, 232, 34

Blandford, R. D. & McKee, C. F. 1982, ApJ, 255, 419

Blandford, R. D. & Znajek, R. L. 1977, MNRAS, 179, 433

Boettcher, M. & Schlickeiser, R. 1997, A&A, 325, 866

Boller, T. & Brandt, W. N. 1999, in Astronomical Society of the Pacific Conference Series, Vol. 175, Structure and Kinematics of Quasar Broad Line Regions, ed. C. M. Gaskell, W. N. Brandt, M. Dietrich, D. Dultzin-Hacyan, & M. Eracleous, 279

Boller, T., Brandt, W. N., Fabian, A. C., & Fink, H. H. 1997, MNRAS, 289, 393

Bottorff, M., Korista, K. T., Shlosman, I., & Blandford, R. D. 1997, ApJ, 479, 200

Brenneman, L. W., Risaliti, G., Elvis, M., & Nardini, E. 2013, MNRAS, 429, 2662

Butler, N., Klein, C., Fox, O., et al. 2012, in Proc. SPIE, Vol. 8446, Ground-based and Airborne Instrumentation for Astronomy IV, 844610

Buttiglione, S., Capetti, A., Celotti, A., et al. 2009, A&A, 495, 1033

Capriotti, E. R., Foltz, C. B., & Peterson, B. M. 1982, ApJ, 261, 35

Carini, M. T., Miller, H. R., Noble, J. C., & Goodrich, B. D. 1992, AJ, 104, 15

Carnerero, M. I., Raiteri, C. M., Villata, M., et al. 2015, MNRAS, 450, 2677

Cellone, S. A., Romero, G. E., & Combi, J. A. 2000, AJ, 119, 1534

Chagelishvili, G. D., Lominadze, J. G., & Rogava, A. D. 1989, ApJ, 347, 1100

Chakrabarti, S. & Titarchuk, L. G. 1995, ApJ, 455, 623

Chakrabarti, S. K. & Wiita, P. J. 1993, A&A, 271, 216

Chang, K. & Refsdal, S. 1979, Nature, 282, 561

Chartas, G., Brandt, W. N., Gallagher, S. C., & Garmire, G. P. 2002, ApJ, 579, 169

Chen, P. S. & Shan, H. G. 2009, MNRAS, 393, 1408

Cid Fernandes, R., Schlickmann, M., Stasinska, G., et al. 2009, in Astronomical Society of the Pacific Conference Series, Vol. 408, The Starburst-AGN Connection, ed. W. Wang, Z. Yang, Z. Luo, & Z. Chen, 122

Condon, J. J. & Backer, D. C. 1975, ApJ, 197, 31

Crenshaw, D. M. & Kraemer, S. B. 2012, ApJ, 753, 75

Cristiani, S., Trentini, S., La Franca, F., & Andreani, P. 1997, A&A, 321, 123

Cristiani, S., Vio, R., & Andreani, P. 1990, AJ, 100, 56

Cutri, R. M., Wisniewski, W. Z., Rieke, G. H., & Lebofsky, M. J. 1985, ApJ, 296, 423

Day, C. S. R., Fabian, A. C., George, I. M., & Kunieda, H. 1990, MNRAS, 247, 15P

de Diego, J. A. 2010, AJ, 139, 1269

de Diego, J. A. 2014, AJ, 148, 93

de Diego, J. A., Dultzin-Hacyan, D., Ramírez, A., & Benítez, E. 1998, ApJ, 501, 69

de Diego, J. A., Kidger, M. R., Gonzalez-Perez, J. N., & Lehto, H. J. 1997, A&A, 318, 331

de Diego, J. A., Polednikova, J., Bongiovanni, A., et al. 2015, AJ, 150, 44

de Vries, M. & Kuijpers, J. 1992, A&A, 266, 77

Dennett-Thorpe, J. & de Bruyn, A. G. 2000, ApJ, 529, L65

di Clemente, A., Giallongo, E., Natali, G., Trevese, D., & Vagnetti, F. 1996, ApJ, 463, 466

Dietrich, M., Kollatschny, W., Peterson, B. M., et al. 1993, ApJ, 408, 416

Dietrich, M., Peterson, B. M., Grier, C. J., et al. 2012, ApJ, 757, 53

Djorgovski, S., Weir, N., Matthews, K., & Graham, J. R. 1991, ApJ, 372, L67

Done, C. & Krolik, J. H. 1996, ApJ, 463, 144

Edelson, R. A. & Krolik, J. H. 1988, ApJ, 333, 646

Eisenstein, D. J., Weinberg, D. H., Agol, E., et al. 2011, AJ, 142, 72

Elvis, M., Maccacaro, T., Wilson, A. S., et al. 1978, MNRAS, 183, 129

Elvis, M., Wilkes, B. J., McDowell, J. C., et al. 1994, ApJS, 95, 1

Fabbiano, G., Willner, S. P., Carleton, N. P., & Elvis, M. 1986, ApJ, 304, L37

Fabrika, S. N. 1980, Soviet Astronomy Letters, 6, 293

Fath, E. A. 1909, Lick Observatory Bulletin, 5, 71

Ferland, G. J. & Osterbrock, D. E. 1986, ApJ, 300, 658

Fitch, W. S., Pacholczyk, A. G., & Weymann, R. J. 1967, ApJ, 150, L67

Fritz, J., Franceschini, A., & Hatziminaoglou, E. 2006, MNRAS, 366, 767

Gaidos, J. A., Akerlof, C. W., Biller, S., et al. 1996, Nature, 383, 319

Garcia, A., Sodré, L., Jablonski, F. J., & Terlevich, R. J. 1999, MNRAS, 309, 803

Gaskell, C. M. 2004, ApJ, 612, L21

George, I. M. & Fabian, A. C. 1991, MNRAS, 249, 352

Gilli, R., Vignali, C., Mignoli, M., et al. 2010, A&A, 519, A92

Giveon, U., Maoz, D., Kaspi, S., Netzer, H., & Smith, P. S. 1999, MNRAS, 306, 637

Goad, M. R., Korista, K. T., De Rosa, G., et al. 2016, ApJ, 824, 11

Gopal-Krishna, Gupta, A. C., Sagar, R., et al. 2000, MNRAS, 314, 815

Gopal-Krishna & Wiita, P. J. 1992, A&A, 259, 109

Goyal, A., Mhaskey, M., Gopal-Krishna, et al. 2013, Journal of Astrophysics and Astronomy, 34, 273

Hartman, R. C., Webb, J. R., Marscher, A. P., et al. 1996, ApJ, 461, 698

Hawkins, M. R. S. 1993, Nature, 366, 242

Hazard, C., Mackey, M. B., & Shimmins, A. J. 1963, Nature, 197, 1037

Heeschen, D. 1982, in IAU Symposium, Vol. 97, Extragalactic Radio Sources, ed. D. S. Heeschen & C. M. Wade, 327

Heeschen, D. S. 1984, AJ, 89, 1111

Heidt, J. & Wagner, S. J. 1996, A&A, 305, 42

Hönig, S. F., Kishimoto, M., Gandhi, P., et al. 2010, A&A, 515, A23

Hook, I. M., McMahon, R. G., Boyle, B. J., & Irwin, M. J. 1994, MNRAS, 268, 305

Hovatta, T., Tornikoski, M., Lainela, M., et al. 2007, A&A, 469, 899

Howell, S. B., Warnock, III, A., & Mitchell, K. J. 1988, AJ, 95, 247

Jang, M. 2001, Ap&SS, 275, 209

Jang, M. & Miller, H. R. 1997, AJ, 114, 565

Jauncey, D. L., Bignall, H. E., Lovell, J. E. J., et al. 2003, in Astronomical Society of the Pacific Conference Series, Vol. 300, Radio Astronomy at the Fringe, ed. J. A. Zensus, M. H. Cohen, & E. Ros, 199

Jaunsen, A. O., Jablonski, M., Pettersen, B. R., & Stabell, R. 1995, A&A, 300, 323

Jones, D. H., Read, M. A., Saunders, W., et al. 2009, MNRAS, 399, 683

Jones, D. H., Saunders, W., Colless, M., et al. 2004, MNRAS, 355, 747

Joshi, R., Chand, H., Gupta, A. C., & Wiita, P. J. 2011, MNRAS, 412, 2717

Joshi, R., Chand, H., Wiita, P. J., Gupta, A. C., & Srianand, R. 2012, MNRAS, 419, 3433

Kedziora-Chudczer, L., Jauncey, D. L., Wieringa, M. H., et al. 1997, ApJ, 490, L9

Kellermann, K. I., Sramek, R., Schmidt, M., Shaffer, D. B., & Green, R. 1989, AJ, 98, 1195

Kellermann, K. I., Sramek, R. A., Schmidt, M., Green, R. F., & Shaffer, D. B. 1994, AJ, 108, 1163

Kelly, B. C., Bechtold, J., Siemiginowska, A., Aldcroft, T., & Sobolewska, M. 2007, ApJ, 657, 116

Kennicutt, Jr., R. C. 1992, ApJS, 79, 255

Kerrick, A. D., Akerlof, C. W., Biller, S. D., et al. 1995, ApJ, 438, L59

Kesteven, M. J. L., Bridle, A. H., & Brandie, G. W. 1976, AJ, 81, 919

Kidger, M., Lario, P. G., & de Diego, J. A. 1992, A&AS, 93, 391

Kidger, M. R., Takalo, L. O., & de Diego, J. A. 1994, A&A, 282, 369

Kim, J.-Y. & Trippe, S. 2013, Journal of Korean Astronomical Society, 46, 65

Kinman, T. D. 1975, in IAU Symposium, Vol. 67, Variable Stars and Stellar Evolution, ed. V. E. Sherwood & L. Plaut, 573–590

Kniffen, D. A., Bertsch, D. L., Fichtel, C. E., et al. 1993, ApJ, 411, 133

Kollatschny, W. & Dietrich, M. 1996, A&A, 314, 43

Kovalev, Y. Y., Aller, H. D., Aller, M. F., et al. 2009, ApJ, 696, L17

Krennrich, F., Bond, I. H., Bradbury, S. M., et al. 2002, ApJ, 575, L9

Kriss, G. A., Peterson, B. M., Crenshaw, D. M., & Zheng, W. 2000, ApJ, 535, 58

Krolik, J. H. & Begelman, M. C. 1988, ApJ, 329, 702

Krolik, J. H., Horne, K., Kallman, T. R., et al. 1991, ApJ, 371, 541

Lang, D., Hogg, D. W., Mierle, K., Blanton, M., & Roweis, S. 2010, AJ, 139, 1782

Li, S.-L. & Cao, X. 2008, MNRAS, 387, L41

Lightman, A. P. & Eardley, D. M. 1974, ApJ, 187, L1

Lightman, A. P. & White, T. R. 1988, ApJ, 335, 57

Lintott, C., Schawinski, K., Bamford, S., et al. 2011, MNRAS, 410, 166

Lorenzetti, D., Spinoglio, L., Massaro, E., & Perola, G. C. 1990, A&A, 235, 35

Lovelace, R. V. E. & Backer, D. C. 1972, Astrophys. Lett., 11, 135

Lynds, C. R. 1967, ApJ, 147, 837

Lyutikov, M. 2003, , 47, 513

Markowitz, A. & Edelson, R. 2001, ApJ, 547, 684

Marscher, A. P. 1992, in American Institute of Physics Conference Series, Vol. 254, American Institute of Physics Conference Series, ed. S. S. Holt, S. G. Neff, & C. M. Urry, 377–385

Marscher, A. P., Gear, W. K., & Travis, J. P. 1992, in Variability of Blazars, ed. E. Valtaoja & M. Valtonen, 85

Mastichiadis, A. & Kirk, J. G. 1997, A&A, 320, 19

Matthews, T. A. & Sandage, A. R. 1963, ApJ, 138, 30

Mattox, J. R., Wagner, S., McGlynn, T. A., et al. 1995, IAU Circ., 6179, 1

Mattox, J. R. & Wagner, S. J. 1996, in Astronomical Society of the Pacific Conference Series, Vol. 110, Blazar Continuum Variability, ed. H. R. Miller, J. R. Webb, & J. C. Noble, 352

Meyer, M. J., Zwaan, M. A., Webster, R. L., et al. 2004, MNRAS, 350, 1195

Miller, H. R. & Wiita, P. J. 1992, Variability of active galactic nuclei (Cambridge University press)

Miller, P., Rawlings, S., & Saunders, R. 1993, MNRAS, 263, 425

Montgomery, D. C. 2013, Design and analysis of experiments, 8th edition. (John Wilet & Sons)

Mor, R. & Netzer, H. 2012, MNRAS, 420, 526

Moran, E. C., Barth, A. J., Kay, L. E., & Filippenko, A. V. 2000, ApJ, 540, L73

Mulchaey, J. S., Mushotzky, R. F., & Weaver, K. A. 1992, ApJ, 390, L69

Nair, A. D. 1997, MNRAS, 287, 641

Nandra, K., George, I. M., Mushotzky, R. F., Turner, T. J., & Yaqoob, T. 1997, ApJ, 476, 70

Nenkova, M., Sirocky, M. M., Ivezić, Ž., & Elitzur, M. 2008, ApJ, 685, 147

Netzer, H. 2009, ApJ, 695, 793

Netzer, H. 2015, ARA&A, 53, 365

Netzer, H., Heller, A., Loinger, F., et al. 1996, MNRAS, 279, 429

Netzer, H. & Marziani, P. 2010, ApJ, 724, 318

Osterbrock, D. E. & Koski, A. T. 1976, MNRAS, 176, 61P

Paliya, V. S., Stalin, C. S., Kumar, B., et al. 2013, MNRAS, 428, 2450

Peterson, B. M. 1999, in Astronomical Society of the Pacific Conference Series, Vol. 175, Structure and Kinematics of Quasar Broad Line Regions, ed. C. M. Gaskell, W. N. Brandt, M. Dietrich, D. Dultzin-Hacyan, & M. Eracleous, 49

Peterson, B. M. 2001, in Advanced Lectures on the Starburst-AGN, ed. I. Aretxaga, D. Kunth, & R. Mújica, 3

Peterson, B. M. 2006, in Lecture Notes in Physics, Berlin Springer Verlag, Vol. 693, Physics of Active Galactic Nuclei at all Scales, ed. D. Alloin, 77

Peterson, B. M., Berlind, P., Bertram, R., et al. 2002, ApJ, 581, 197

Peterson, B. M., Denney, K. D., De Rosa, G., et al. 2013, ApJ, 779, 109

Peterson, B. M., Wanders, I., Bertram, R., et al. 1998, ApJ, 501, 82

Piconcelli, E., Jimenez-Bailón, E., Guainazzi, M., et al. 2005, A&A, 432, 15

Pier, E. A. & Krolik, J. H. 1992, ApJ, 401, 99

Pogge, R. W. & Peterson, B. M. 1992, AJ, 103, 1084

Polednikova, J., Ederoclite, A., Cepa, J., et al. 2015, ArXiv e-prints

Polednikova, J., Ederoclite, A., de Diego, J. A., et al. 2016, ArXiv e-prints

Pringle, J. E., Rees, M. J., & Pacholczyk, A. G. 1973, A&A, 29, 179

Qian, S. J., Quirrenbach, A., Witzel, A., et al. 1991, A&A, 241, 15

Quirrenbach, A., Witzel, A., Kirchbaum, T. P., et al. 1992, A&A, 258, 279

R core team. 2013, A Language and Enviroment for Statistical Computing, R Foundation for Statistical Computing

Ramírez, A., de Diego, J. A., Dultzin, D., & González-Pérez, J.-N. 2009, AJ, 138, 991

Ramírez, A., de Diego, J. A., Dultzin-Hacyan, D., & González-Pérez, J. N. 2004, A&A, 421, 83

Ramírez, A., Dultzin, D., & de Diego, J. A. 2010, ApJ, 714, 605

Rees, M. J. 1978, Nature, 275, 516

Reyes, R., Zakamska, N. L., Strauss, M. A., et al. 2008, AJ, 136, 2373

Risaliti, G., Elvis, M., Fabbiano, G., Baldi, A., & Zezas, A. 2005, ApJ, 623, L93

Risaliti, G., Salvati, M., Elvis, M., et al. 2009, MNRAS, 393, L1

Romero, G. E., Cellone, S. A., & Combi, J. A. 1999, A&AS, 135, 477

Schmidt, M. 1963, Nature, 197, 1040

Schmidt, M. 1969, ARA&A, 7, 527

Schödel, R., Krips, M., Markoff, S., Neri, R., & Eckart, A. 2007, A&A, 463, 551

Sesar, B., Ivezić, Ž., Lupton, R. H., et al. 2007, AJ, 134, 2236

Seyfert, C. K. 1943, ApJ, 97, 28

Shapovalova, A. I., Doroshenko, V. T., Bochkarev, N. G., et al. 2004, A&A, 422, 925

Shapovalova, A. I., Popović, L. Č., Burenkov, A. N., et al. 2012, ApJS, 202, 10

Sikora, M., Stawarz, Ł., & Lasota, J.-P. 2007, ApJ, 658, 815

Slipher, V. M. 1917, Lowell Observatory Bulletin, 3, 59

Soifer, B. T., Sanders, D. B., Madore, B. F., et al. 1987, in NASA Conference Publication, Vol. 2466, NASA Conference Publication, ed. C. J. Lonsdale Persson, 523–530

Spada, M., Ghisellini, G., Lazzati, D., & Celotti, A. 2001, MNRAS, 325, 1559

Stalevski, M., Fritz, J., Baes, M., Nakos, T., & Popović, L. Č. 2012, MNRAS, 420, 2756

Stalin, C. S., Gopal-Krishna, Sagar, R., & Wiita, P. J. 2004, MNRAS, 350, 175

Starling, R. L. C., Siemiginowska, A., Uttley, P., & Soria, R. 2004, MNRAS, 347, 67

Takalo, L. O., Kidger, M. R., de Diego, J. A., Sillanpaa, A., & Nilsson, K. 1992, AJ, 104, 40

Taylor, M. B. 2005, in Astronomical Society of the Pacific Conference Series, Vol. 347, Astronomical Data Analysis Software and Systems XIV, ed. P. Shopbell, M. Britton, & R. Ebert, 29

Teng, S. H., Wilson, A. S., Veilleux, S., et al. 2005, ApJ, 633, 664

Terlevich, R., Tenorio-Tagle, G., Franco, J., & Melnick, J. 1992, MNRAS, 255, 713

Terrell, J. 1986, ApJ, 300, 669

Thompson, D. J., Bertsch, D. L., Dingus, B. L., et al. 1995, ApJS, 101, 259

Tommasin, S., Spinoglio, L., Malkan, M. A., & Fazio, G. 2010, ApJ, 709, 1257

Torrealba, J., Chavushyan, V., Cruz-González, I., et al. 2012, , 48, 9

Torricelli-Ciamponi, G., Foellmi, C., Courvoisier, T. J.-L., & Paltani, S. 2000, A&A, 358, 57

Tran, H. D., Cohen, M. H., & Villar-Martin, M. 2000, AJ, 120, 562

Trevese, D., Kron, R. G., Majewski, S. R., Bershady, M. A., & Koo, D. C. 1994, ApJ, 433, 494

Turner, T. J., George, I. M., Nandra, K., & Turcan, D. 1999, ApJ, 524, 667

Turnshek, D. A., Grillmair, C. J., Foltz, C. B., & Weymann, R. J. 1988, ApJ, 325, 651

Ulrich, M.-H., Maraschi, L., & Urry, C. M. 1997, ARA&A, 35, 445

Urry, C. M. & Padovani, P. 1995, PASP, 107, 803

Uttley, P. & McHardy, I. M. 2001, MNRAS, 323, L26

Valtaoja, E. & Teraesranta, H. 1996, A&AS, 120, C491

Valtaoja, E. & Terasranta, H. 1995, A&A, 297, L13

van Dokkum, P. G. 2001, PASP, 113, 1420

Vanden Berk, D. E., Wilhite, B. C., Kron, R. G., et al. 2004, ApJ, 601, 692

Véron-Cetty, M.-P. & Véron, P. 2010, A&A, 518, A10

Villar-Martin, M. 1996, Dust and gas in active galaxies (ESO)

Voges, W., Aschenbach, B., Boller, T., et al. 1999, A&A, 349, 389

Wagner, S. J. & Witzel, A. 1995, ARA&A, 33, 163

Walker, M. F. 1968, ApJ, 151, 71

Wamsteker, W., Rodriguez-Pascual, P., Wills, B. J., et al. 1990, ApJ, 354, 446

Wanders, I., Goad, M. R., Korista, K. T., et al. 1995, ApJ, 453, L87

Wanders, I., Peterson, B. M., Alloin, D., et al. 1997, ApJS, 113, 69

Wilhite, B. C., Brunner, R. J., Grier, C. J., Schneider, D. P., & vanden Berk, D. E. 2008, MNRAS, 383, 1232

Willett, K. W., Lintott, C. J., Bamford, S. P., et al. 2013, MNRAS, 435, 2835

Witzel, A., Heeschen, D. S., Schalinski, C., & Krichbaum, T. 1986, Mitteilungen der Astronomischen Gesellschaft Hamburg, 65, 239

Wold, M., Brotherton, M. S., & Shang, Z. 2007, MNRAS, 375, 989

Xue, Y., Yuan, F., & Cui, W. 2006, ApJ, 647, 194